Assessment of pediatric shoulder range of motion and loading response to evaluate the biofidelity of the Large Omni-directional Child (LODC) Anthropomorphic Test Device (ATD) shoulder design

Thesis

Presented in Partial Fulfillment of the Requirements for the Degree Master of Science in the Graduate School of The Ohio State University

By

Matthew David Isakson, BS

Graduate Program in Biomedical Engineering

The Ohio State University

2023

Thesis Committee:

Julie A. Mansfield, PhD, Advisor

John H. Bolte, IV, PhD, Committee Member

Abstract

The shoulder girdle complex, through engagement with the seat belt, influences motor vehicle occupant upper body movement during frontal impacts, affecting the movement of the head, neck, and thorax. The recently developed LODC ATD was designed with flexible shoulder girdle structures that capture the unique kinematics in pediatric occupants. However, the LODC shoulder has not been evaluated for biofidelity due to the lack of biomechanical data available on pediatric shoulder responses. This study evaluated quasi-static pediatric shoulder girdle complex responses through non-invasive displacement measurements. These data were obtained to compare to the LODC ATD, to assess its biofidelity. Shoulder range of motion and anthropometric measurements were obtained from 25 pediatric volunteers, ages 8-12 years old. Loads were applied bilaterally exclusively to the shoulder complexes in increments of 25 N up to 150 N per shoulder at 90, 135, and 170 degrees of shoulder flexion. Still photos were used to determine shoulder displacement in the sagittal plane from images captured prior to and following the load applications. Data analysis consisted of motion tracking to evaluate the absolute and relative displacement of the right acromion and T1. The displacements for each volunteer were normalized based on the volunteer's shoulder width compared to the shoulder width of the LODC ATD. For the 90° load, the acromion moved relative to T1 an average of 28.1 mm forward and 3.1 mm downward at maximum displacement. For

the 135° load, the acromion moved relative to T1 an average of 12.4 mm forward and 40.0 mm upward at maximum displacement. Similar displacements at higher loads indicated that the volunteers achieved their maximum range of motion. The same test procedure was completed for the LODC ATD, resulting in a biofidelity comparison in displacements using Biofidelity Ranking Score. Results from this analysis indicated that the LODC was found to have better biofidelity in the forward direction than the upward direction. All of the displacement data for the volunteers and LODC were transformed into a single stiffness that characterized the force-displacement relationship. The LODC was found to be outside one standard deviation for the upward direction of the 135° series and within one standard deviation for the forward direction of the 90° and 135° series. Overall, the LODC was compared to the normalized 8–12-year-old shoulder girdle response to anterior and superior loading, with the anterior response being more biofidelic than the superior response.

Dedication

I wanted to dedicate this work to my family of Paul, Cathy, and Jake Isakson, as well as any friends who supported me during this process. They helped me strive to be the best version of myself each and every day. It cannot be overstated how much of a positive influence they all have had on me as a person.

Acknowledgments

The researchers wanted to thank the 25 pediatric volunteers and their families for participation in this study. Their contribution will be useful in improving the biofidelity of ATDs, and therefore, passenger safety in vehicles. Additionally, thanks to all of the faculty and students in the Injury Biomechanics Research Center at The Ohio State University who helped at any point with the completion of this project, specifically, Dr. Julie Mansfield, PhD and Rosalie Connell for their guidance and contributions throughout the project. Lastly, thanks to the mentors from NHTSA Vehicle Research & Technology and the Transportation Research Center, Inc. for their contributions to the study.

Vita

April 24, 2000……Born – Cincinnati, OH

May 2022……B.S. Biomedical Engineering
The Ohio State University

August 2022 – May 2023……Graduate Research Associate
The Ohio State University

Fields of Study

Major Field: Biomedical Engineering

Table of Contents

List of Tables

List of Figures

Chapter 1: Introduction

Motor Vehicle Crashes

Motor vehicle crashes are the most common source of severe unintentional injury worldwide (Chandran et al., 2010), causing 1.2 million deaths per year (Jindal and Mukherji, 2005). Within the United States in 2020, there were over 25,000 deaths and 2 million injuries from motor vehicle crashes, the most common type of which was a frontal collision (National Center for Statistics and Analysis, 2022). These fatality statistics were the leading cause of death for those aged 1-44 (National Center for Injury Prevention and Control Centers for Disease Control and Prevention, 2021). For all occupants, the most common injuries resulting in death during collisions are located in the head (Forman et al., 2015). During the collision, occupants have their velocity decreased by safety restraint systems that increase the "ride-down" time. As a result, the peak forces experienced are decreased and less likely to cause injury. Safety restraint systems often include airbags and 3-point safety belts, commonly known as seat belts (Hynd et al., 2012). The shoulder belt of the 3-point safety belts is designed to interact with the body from the clavicle to the pelvis. The shoulder belt applies an anterior to posterior load across the entire webbing, therefore interacting with the shoulder, thorax, abdomen, and pelvis. As a result, the shoulder belt limits forward excursion of the torso,

decreasing head excursion, thus decreasing the chance of serious head injuries (Isaacs et al., 2022).

Shoulder Anatomy Background

The shoulder girdle complex is composed of the clavicle and the scapula, with articulation to the manubrium of the sternum and to the proximal humerus, seen in Figure 1. Four joints are present in the shoulder girdle complex: the sternoclavicular (SC), acromioclavicular (AC), scapulothoracic, and glenohumeral joints. This unique set of joints allows for complex motions of the upper extremity (Javed et al., 2022; Miniato et al., 2022). The SC joint is the only articulation between the upper limb and axial skeleton, and it helps with shoulder motion and stability of the upper extremity. The sternoclavicular, interclavicular, and costoclavicular ligaments comprise the synovial joint capsule. The AC joint connects the distal end of clavicle to the acromion of the scapula. This joint is stabilized by the acromioclavicular ligament superiorly and coracoclavicular ligament inferiorly. The scapulothoracic joint is not a traditional joint, but it is used to characterize the sliding of the scapula over the posterior thoracic cage. Lastly, the glenohumeral joint is a ball and socket synovial joint that is recognized as extremely mobile at the expense of being relatively unstable. This joint consists of the head of the humerus articulating with the glenoid fossa of the scapula. The ligaments that create the joint capsule are the superior, middle, and inferior glenohumeral ligaments. The coracoacromial ligament also stabilizes the glenohumeral joint by creating a superior border to upward motion of the humerus. The tendons consisting of the rotator cuff as

well as the proximal tendons of biceps and triceps brachii stabilize the glenohumeral joint. Overall, these ligaments and tendons allow for the complex range of motion for the joints of the shoulder girdle complex.

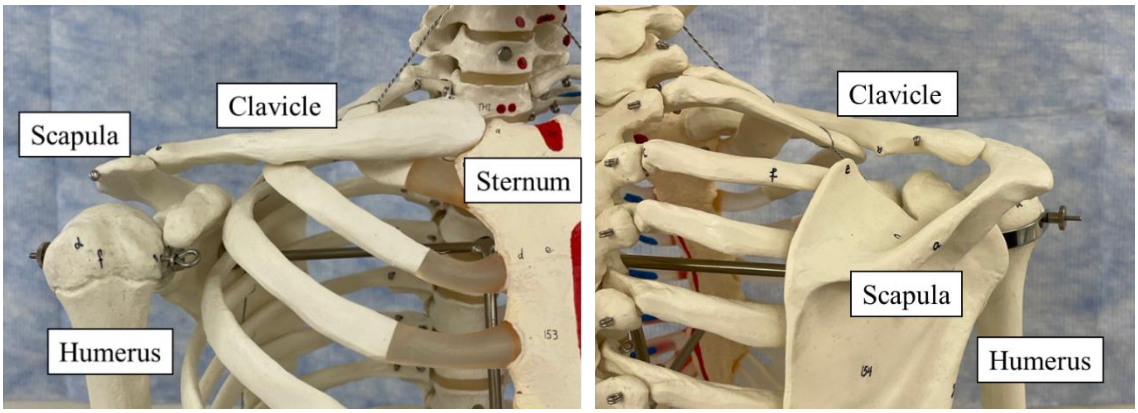

Figure 1: Bones of the right shoulder girdle from anterior view (left) and posterior view (right)

For the glenohumeral joint, there are several common movements. Abduction is the upward and lateral movement of the humerus away from the body in the coronal plane, and adduction is the downward and medial movement of the humerus toward the body in the coronal plane. Flexion is the movement of the humerus forward and upward in the sagittal plane, and extension is the movement of the humerus backward and upward in the sagittal plane. Internal and external rotation are the movement of the humerus around its long axis away and toward the body, respectively. For the scapulothoracic joint, elevation and depression are the upward and downward motions, respectively, along the rib cage. Protraction and retraction characterize the horizontal movement of the scapula

laterally and medially, respectively. With each of these motions, there is also a rotational component of the scapula so that it maintains constant contact with the thoracic cage.

The musculature of the shoulder girdle complex determines these movements of the joints. The anterior muscles consist of pectoralis major and minor and serratus anterior. Pectoralis major flexes, adducts, and internally rotates the shoulder from attachments to the clavicle, sternum, ribs 1-7, and the bicipital groove of the humerus. Pectoralis minor protracts and depresses the scapula due to attachments to ribs 3-5 and the coracoid process of the scapula. Serratus anterior protracts and holds the scapula to the thoracic wall from its attachments to ribs 1-8 and the anterior-medial border of the scapula. The posterior muscles affect shoulder motion as well. Trapezius elevates, retracts, and depresses the scapula from its origins on the skull and spinous processes of C7-T12 and insertions to the clavicle, acromion, and spine. Latissimus dorsi attaches from the spinous processes of T7-T12 and the pelvis to the anterior aspect of the humerus, allowing it to control adduction and internal rotation. Levator scapulae elevates the scapula and depresses the glenoid cavity by its origin on C1-C4 and its insertion on the superior angle of the scapula. Lastly, the rhomboid major and minor muscles retract the scapula, depress the glenoid cavity, and hold the scapula close to the thoracic wall by attaching from the spinous processes of C7-T5 to the medial border of the scapula. These anterior and posterior muscles help control the positioning of the shoulder girdle complex.

The scapulohumeral muscles are comprised of the rotator cuff and deltoid and teres major muscles. The rotator cuff around the glenohumeral joint consists of the supraspinatus, infraspinatus, teres minor, and subscapularis muscles. Supraspinatus assists with the initiation of shoulder abduction, teres minor and infraspinatus assist with external rotation, and subscapularis assists with internal rotation. All of these muscles cross the glenohumeral joint, with origins on the scapular and insertions on the humerus. These four muscles in the rotator cuff all contribute greatly to the stability and flexibility of the glenohumeral joint. The deltoid controls abduction, flexion through its anterior fibers, and extensions though its posterior fibers. The deltoid attaches to the lateral third of the clavicle, the acromion, and the scapular spine and inserts to the deltoid tuberosity of the humerus. Lastly, the teres major muscle internally rotates, adducts, and extends the shoulder from its attachments to the scapula and humerus.

Within the upper extremity, biceps brachii, coracobrachialis, and triceps brachii control shoulder movements as well. Biceps brachii flexes the shoulder with its short head attaching at the coracoid process, its long head attaching at the supraglenoid tubercle, and its distal end inserting on the bicipital tuberosity. Coracobrachialis flexes and adducts the shoulder from attaching at the coracoid process and mid-medial humerus. Lastly, triceps brachii extends the shoulder from proximal attachments to the infraglenoid tubercle and posterior humerus and distal attachments to the olecranon of the ulna. Overall, all of these muscles control the complex motion of the scapulothoracic and glenohumeral joints.

Shoulder Crash Kinematics

Recent studies have observed the shoulder belt slipping off occupants and ATDs during frontal and oblique collisions and maneuvers, eliminating the benefits of the belt (Baker et al., 2018; Bohman et al., 2018, 2011; Horsch and Hering, 1989). During the collision, the mass of the upper extremity combined with the velocity before the crash causes the upper extremity to rotate upward about the shoulder, observed as shoulder flexion (Horsch and Hering, 1989). Simultaneously, the shoulder belt is applying a posterior load to the clavicle, limiting the forward excursion of the shoulder girdle complex. As a result, an anterior and superior load is applied to the shoulder girdle complex from the arms translating forward and rotating upward while the clavicle is being restrained by the shoulder belt. These forces are only a few that determine the positioning of the shoulder girdle complex during frontal collisions. Others include any pre-crash maneuvers and belt pre-tensioners that influence the position of the torso and shoulder. All of these forces together determine whether the shoulder belt will slip off the occupant (Hontschik and Ruter, 1980).

Outside of this scenario of belt-slipping, the shoulder girdle complex is also important because of its effect on the response of the thorax, head, and neck. Thoracic injuries are affected by the proportion of the shoulder belt load that is applied through the shoulder instead of the sternum. A previous study concluded that well over half of the shoulder belt load could be directed through the shoulder (Kent et al., 2003). With the interactions of the shoulder and thorax to the head and neck, injuries to the head and neck are

therefore also affected by the shoulder girdle complex. Overall, it is important that the shoulder design of the ATDs is biofidelic of the populations they are representing. Otherwise, incorrect conclusions can be drawn with the design of shoulder belts with either over- or underpredicting the belt slipping off the shoulder. Additionally, injury values with head acceleration, head excursion, neck forces, and chest deflection are also influenced shoulder stiffness, therefore requiring ATDs to have a biofidelic shoulder girdle complex. With how important the shoulder belt is with affecting injury metrics, it is important to have a biofidelic shoulder design of the ATDs.

Pediatric Vehicle Occupants

For children aged 1-18, motor vehicle crashes serve as the leading cause of death (National Center for Injury Prevention and Control Centers for Disease Control and Prevention, 2021). Head injuries for pediatrics are believed to be most frequently caused by the head coming into contact with objects, including parts of the vehicle (Arbogast et al., 2010). When the shoulder belt slips off and head excursion increases, these head injuries are then more likely to occur (Bohman et al., 2018). Pediatric occupants utilize the shoulder belt when they are sitting in a belt-positing booster seat or sitting without any type of child restraint system. These two conditions are typically present for pediatrics aged 8 and above (NHTSA, n.d.). Therefore, it is important that the ATDs designed for children within this range are biofidelic in the shoulder girdle complex.

Differences in shoulder girdle kinematics between children and adults have been documented due to differences in scapulae position and musculature (Dayanidhi et al., 2005; Struyf et al., 2011). Specifically, pediatric musculature is observed to be much less stiff than that of adults, significantly affecting the kinematics of the pediatric shoulder girdle complex compared to adults. As a result, adult ATDs cannot be simply scaled down to the size of pediatrics and exhibit the same biofidelity as adults.

Previous testing of the Q3 and Hybrid-III 6-year-old ATDs have concluded that these pediatric ATDs do not replicate nuanced shoulder responses of their represented populations (Bohman et al., 2018; Ita et al., 2014). The National Highway Traffic Safety Administration (NHTSA) recently developed a novel ATD with flexible shoulder girdle structures that can capture the unique kinematics of pediatric populations. The Large Omnidirectional Child (LODC) ATD has shoulders with human anatomical components including a clavicle with a pectoral surface and a pivoting scapula (Stammen et al., 2016). Currently, the LODC has not been evaluated for biofidelity in the shoulder region due to the lack of biomechanical data available on pediatric shoulder responses. Previous work has successfully evaluated adult volunteer shoulder responses for validation of the Hybrid III 50th male and THOR-50M ATDs (Davidsson, 2013; Törnvall et al., 2010).

Objective

The objective of this study was to quantify characteristics of the pediatric shoulder girdle complex using anthropometric and range of motion measurements and quasi-static

responses that were then compared to the Large Omni-Directional Child (LODC) Anthropomorphic Test Device (ATD) to assess its biofidelity.

Chapter 2: Materials and Methods

Overview of Methods

All volunteer protocols were approved by the Ohio State University Institutional Review Board (protocol #2018H0137). Shoulder range of motion and anthropometric measurements were obtained from pediatric volunteers (n=25), ages 8-12 years old. Loads were applied bilaterally to the shoulders in a custom fixture in increments of 25 N up to 150 N per shoulder at 90°, 135°, and 170° of shoulder flexion. A volunteer that completed a full trial therefore had six loads applied at each angle. The positions of T1 and right acromion were recorded with still-frame photographs in unloaded and loaded positions. These methods were adapted from previous studies that had evaluated adult shoulder responses with applied quasi-static loads (Davidsson, 2013; Törnvall et al., 2010). The LODC also underwent the same testing procedure to have data to be compared to the volunteers.

Test Setup

A custom test fixture consisting of a captain's chair from a sedan and adjustable cables was used to apply loads to the shoulder complex (Figure 2). Elbow flexion was constrained with arm braces (Figure 3). Each elbow brace was loaded by its own cable, which originated from a single attachment point behind the captain's chair, located left of

the apparatus in Figure 2. Known counterweights were applied at the attachment point, applying an equal load through the left and right cables. For the first 13 volunteers, sandbags placed in a bucket served as the known weight source. For the last 12 volunteers and LODC, free weights were hung from a hook. This change was made to decrease the size of the weight source since the bucket for the sandbags was large. A drop table was located under the weights, allowing for the weights to be either supported in the pre-loading condition or free hanging in the post-loading condition.

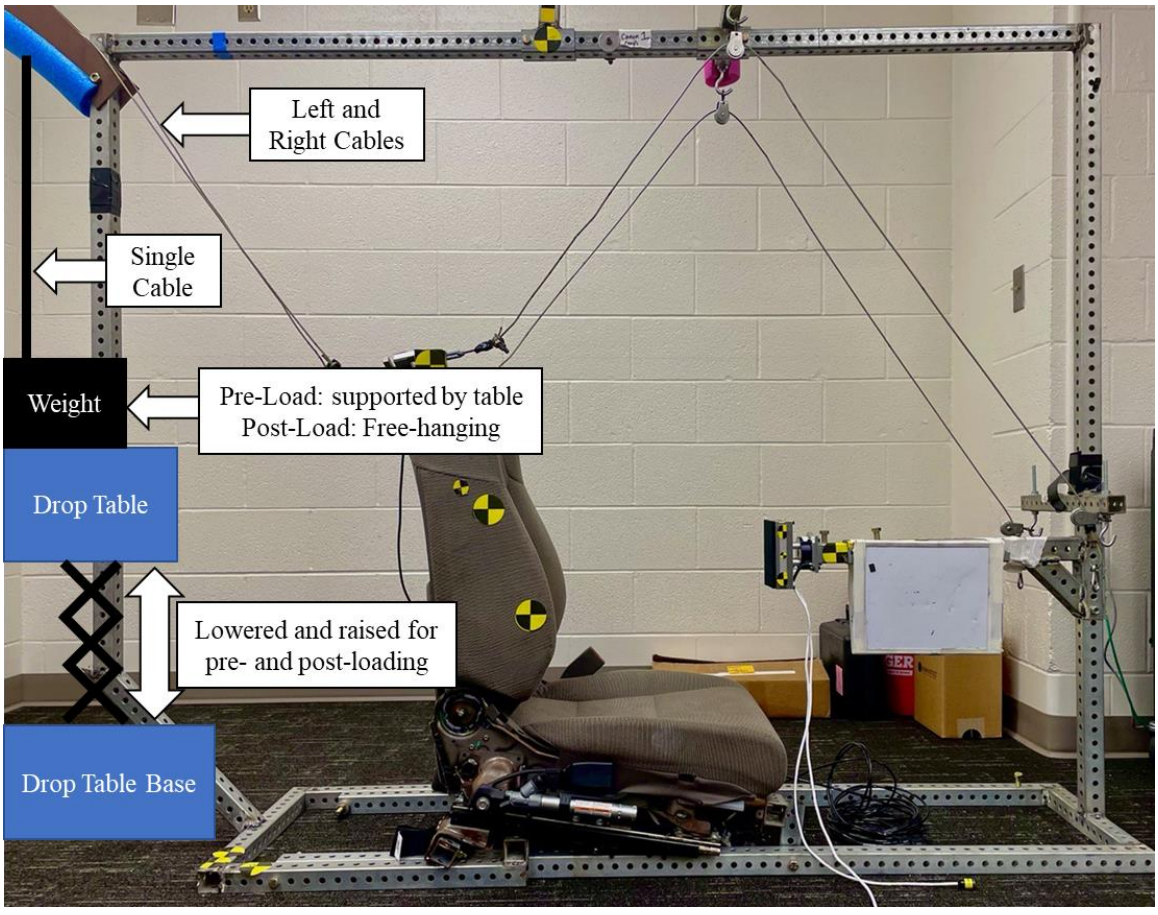

Figure 2: Custom test fixture with drop table and weight locations

Figure 3: Elbow braces with cable attachment point

Foam was placed between the seatback and the volunteer so that the sagittal view of the spine was not obstructed by the outer wings of the seat (Figure 4). A chest support was centered just below the sternal notch of each volunteer to restrict displacement of the torso (Figure 4). Therefore, the 90° series had the loads applied in the same relative spot for each volunteer despite any size differences. However, for the 135° and 170° series, the slidable mount on top of the fixture was placed in the same location for each volunteer. Therefore, volunteers that varied in seated height resulted in slightly different angles of applied load. Specifically, a taller volunteer would experience a loading angle slightly below 135°, and a shorter volunteer would experience a loading angle slightly above 135° of shoulder flexion. Although these differences in angles were not quantified, the differences were believed to be insignificant in the response to the load.

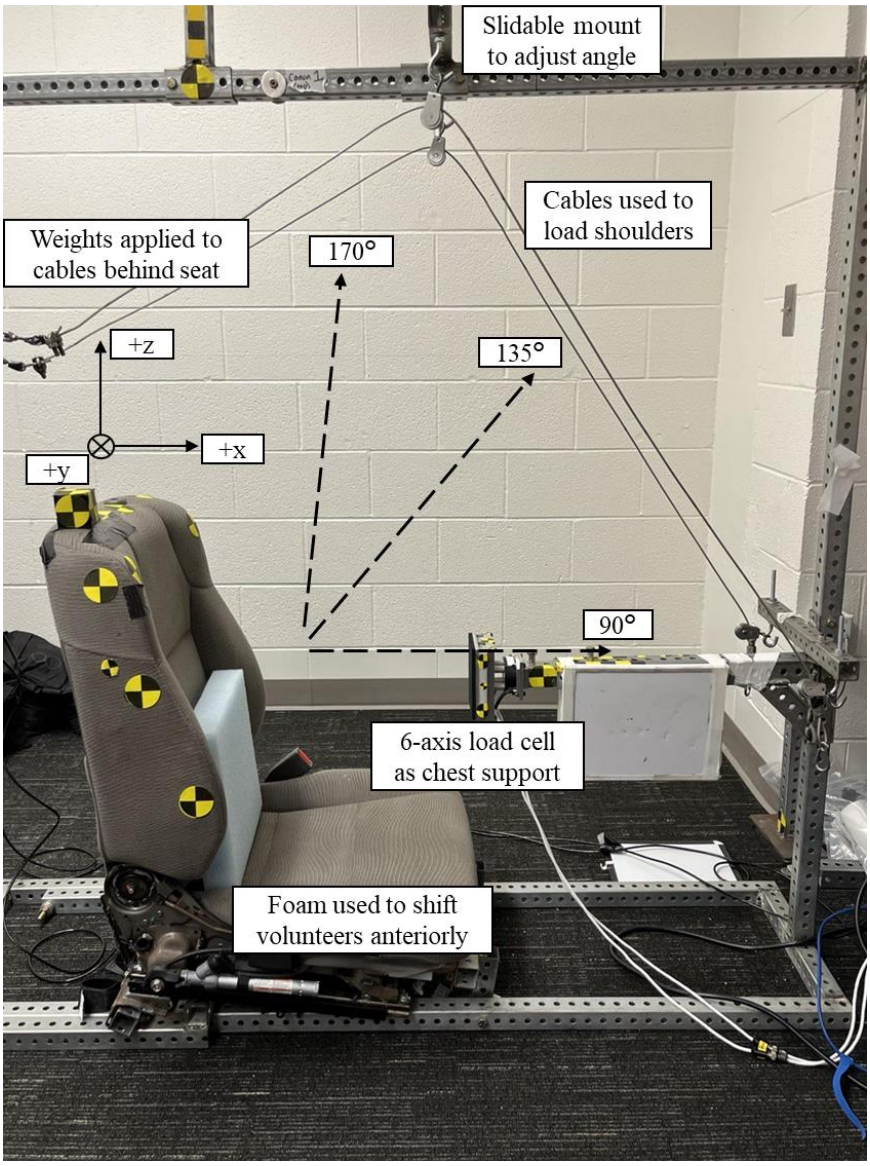

Figure 4: Test fixture to isolate loading angles on shoulder complex with coordinate axes system

The LODC underwent the same testing procedure in the same test fixture. However, the elbow braces were not utilized due to the forearms being removed, allowing for a simple attachment of the cable to the arm of the LODC ATD. The removal of the forearms was

believed to have the same loading pattern as the volunteers with elbow braces since the load was applied at the distal humerus, and the glenohumeral joint was the first joint affected by the load. Additionally, the testing of the LODC ATD differed by using a lap belt for the 135° and 170° loading angles. Without the belt, the LODC ATD was elevated from the seat at higher loads. This trend was not observed in volunteers except for several at the higher loads for the 170° series. Since the purpose of this testing was to characterize the shoulder girdle complex, the lap belt was included so that the boundary conditions were as similar as possible for the shoulder region between most of the volunteers and the ATD.

Instrumentation

Three cameras were placed on the test fixture to capture views of frontal, sagittal, and transverse planes of the volunteers. An x-y-z coordinate system (Figure 4) was established based on the coordinate system used in previous studies (Davidsson, 2013; Törnvall et al., 2010). This system was used to identify the positioning of the volunteers in pre- and post-loading conditions in each camera view (Figure 5).

Fiducials were placed on anatomical landmarks such that they could be tracked from the three camera views (Figure 5). T1 and acromion landmarks were visualized using three dimensional fiducial blocks, ensuring optimal visibility from multiple camera angles. The exact location of T1 and acromion on the surface of each volunteer's skin was identified by using the three-dimensional blocks as a guide.

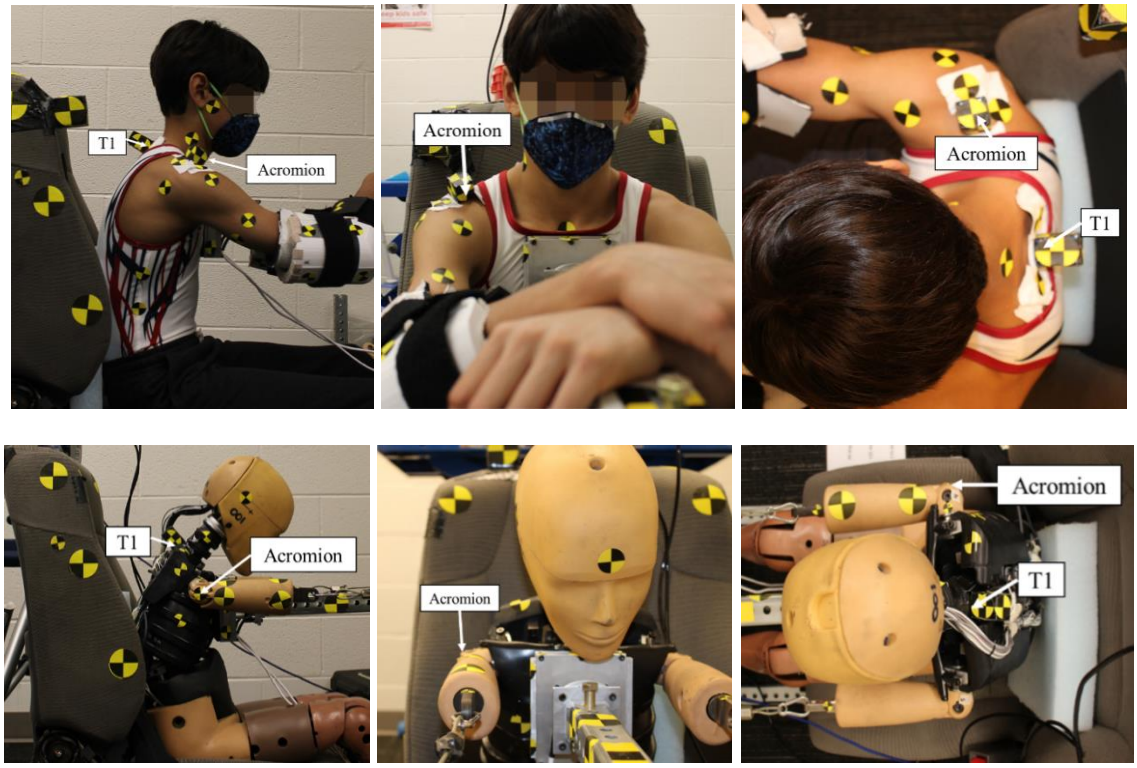

Figure 5: Camera views of side (left column), front (middle column), and top (right column) with fiducial placement for example volunteer (top row) and LODC (bottom row)

Uniaxial load cells were included along the cables of the testing fixture to assess an equal, bilateral application of the weights (Figure 6). These two unidirectional tension load cells were used to record the forces transmitted from the weight source to the left and right sides. Since the right acromion was visible from the sagittal view, the effective load being applied to the right elbow brace was quantified using the values from these load cells. Additionally, a six-axis load cell was placed in the chest support plate of the frame (Figure 6). When loading occurred, linear forces and moments were recorded in

the x, y, and z directions as the volunteer was pulled towards the chest support plate. By rigidly absorbing the load, this load cell limited the motion of the torso, helping isolate the applied force on the shoulder complex. The data of the uniaxial and 6-axis load cells from the volunteers were compared to that of the LODC ATD to ensure similar loading patterns from the test fixture.

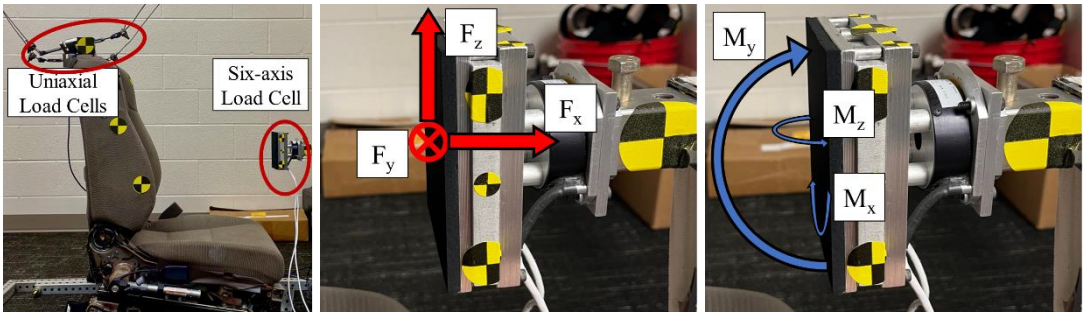

Figure 6: Uniaxial load cells and 6-axis chest plate (left) with chest plate forces (middle) and moments (right)

Test Procedure

Anthropometric measurements were collected for each volunteer (Table 1). Next, active assisted range of motion measurements listed in Table 2 were collected using a goniometer (Jamar E-Z Read). Diagrams depicting anthropometric and active assisted range of motion (ROM) measurements can be found in the appendix (Figures A1 and A2). Volunteer sex and arm dominance were also recorded. For the LODC, the anthropometric measurements utilized were those already reported for the ATD

(Stammen et al., 2016). As a result, there are no ROM measurements to report for the LODC.

Table 1: Anthropometric measurements

Anthropometric Measurements	
Age	Right Clavicular Length
Height	Right Humeral Length
Weight	Chest Width
Seated Heigh	Chest Depth
Shoulder Width	Chest Circumference
Bi-acromial Distance	Right Arm Circumference

Table 2: Active assisted shoulder ROM

Active Assisted Shoulder ROM Measurements
Flexion
Extension
Abduction
Internal Rotation
External Rotation

After anthropometry and range of motion data collection, the shoulder girdle loading sequence occurred with the volunteer seated in the test fixture. The order of the three loading angles was randomized for each volunteer prior to testing. Each loading sequence began with nominal loads of 25 N per shoulder and was incrementally increased by 25 N per shoulder up to 150 N for each angle. Previous testing with adult volunteers reached 200N per shoulder (Davidsson, 2013; Törnvall et al., 2010). Volunteers were able to stop testing if a personal threshold of discomfort was reached. At this point, the volunteer would move to the next angle of loading and restart with the lowest load of 25 N per shoulder. Throughout testing, volunteers were asked to remain relaxed, not to tense their muscles against the motion, and to refrain from bracing their feet against the floor.

Data were collected at two instances for each load: pre-loading and post-loading. The pre-loading condition occurred while the weights were still supported by the drop table, resulting in zero tension in the cables, and therefore, no applied load to the volunteer. The pre-loading position and load were instantaneously recorded through still photos from all three camera views and the load cells, respectively. Following the pre-loading condition, the drop table was lowered, allowing weights to hang freely from the cable, resulting in the weight being delivered through the cables to the shoulder complexes. The post-loading condition was determined when the volunteer reached an equilibrium observed by no motion. Once again, synchronized pictures from each camera and the load cell data were captured in the post-loading condition. From this procedure, each post-loading

condition had a corresponding pre-loading condition. An example of a pre-loading and post-loading photos for the two testing angles are shown in Figure 7.

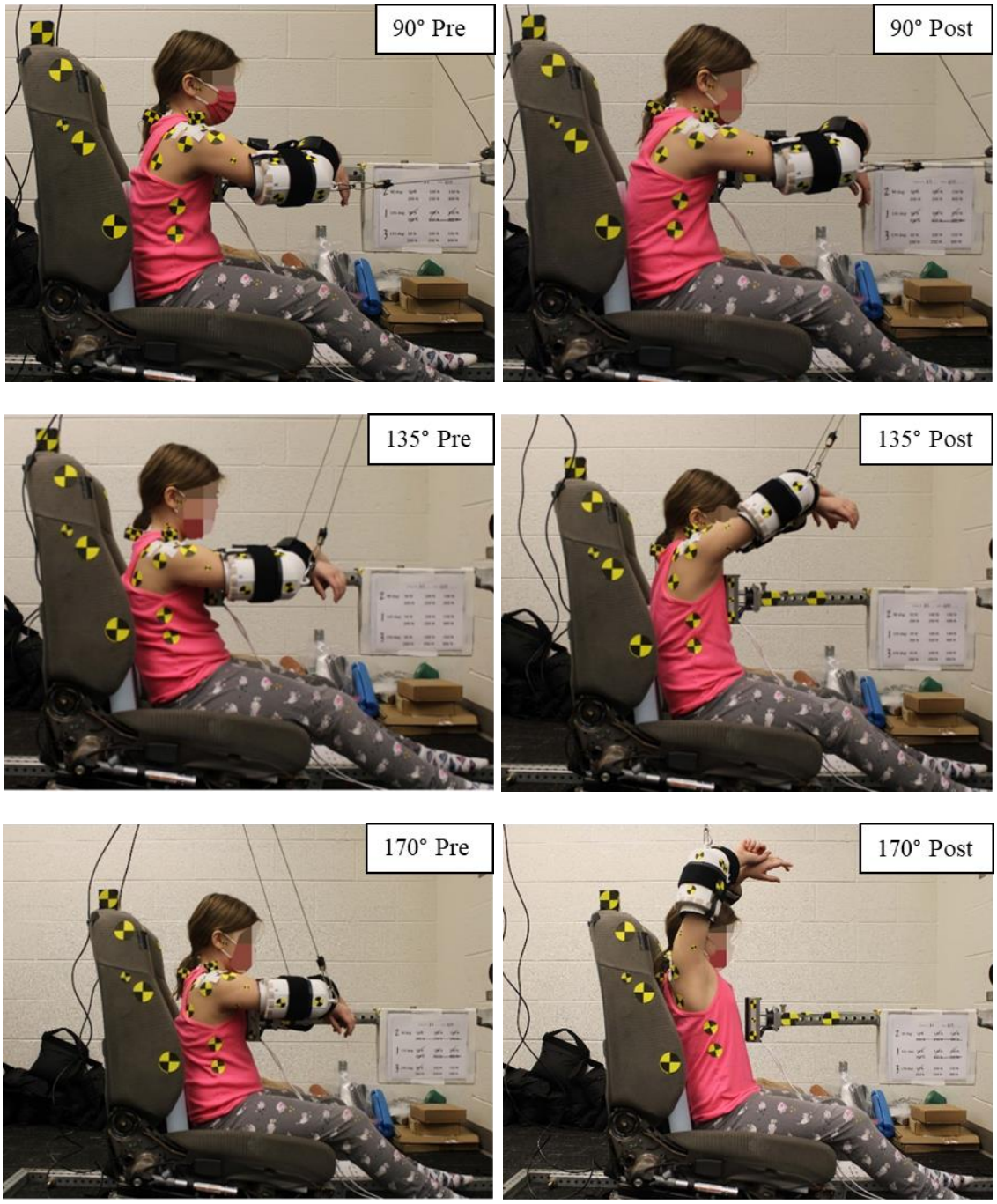

Figure 7: Example volunteer of pre-loading at 90° (upper left), 135° (middle left), and 170° (lower left) and post-loading photos at 90° (upper right), 135° (middle right), and 170° (lower right) from sagittal view

The same test procedure was completed for the LODC ATD following the 25 volunteers. For the 90° series, each pre-loading photo was matched to a corresponding post-loading photo, utilizing the same procedure as the volunteers. Example pre- and post-loading photos for the 90° series are shown in Figure 8. However, the LODC underwent a different pre-load positioning process for the 135° and 170° series. For both of these series, the LODC shoulder would become dislocated during the loaded shoulder flexion that occurred between the pre- and post-loading conditions. Since the objective of this study was to quantify quasi-static displacement with respect to an applied load, the kinematics of shoulder flexion could be ignored. Therefore, the pre-loading position for the LODC for the 135° and 170° series occurred with the shoulder already positioned approximately to those respective angles of flexion. However, to accurately compare the displacement between pre- and post-loading to the volunteers, a single pre-loading position at 90° of shoulder flexion was collected for the 135° and 170° series. As a result, even though pre-loading photos were collected for each load in the 135° and 170° series, only the single pre-loading photo at 90° of shoulder flexion was utilized for the analysis of shoulder displacement. These pre-loading photos at 90° of shoulder flexion are shown in Figure 9 with examples of unused pre-loading photos at 135° and 170° of shoulder flexion and post-loading photos for the 135° and 170° series.

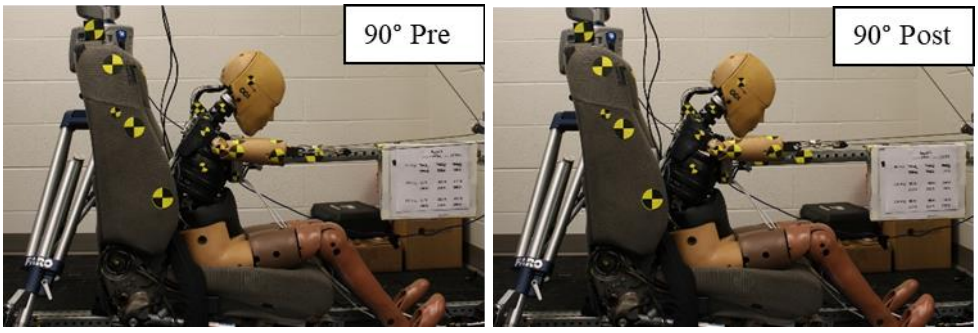

Figure 8: LODC pre-loading (left) and post-loading (right) for 90° series from sagittal view

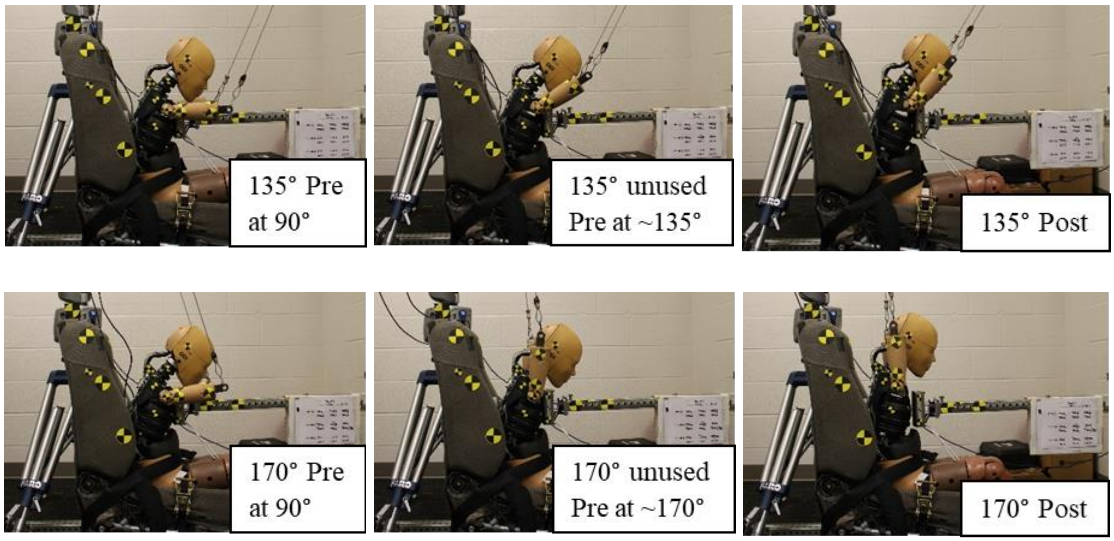

Figure 9: LODC pre-loading photos used for 135° (upper left) and 170° (lower left), with examples of unused pre-loading photos at 135° (upper middle) and 170° (lower middle), and examples of post-loading photos at 135° (upper right) and 170° (lower right) from sagittal view

Displacement Data Analysis

Displacement was quantified using the video analysis software Tracker (version 6.0.6, Open Source Physics). Manual tracking was completed for the T1 and right acromion fiducials. Even though the left acromion was not quantified, it was still important to apply a bilateral load to limit any torso rotation. Additionally, the left shoulder response was assumed to be equivalent to the right shoulder. From the sagittal view, the x-z coordinates for pre- and post-loading conditions were isolated from these landmarks. The coordinate pairs were exported to Microsoft Excel and MATLAB for computational analyses. The goal was to subtract the x-z coordinates of the pre-loading photos from the x-z coordinates of the post-loading photos to determine the displacement of each landmark in the x and z directions. However, volunteers were not always in the same neutral position during the pre-loading phases. Specifically, at higher loads, volunteers would typically be positioned further forward in the pre-loading conditions than during the lower loads, resulting in skewed calculations of displacement. Therefore, for each volunteer at each loading angle, a single pre-loading position was utilized for comparison to post-loading positions. This single pre-loading position was found for T1 and the acromion by using the median x and z coordinates for each landmark in each collected pre-loading position. The median was selected instead of the mean to limit the influence of outliers in positioning. Displacement values were then calculated in the x and z directions for each applied load for the two identified landmarks by subtracting the median pre-loading position from each different post-loading position.

The displacement of T1 relative to right acromion was calculated by taking the difference between the two displacements. Averages and standard deviation values were calculated for these metrics, allowing for the characterization of the healthy 8–12-year-old pediatric population. The displacement values were also normalized to the LODC with respect to shoulder width to account for size differences in the sample of volunteers and for an accurate comparison of the volunteers to the LODC.

The test setup was evaluated to determine precisely how much of the load being suspended via weights (the "nominal" load) was effectively being delivered to the volunteers' shoulders. The left and right cable load cells revealed that the fixture was not perfectly symmetrical; an average of 53% of the nominal load went through the right cable at all loads. Even though this difference appears minimal, it is still important to quantify the actual load being applied to the volunteers for an accurate force-displacement relationship. Additionally, the network of pulleys and cables introduced substantial friction into the system, resulting in less than the nominal loads actually acting on the volunteers' shoulders. A digital tension meter was used to measure the sum of the force magnitudes actually applied at the two elbow braces together. From the asymmetry and friction reduction, the actual load applied to volunteers (the "effective" load) was calculated. Table 3 depicts the effective load at each given nominal load for the two tested angles. Since the cable configurations varied between the loading angles, each angle had different effective loads acting on the volunteers. For the lower nominal loads, several of the right effective loads exceeded the nominal load due to the digital tension

meter reading 100% of the nominal load and the load cells indicating asymmetry of up to 54.4% of the load being applied through the right cable. Nominal loads were utilized for comparisons across loading series, and effective loads were utilized for all calculations.

Table 3: Resultant effective loads experienced by right shoulder

R Shoulder Nominal Load (N)	90° Resultant		135° Resultant		170° Resultant	
	Effective Load (N)	% of Nominal Load (%)	Effective Load (N)	% of Nominal Load (%)	Effective Load (N)	% of Nominal Load (%)
25	23.6	94.5	27.2	109.0	25.9	103.7
50	41.0	82.0	44.2	88.4	44.4	88.8
75	68.2	90.9	69.8	93.1	72.1	96.2
100	83.8	83.8	87.4	87.4	86.4	86.4
125	105.3	84.3	104.2	83.4	108.9	87.1
150	125.3	83.6	123.3	82.2	118.0	78.7

For each loading series, each effective load can be thought of as either a single resultant force vector or can be broken into x and z components. For the 90° series, all of the force was loaded in the x direction, so the x component effective load is the same as the resultant effective load. For the 135° series, the effective load was broken into equivalent x and z components. Lastly, the 170° series was broken into x and z components

proportional to the 170° direction. For each loading angle, resultant effective loads are listed in Table 4.

Table 4: Effective loads by component on the right shoulder

R Shoulder Nominal Load (N)	**90° Effective Load by Component (N)**		**135° Effective Load by Component (N)**		**170° Effective Load by Component (N)**	
	x	z	x	z	x	z
25	23.6	0.0	19.3	19.3	4.6	26.0
50	41.0	0.0	31.3	31.3	7.8	44.3
75	68.2	0.0	49.4	49.4	12.7	72.0
100	83.8	0.0	61.8	61.8	15.2	86.2
125	105.3	0.0	73.7	73.7	19.1	108.4
150	125.3	0.0	87.2	87.2	20.9	118.4

Biofidelity Ranking System

For assessing the biofidelity of the LODC ATD, an adapted Biofidelity Ranking System (BRS) was utilized (Hagedorn et al., 2022). The only difference incorporated into the assessment of the LODC was the removal of the phase shift calculation. This value was previously removed from the BRS score but was suggested to still be reported (Hagedorn et al., 2022; Rhule et al., 2018). Since these values were collected from quasi-static responses, there is no time component of the data collection. The relative acromion to T1

displacement data were utilized for this comparison to analyze the biofidelity of the shoulder girdle complex. For this analysis, the volunteer displacements created a corridor of ±1 standard deviation of displacement at each effective load. This corridor was used to compare to the LODC ATD at each effective load by component. This deviation from ATD to volunteer was compared to the standard deviation of the volunteer sample. From the calculations shown in Equation 1, a score of 2 or less is deemed to have "good biofidelity", and a score of greater than 2 is determined to have "poor biofidelity".

$$BRS\ Score = \frac{\sum|Displacement_{LODC} - Displacement_{Vol\ Avg}|}{\sum(Displacement_{Vol\ SD})} \quad \text{(Eqn. 1)}$$

All BRS scores were calculated and reported for each component of a loading direction. Each x component was averaged together to find a BRS score for the x direction. This process was repeated for the z direction. Then, the average of the BRS scores for the x and z directions was found in order to have one score for the overall biofidelity of the LODC ATD.

Stiffness Analysis

Stiffness was defined as the linear relationship between effective load and relative displacement for each volunteer (Agnew et al., 2015). This linear relationship was estimated by performing a linear regression on the displacement and effective load data, utilizing the slope of the linear estimate. Stiffness was calculated for both resultant effective loads and by each component. Therefore, stiffness in the x and z directions

could be compared. This same method was applied to finding the stiffness of the LODC ATD for comparison to volunteers. All statistical analyses were performed in JMP Pro 15.2 with a significance level of 0.05.

Chapter 3: Pediatric Volunteer Results and Discussion

Anthropometry and Range of Motion

Summarized anthropometric and range of motion data from all 25 volunteers are shown in Table 5 and Table 6, respectively. Full tabulated data can be found in Appendix A (Tables A1 and A2). The shoulder anthropometry and active assisted range of motion data in this study provide insight to the shoulder girdle complex of the healthy 8–12-year-old pediatric population.

Table 5: Summary of anthropometry data

Measurement	**Average (SD)**	**Measurement**	**Average (SD)**
Age (years)	11.0 (1.3)	**R Clavicular Length (mm)**	153 (13)
Mass (kg)	42.7 (12.7)	**R Humeral Length (mm)**	275 (20)
Stature (m)	1.48 (0.11)	**Chest Width (mm)**	249 (27)
Seated Height (mm)	748 (51)	**Chest Depth (mm)**	173 (24)
Shoulder Width (mm)	367 (37)	**Chest Circumference (mm)**	728 (152)
Biacromial Distance (mm)	306 (30)	**Arm Circumference (mm)**	224 (37)

Table 6: Summary of range of motion data

Shoulder ROM Measurement	Average (SD) (°)
Flexion	174.3 (10.9)
Extension	69.6 (15.9)
Abduction	178.5 (6.0)
Internal Rotation at 90°	82.1 (20.6)
External Rotation at 90°	101.0 (8.0)

Quasi-Static Loading

In the quasi-static loading sequence, the 170° loading series was removed due to difficulties observing the acromion fiducial in the sagittal plane. Additional camera views were also heavily obscured, so x and z coordinates could not be established. These obstructed views from all three camera positions are seen in Figure 10. Due to these difficulties with the 170° loading series, all analyses utilized the 90° and 135° loading series results.

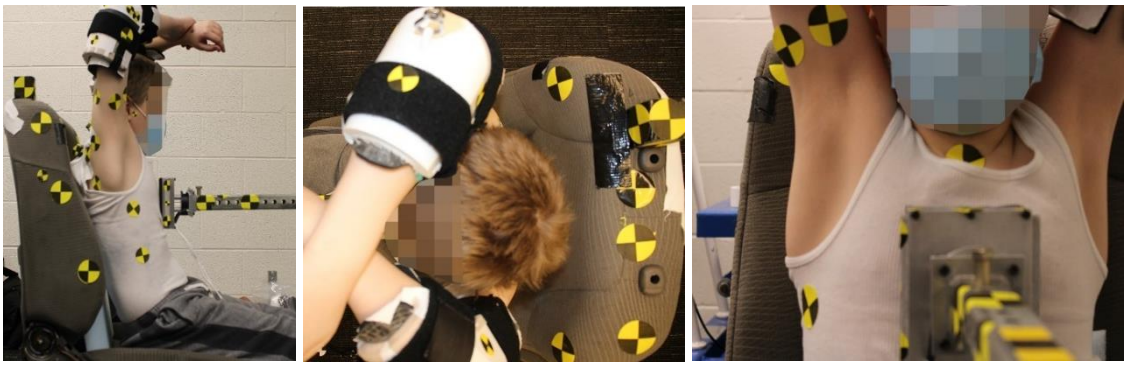

Figure 10: Sagittal (left), transverse (middle), and frontal (right) images for sample 170° post-loading condition

Given that volunteers were able to cease testing at their own discretion, sample size at each nominal load differed by direction. Additionally, higher nominal loads that resulted in greater displacement sometimes caused the weights to be lowered all the way to the drop table at its lowest position. Therefore, the known weights were not exclusively being supported by the loading cables; the drop table was applying an unknown normal force to the weights, resulting in an unknown load being applied to the volunteers. This occurrence of "bottoming out" happened for 6 volunteers during various loads at the 135° loading angle. This occurrence of bottoming out only occurred with the large bucket with sandbags, which is why the weight source was changed to free weights for the last 12 volunteers and LODC. Table 7 displays how many volunteers had data collected at each load for each testing angle, omitting all trials where bottoming out occurred. Descriptive statistical calculations utilized the different sample sizes collected for each nominal load. Examples of all six post-loading conditions are shown in Figure 11 for the 90° and 135° loading series. For the example volunteer in the 135° series, even though the cables were

in the same position for all loads, it was observed that the shoulder did not reach 135° of shoulder flexion until the 75N load. This trend was observed across volunteers that were able to reach higher loads. This trend suggests that different musculature is under tension as load increases in a given direction.

Table 7: Number of volunteers completed at each nominal load

R Shoulder Nominal Load (N)	**90° (# of volunteers with usable data)**	**135° (# of volunteers with usable data)**
25	25	25
50	25	25
75	21	23
100	17	19
125	12	11
150	11	9

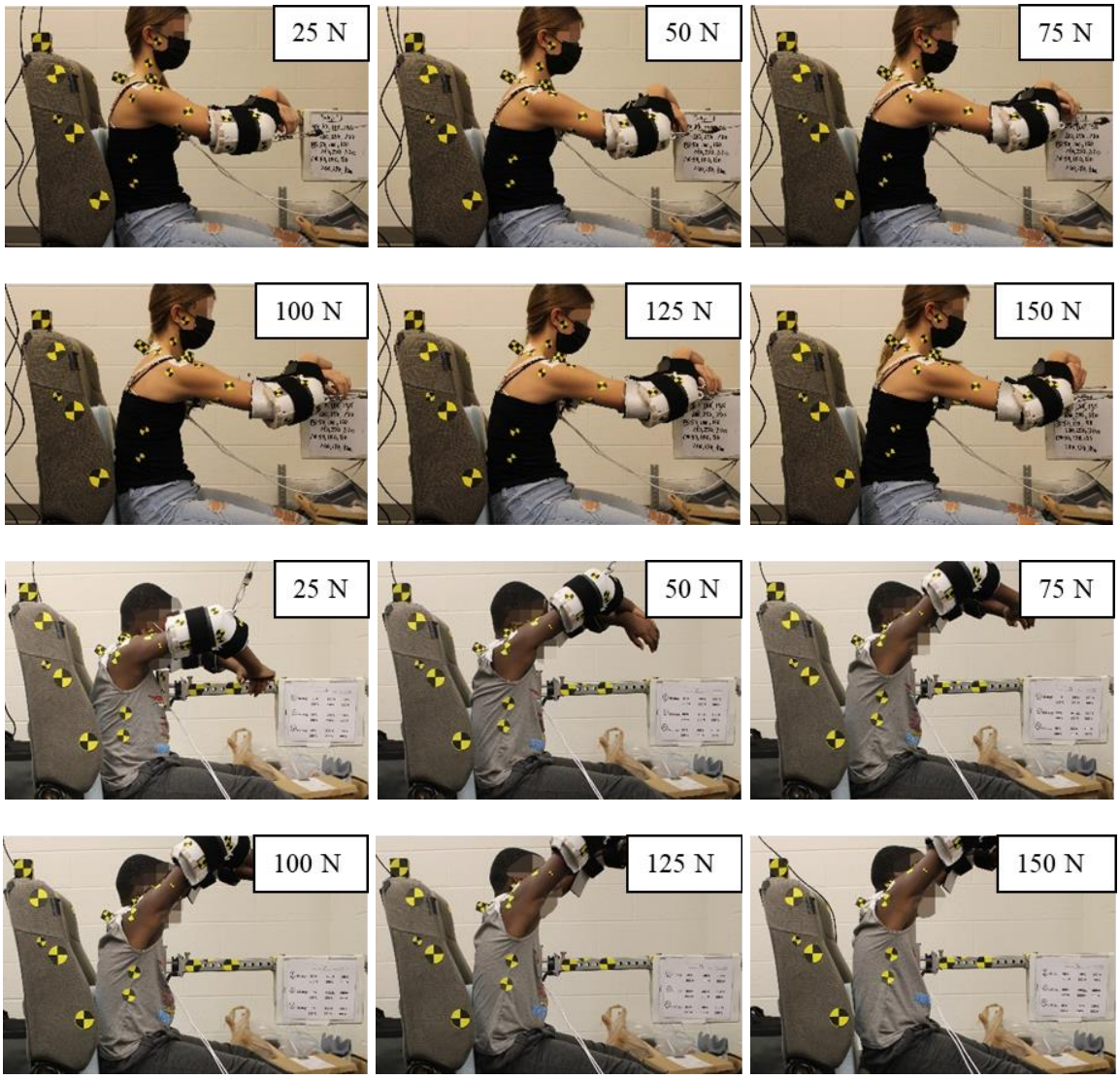

Figure 11: Example volunteers post-loading photos for 90° (top two rows) and 135° (bottom two rows) loading series

Average right acromion and T1 displacements are shown in Figure 12. Full tabulated data can be found in Appendix B (Tables B1-B4). For the 90° load, there is greater displacement in the x direction than the z direction. For the 135° load, the opposite is true, with greater displacement in the z direction than the x direction. This trend is

interesting for the 135° series since there is an equal effective load in the x and z directions, suggesting different responses to upward and forward loading of the shoulder. Each of the circles in the plots indicates increasing nominal loads by increments of 25 N. Therefore, it can be determined that increasing the nominal load by 25 N results in less overall displacement at higher loads (125 N and 150 N) compared to lower loads (25 N and 50 N). This pattern suggests that the volunteers are nearing the end of their comfortable ranges-of-motion at the higher loads.

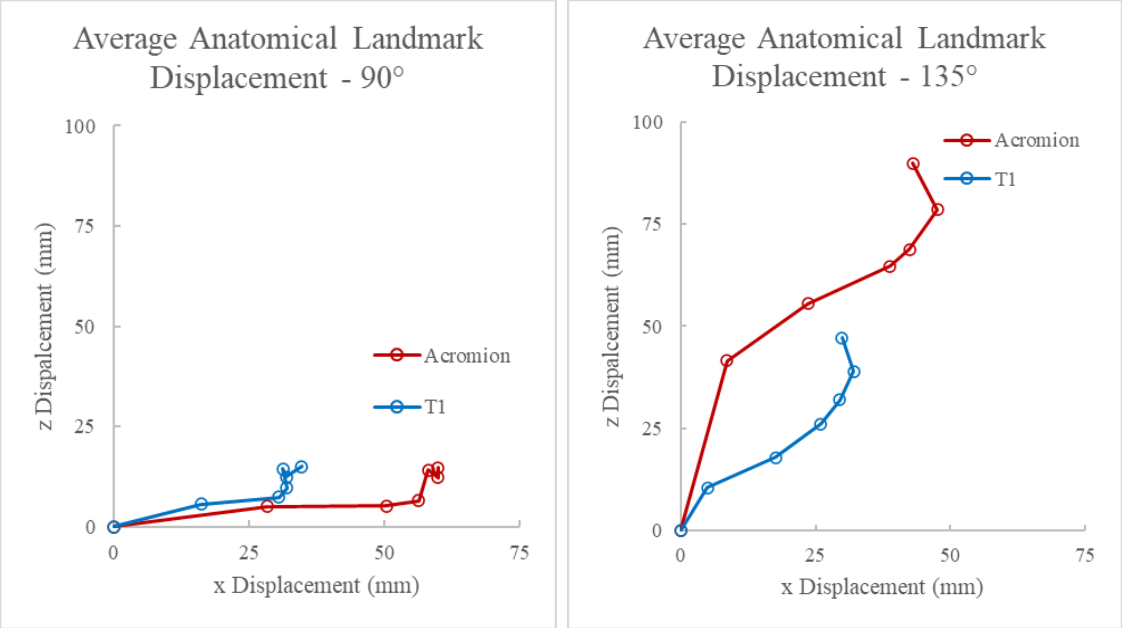

Figure 12: Acromion and T1 displacement in x and z directions at nominal loads

Each circle indicates increasing nominal loads by increments of 25 N.

Relative displacements were analyzed to characterize the response of the shoulder girdle complex itself, following the methods of previous adult studies (Davidsson, 2013). Specifically, the acromion x-z displacement was converted to a relative metric by subtracting the x-z components of T1 for each volunteer at each load. These values of the acromion relative to T1 displacement are shown in Figure 13 as the mean displacement with standard deviations. Since x and z are both response variables with their own standard deviations, the upper standard deviation curve indicates the addition of one standard deviation to x and z, and the lower standard deviation curve indicates the subtraction of one standard deviation from x and z. For the 90° series, volunteers experienced greater displacement in the x direction than the z direction, and for 135° series, volunteers experienced greater displacement in the z direction than the x direction. Additionally, higher loads correspond to less change in relative x and z displacements, even more so than the non-relative displacement.

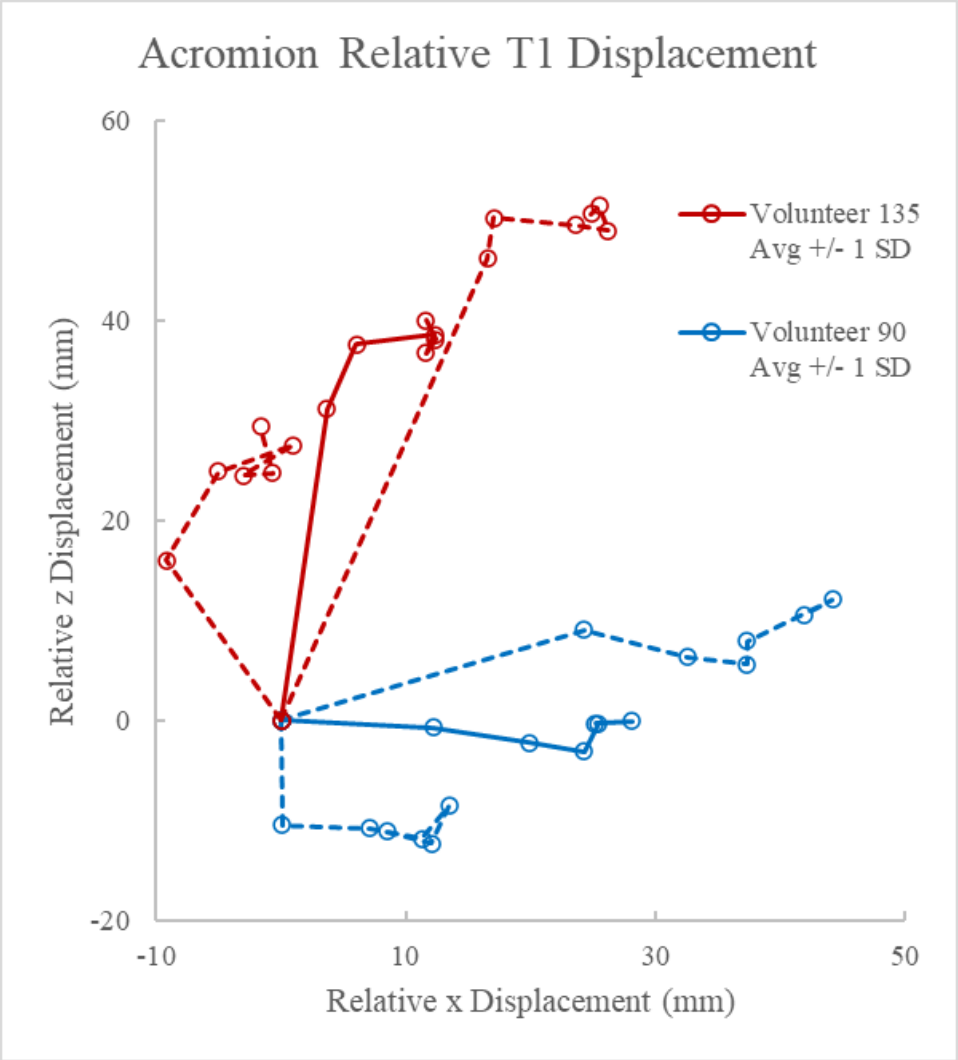

Figure 13: Acromion relative to T1 x-z displacement with standard deviation

Each circle indicates increases in nominal load by increments of 25 N.

Relative displacements (Figure 13) were translated into the x component for the 90° series and the x and z components and resultant vector for the 135° series as a function of effective load (Figure 14). Effective load was shown to depict how the actual force acting on the volunteer would affect the measured displacement. The z component of the 90°

series was not displayed due to there being no effective load in this direction. Therefore, the resultant vector for the 90° series would also be equivalent to the x component. This figure also includes all 25 volunteers to display the variation across the different loading directions. The cluster of data points at higher loads seen in Figure 13 is also observable from the flattening of all four average curves above 100 N in Figure 14. This trend indicates that volunteers reached the limit of their acromion relative to T1 displacement before the maximum nominal load of 150N. For the 90° loading series, the average acromion relative to T1 displacement peaked at 28.1 mm and 3.1 mm in the forward and downward directions, respectively. The concentration of data points around these values as loading increased indicates that the maximum range of motion was achieved (in a tolerable, non-injurious range). In the 135° loading series seen in Figure 13 and Figure 14, the average relative shoulder displacement peaked at 12.4 mm and 40.0 mm in the forward and upward directions, respectively. Like the 90° series, the 135° series also contained a concentration of data points associated with increased loads near these maximum values. Therefore, the results suggest that the maximum range of motion was achieved in both loading series.

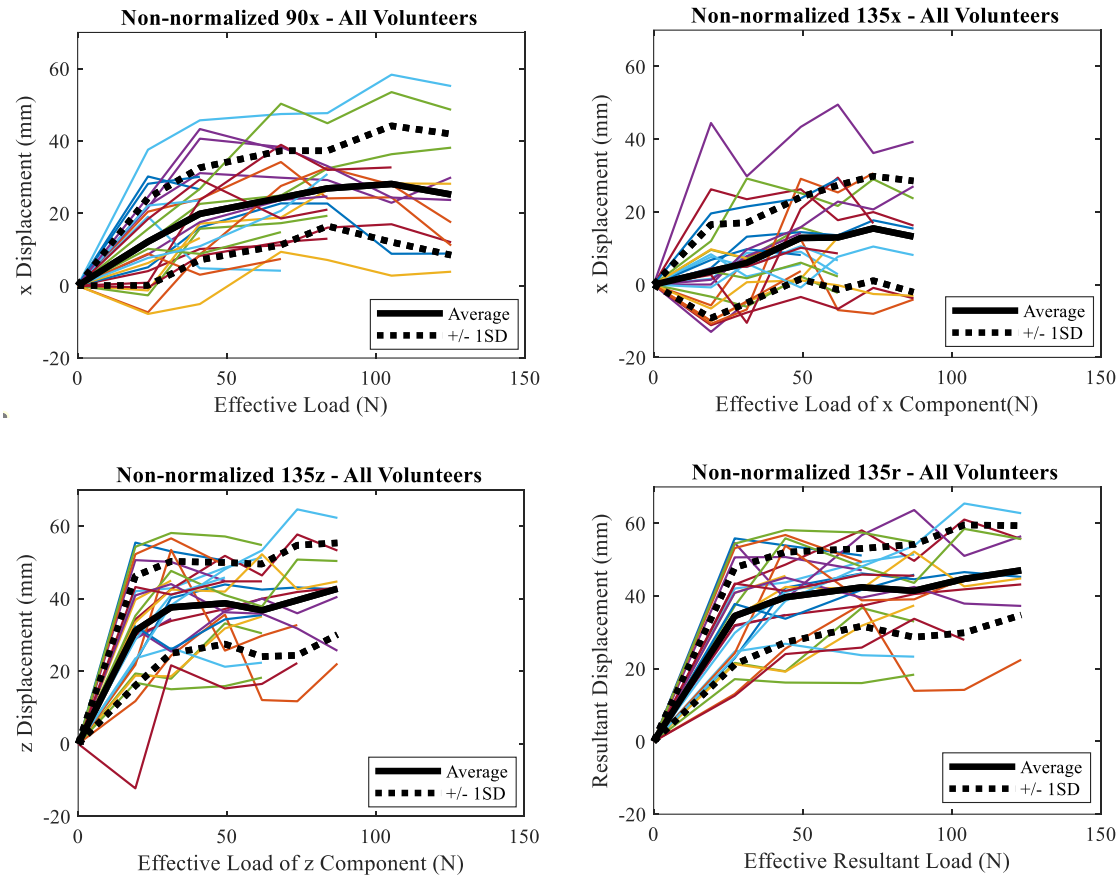

Figure 14: Acromion relative to T1 displacement of all volunteers by component

Each vertex corresponds to the effective load at each condition, in increments of 25 N of nominal load.

Results from the 135° loading series also point to differences in how the shoulder operates during shoulder protraction (anterior motion of the shoulder) and shoulder elevation (superior motion of the shoulder). Given the effective loads in the x and z direction for the 135° loading series were equal, greater displacement in the z direction indicated the musculature under tension during shoulder protraction is stiffer than the

musculature under tension during shoulder elevation. This trend of greater musculature stiffness in shoulder protraction compared to shoulder elevation was also observed in adults who underwent the same testing procedure (Törnvall et al., 2010).

Data Normalization

Previous literature has suggested that shoulder width may influence acromion to T1 displacements for adults (Davidsson, 2013). With the age range of 8 to 12 years old, there was a noticeably large spread of shoulder width measurements for the 25 volunteers. Therefore, the displacements calculated for each volunteer were normalized with respect to the shoulder width of the LODC ATD, 340mm. Specifically, each of a volunteer's displacements were multiplied by the ratio of the LODC ATD shoulder width to the volunteer shoulder width, seen in Equation 2. Figure 13 and Figure 14 have been reproduced using these normalized displacement data (Figure 15 and Figure 16, respectively).

$$Normalized\ Displacement = NonNormalized\ Displacement * \frac{Shoulder\ Width_{LODC}}{Shoulder\ Width_{Vol}}$$

(Eqn. 2)

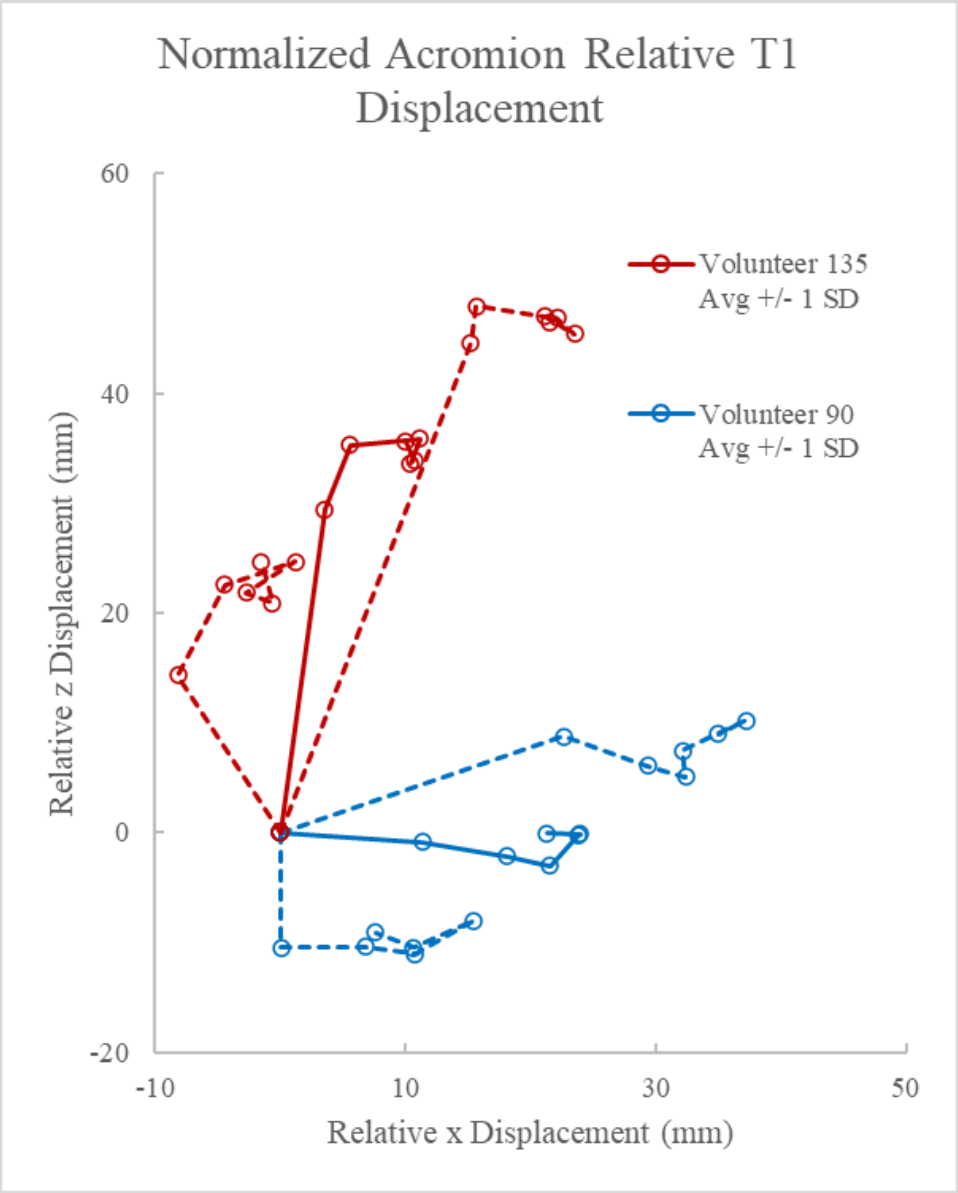

Figure 15: Normalized acromion relative to T1 x-z displacement with standard deviation

Each circle indicates increases of nominal load by increments of 25 N.

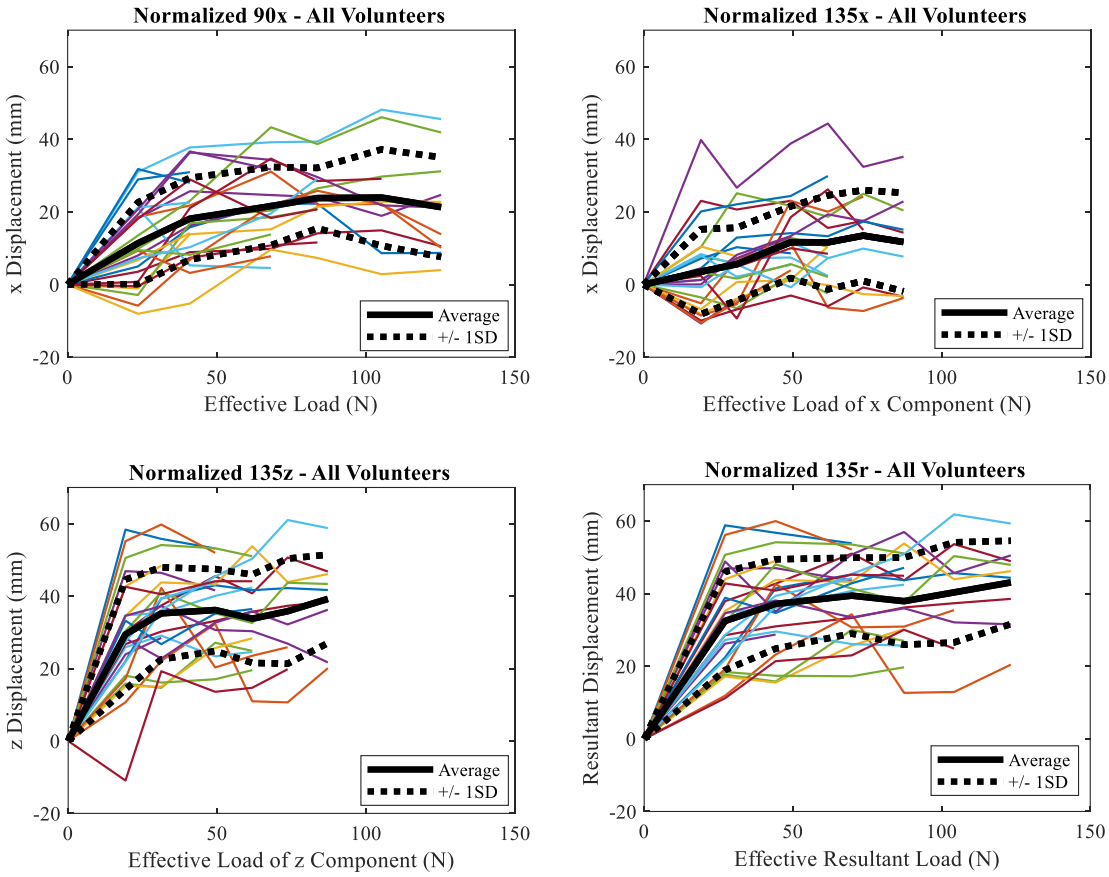

Figure 16: Normalized acromion relative to T1 displacement of all volunteers by direction

Each vertex corresponds to the effective load at each condition, in increments of 25 N of nominal load.

For the 90° loading series seen in Figure 15 and Figure 16, the average acromion relative to T1 displacement peaked at 23.9 mm and 3.0 mm in the forward and downward directions, respectively. In the 135° loading series, the average relative shoulder displacement peaked at 11.1 mm and 35.9 mm in the forward and upward directions,

respectively. These average values are less in magnitude than the respective non-normalized averages, which is explained by the volunteer sample having a larger shoulder width on average.

The normalization procedure was incorporated based on previous literature that suggested acromion displacement relative to T1 was influenced by shoulder width (Davidsson, 2013). This observation is supported by the idea that volunteers with a greater shoulder width should be able to be pulled further anteriorly and superiorly. Since the volunteer age range was 8-12 years old, there was a wide variety in shoulder widths explained by different developmental levels of each volunteer. Therefore, normalized displacement data were utilized for all comparisons to the LODC ATD.

Stiffness Analysis

A metric used to characterize the shoulder gridle complex is stiffness, which is the amount of force required for 1 mm of displacement. Stiffness is recognized as the linear relationship between force and displacement (Agnew et al., 2015). Due to volunteers reaching the end of their non-injurious range of motion, lower effective loads demonstrated this linear relationship, but higher effective loads resulted in no increased displacement. Therefore, the linear portion of the force-displacement relationship was isolated to calculate stiffness for each subject in the different loading directions. Due to each volunteer having between 2 to 6 data points, a novel, repeatable method of identifying the linear portion was developed. For a volunteer with a given loading

direction, the maximum displacement and corresponding effective load were identified. The displacement was evaluated by comparing it to the displacement at the previous effective load. If the maximum displacement increased by less than 20% of that preceding displacement, then the maximum displacement was determined not to be in the linear stiffness region. This process was repeated, working backwards until a 20% difference in displacement was observed between consecutive effective loads. A 20% difference was selected as a consistent value that visually appeared to repeatedly identify the start of the plateau for each volunteer. This identified point was determined to be the end of the linear stiffness region, and all data at higher effective loads were cut from the stiffness analysis. A linear regression was then performed for the force-displacement values that were in the linear region. The slope was inverted to achieve units of N/mm, which was then determined to be the stiffness.

To best estimate the stiffness of a healthy 10-year-old, all normalized displacement data and effective loading data were used in the stiffness calculation. For the 90° series, the x component was analyzed for stiffness, and for the 135° series, the x and z components and resultant vector were analyzed for stiffness. This process of finding the cut point for linear stiffness for the different components is shown for an example volunteer in Figure 17. All data points are displayed, and the circled point indicates where the linear stiffness region was cut. Figures with each volunteer's displacement and effective loading data in the four directions analyzed (90x, 135x, 135z, and 135r) are displayed in Appendix C (Figures C1-C25). Additionally, all stiffness results for each volunteer were tabulated in

Appendix C (Tables C1-C2). The average stiffness results for the 25 volunteers are shown in Figure 18.

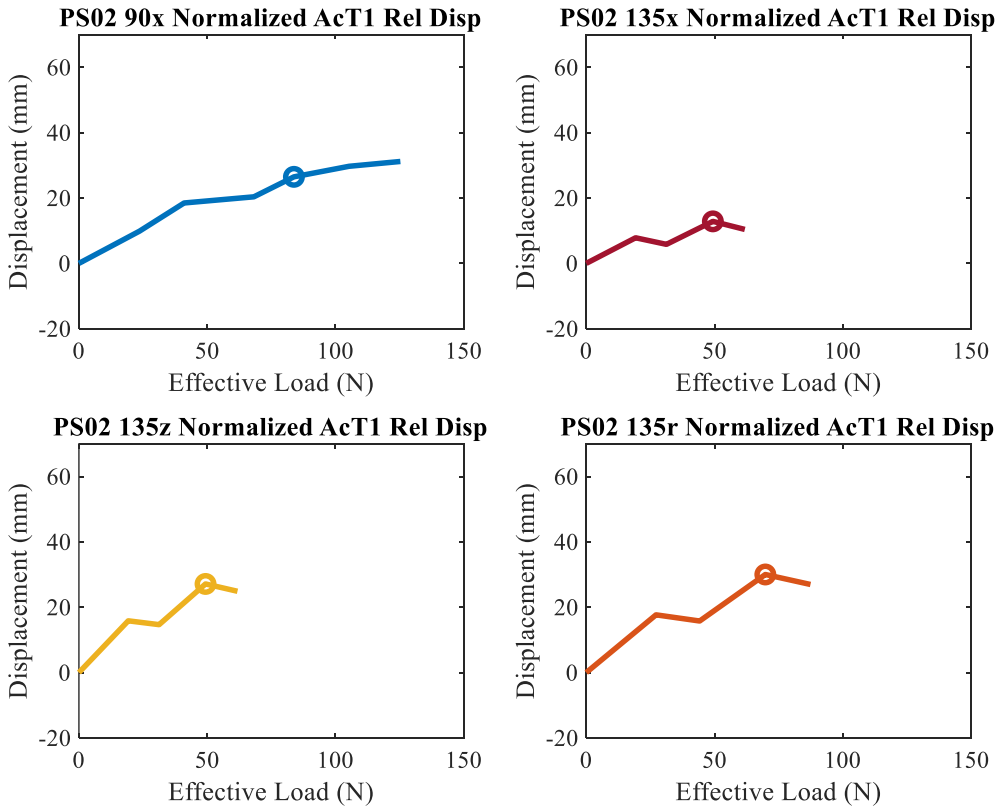

Figure 17: Example volunteer displacement data with marker of end of linear stiffness region

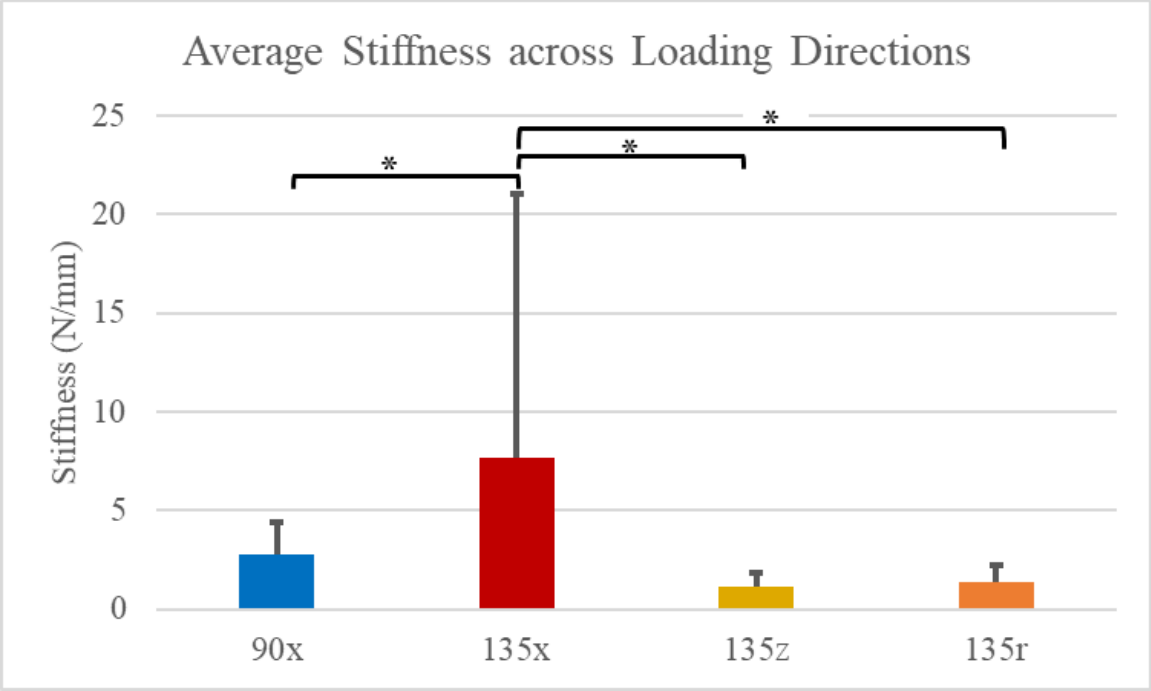

Figure 18: Average volunteer stiffness with one standard deviation in different loading directions

* Denotes significance ($p<0.05$)

These stiffnesses suggest that in the x direction, the angle of loading influences the stiffness of the shoulder girdle complex. This trend was observed with the average stiffness of the x component in the 90° series being significantly different than the x component of the 135° series. A similar observation was found in adult anterior and superior shoulder loading (Törnvall et al., 2010). These stiffnesses also provide insight on how the shoulder girdle complex does not have the same stiffness under the same loading condition across different directions. For the 135° loading series, the x component was found to be significantly different than the z component, even though both directions had

equivalent effective loads. These results suggest that there are different stiffnesses associated with shoulder elevation and shoulder protraction.

The x component of the 135° series also had the greatest variation in stiffness across the 25 volunteers. Variability could have been introduced based on the load at which the shoulders were fully flexed to the 135° loading angle. However, it is interesting that the z component of the 135° series was not nearly as variable given that they have the same loading input. One reason for this difference is the presence of the chest plate that restricted anterior displacement of the torso. The chest plate in conjunction with the variability in fully flexed arms can be attributed to the high variation for the x component of the 135° series but not the z component. Another possible explanation for this variation is the musculature differences between volunteers. Many of the volunteers participated in a variety of sports involving the upper extremity (baseball, basketball, volleyball, gymnastics), leading to different muscular developmental levels. Future work could quantify how involvement in these sports, and other anthropometric measurements, could be confounding variables in shoulder stiffness. With the anthropometric, active-assisted ROM, displacement, and stiffness data from 25 volunteers, the 10-year-old shoulder girdle was characterized and able to be compared to the results of the LODC ATD.

Overall, the 25 pediatric volunteers had the shoulder girdle complex characterized from anthropometric and active assisted range of motion measurements. These values are

useful not only for comparison to ATDs but also in general for quantifying the healthy 8–12-year-old population. Under quasi-static loading, displacements of the acromion relative to T1 were found across effective loads to quantify position in the x and z direction for 90° series and 135° series. These values were normalized by shoulder breadth to account for size differences across the sample. The normalized displacements were used to find the stiffness by each component, which were observed by the positive, linear portions of the force-displacement relationship. The stiffness in the x direction of the 135° series was found to be significantly different than all other directions, suggesting stiffness is influenced by the component for a given load and influenced by the direction of the loading for a given direction. The stiffnesses and displacements were useful for detecting differences across and within the loading series and for comparison to the LODC.

Chapter 4: Comparison of Volunteers to LODC ATD

Anthropometry Comparison

Volunteer anthropometric averages were compared to reported anthropometry of the LODC ATD (Stammen et al., 2016). Age, height, and weight are shown in Table 8. These values indicate that the volunteer sample is older and larger than the ATD, seen by the stature of the LODC being outside one standard deviation of the volunteer average. These differences also suggest the need for normalization when comparing displacements under quasi-static loading. For other anthropometric measurements, the ATD values were compared to see if they were within one standard deviation of the volunteer sample in Figure 19. The trend of the LODC being smaller than the volunteer average continued for the seated height and shoulder width, with the LODC being more than one standard deviation below the volunteer average for seated height. Since seated height affects the actual angle the load was applied for the 135° series, the LODC may have experienced slightly different loading conditions. Future analysis could evaluate the true loading angles for the volunteers and LODC. Interestingly, the other reported measurements of chest depth and chest circumference for the LODC were both above the volunteer average. This change in relationship to the volunteers suggests that a proportion used in the LODC design could be inaccurate. However, for both chest depth and circumference, the LODC was within one standard deviation of the volunteer averages.

Table 8: Age, height, and weight measurements of volunteers and LODC ATD

Measurement	Volunteer Average (SD)	LODC
Age (years)	11.0 (1.3)	10
Mass (kg)	42.7 (12.7)	34.6
Stature (m)	1.48 (0.11)	1.30*

* Denotes LODC outside one standard deviation of volunteer average

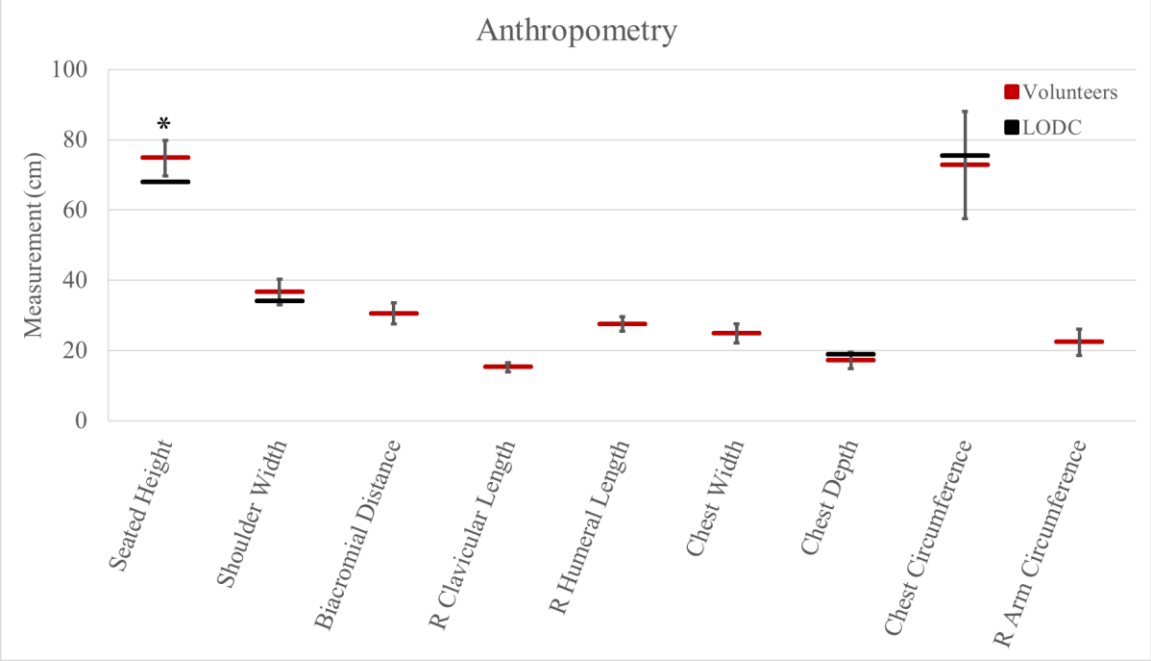

Figure 19: Anthropometric comparison of the volunteer sample to the LODC ATD

* Denotes LODC outside one standard deviation of volunteer average

While many anthropometric measurements for the LODC have not been published, stature and seated height were the reported LODC ATD values that existed outside one

standard deviation of the volunteer sample. Therefore, it can be concluded that normalization is necessary for comparisons between the volunteer sample and the LODC. Future testing of the LODC ATD can be completed to quantify the remaining anthropometric and active assisted range of motion measurements to determine if all dimensions are representative of the population.

Quasi-Static Loading Comparison

The next step in comparing the LODC to the volunteers was to ensure the loading scenarios were comparable between volunteers and ATD. Uniaxial load cell data from the right cable are shown in Figure 20. The right load cell was analyzed since that cable was the source of the load acting on the measured shoulder of the volunteers and LODC. The left load cell results can be found in Appendix D (Figures D1-D2). Fully tabulated load cell data can also be found in Appendix D (Tables D1-D6). Even though the trials for the LODC tended to exhibit a higher measured load compared to the volunteer average, the LODC was not outside one standard deviation at higher loads. One explanation for this difference in loading inputs is that the LODC kinematics of loading could have resulted in higher tension and the friction of the cable system then held that tension value while the post-loading collection occurred. Another explanation is the change from sandbags to free weights as the known weight source. This shift also might be responsible for the relatively high standard deviations observed for what should be consistent input loading. These input conditions were determined to be sufficiently similar for comparison of the LODC to the volunteers. However, these reported

differences in loading input should be noted when utilizing these results to assess the shoulder biofidelity of the LODC.

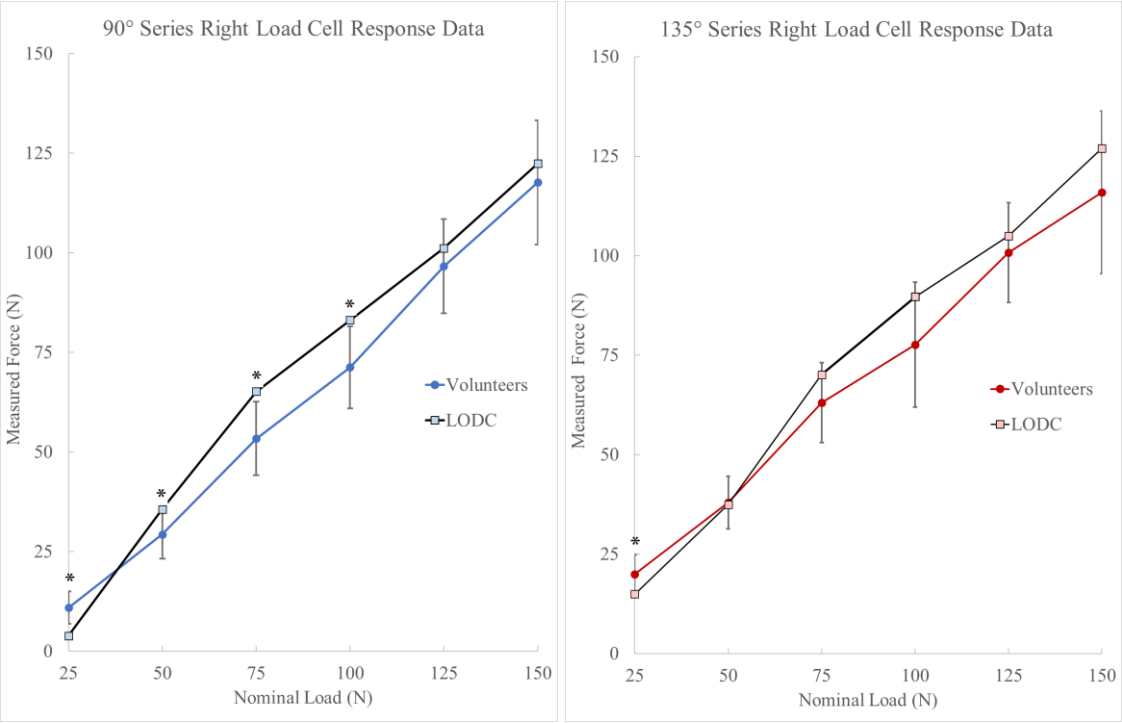

Figure 20: Right load cell measured force across nominal loads

* Denotes LODC outside 1 standard deviation of volunteer average

Data were collected from the 6-axis load cell to evaluate the response of the torso from loading of the shoulder girdle complex. The same coordinate system was used for the forces and moments of the load cell, seen in Figure 21. For the forces, *Fz* and *Fy* quantified the shear force in the forward and upward directions, respectively, and *Fx* quantified the force directed into the force plate. For the moments, *My* quantified uneven loading from the bottom to the top of the plate, and *Mz* quantified uneven loading from

the left to the right. *Mx* was the value of the angular shear force on the chest plate. Overall, *Fy*, *Mx*, and *Mz* were used to quantify the symmetry and uniformity of the torso response, and *Fz*, *Fx*, and *My* were used to quantify the response of the torso to loading in those directions.

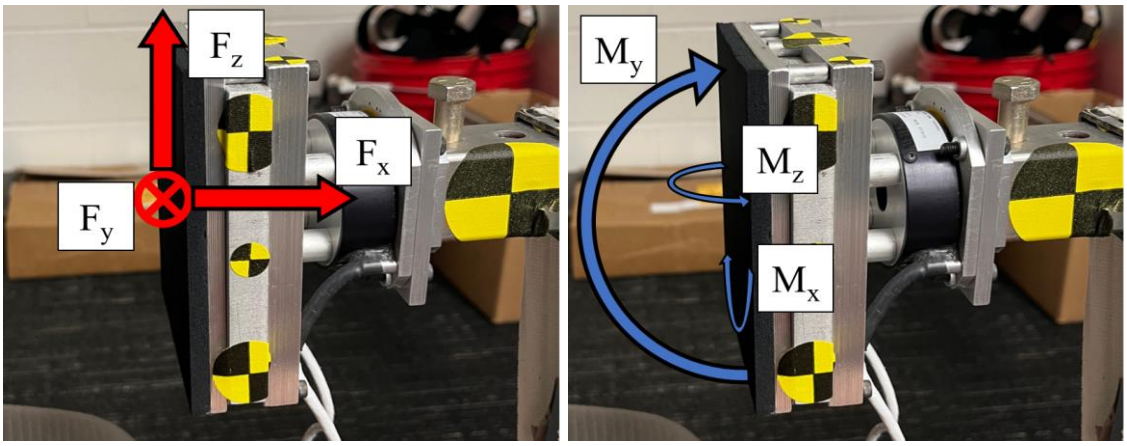

Figure 21: Forces (left) and moments (right) of six-axis load cell

For the force data, *Fy* was close to zero at all loads in the 90° series (Figure 22). There was a noticeable trend upward at higher nominal loads for volunteers but downward for the LODC. However, these magnitudes for the volunteer average and LODC were relatively small, never exceeding 5 N, suggesting there is little shear force from right to left. There were no observable trends in the 135° series, and all force magnitudes for the volunteer average and LODC were less than 3 N (Figure 23).

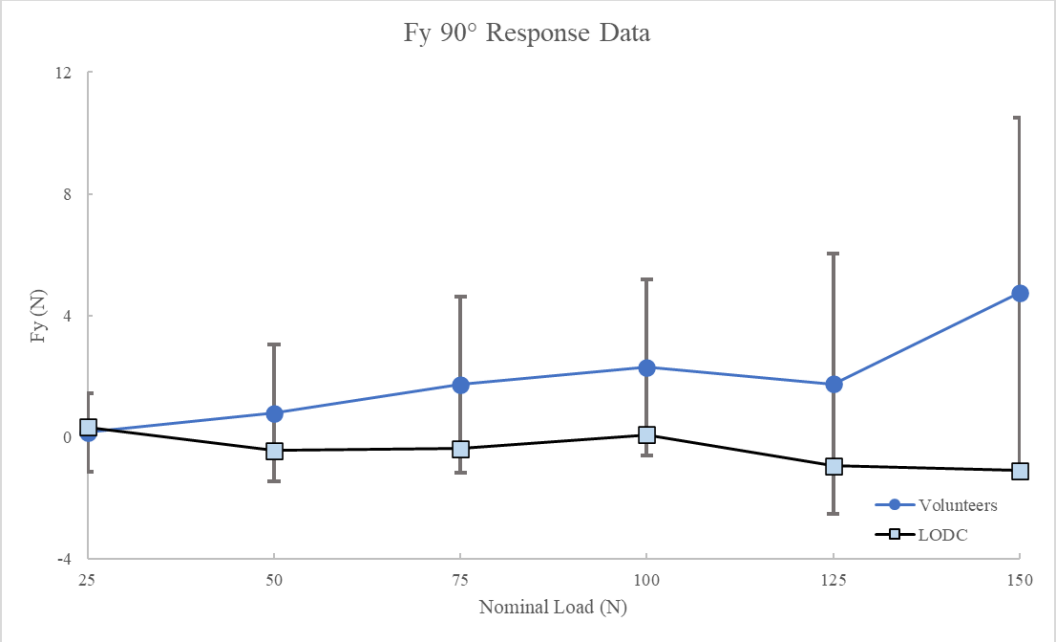

Figure 22: *Fy* for 90° series for volunteers (average ± 1 SD) and LODC

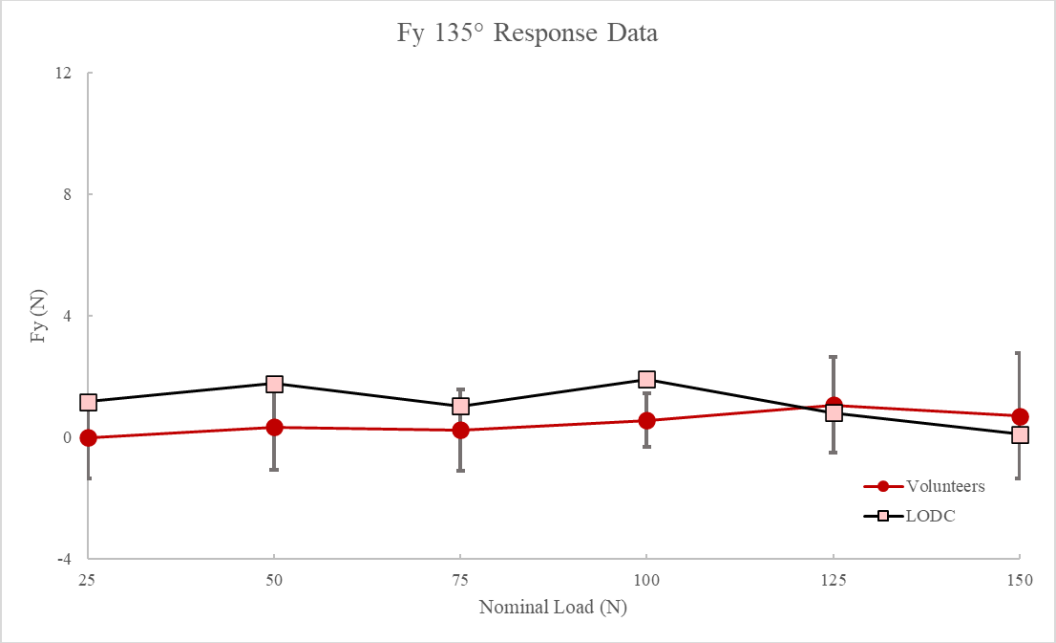

Figure 23: *Fy* for 135° series for volunteers (average ± 1 SD) and LODC

Fx was greater in the 90° series (Figure 24) than the 135° series (Figure 25) since all of the nominal load was applied in the x direction. The LODC was near one standard deviation above the volunteer average for the 90° series and near one standard deviation below the volunteer average for the 135° series at each nominal load. For both series, there appeared to be a linear relationship between the magnitude of the effective load in the x direction and the resultant *Fx* measurement.

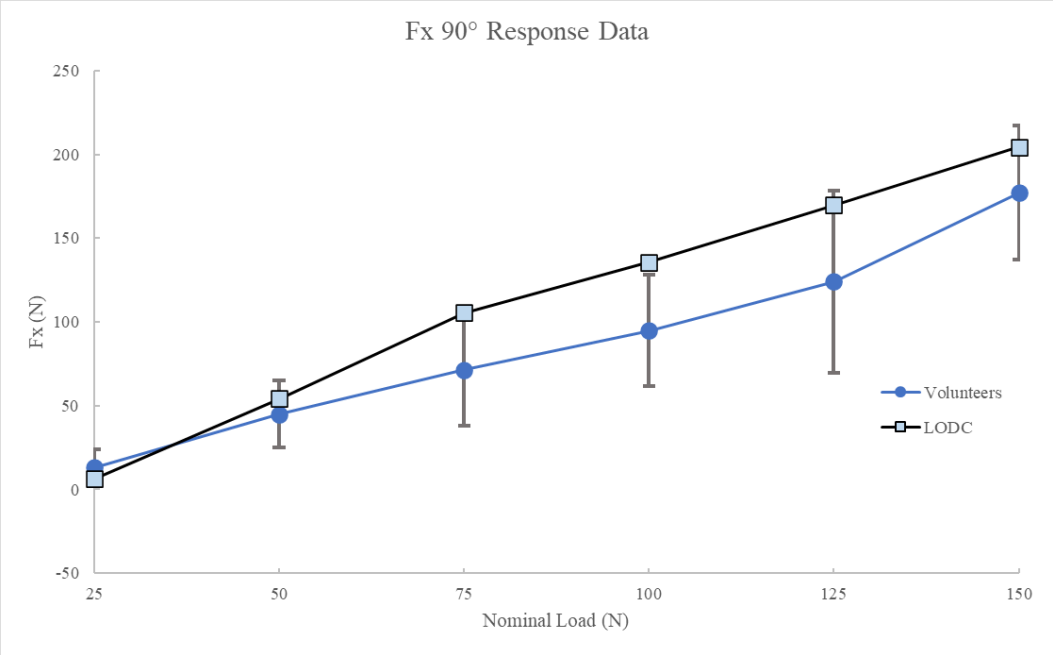

Figure 24: *Fx* for 90° series for volunteers (average ± 1 SD) and LODC

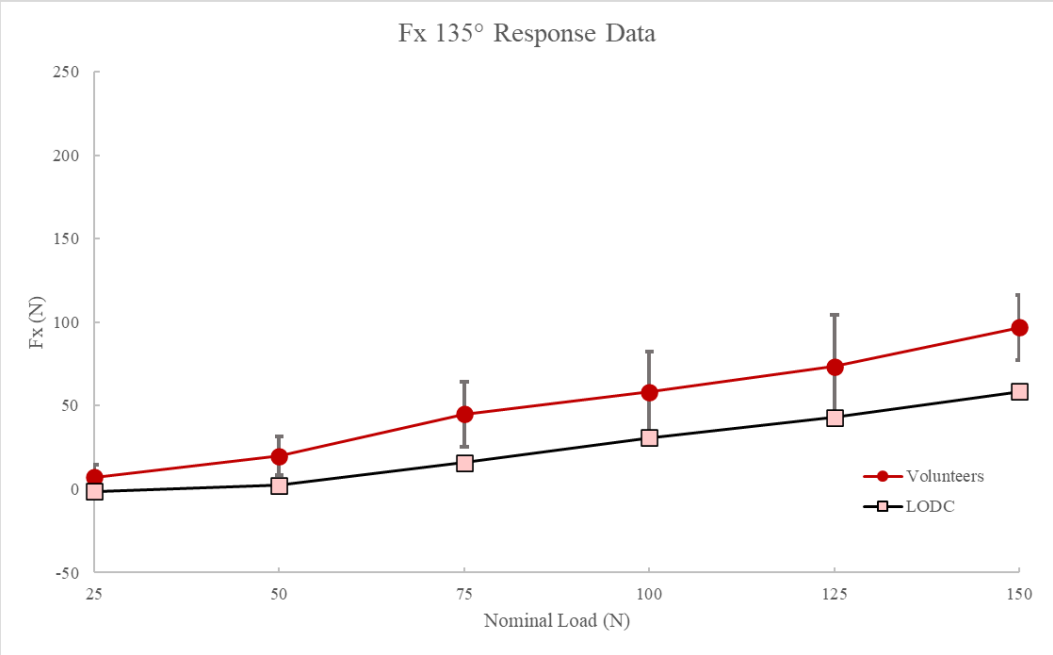

Figure 25: *Fx* for 135° series for volunteers (average ± 1 SD) and LODC

For *Fz*, the volunteer average and LODC trended downward for the 90° series (Figure 26), and both trended upward for the 135° series (Figure 27). With regards to the magnitude, the 90° series had a lower magnitude of 29 N downward at the maximum nominal load compared to the 135° series which had a magnitude of 34 N upward at the maximum nominal load. These results for the 135° series are validated by the upward component of the effective load on the volunteers and LODC; however, there was no downward effective load in the 90° series, suggesting an external factor outside of the loading, such as gravity and slouching resulted, in the downward shear. For the 90° series, the LODC tended to be around one standard deviation above the volunteer average. However, in the 135° series, the LODC was well above one standard deviation

of the volunteer average. These trends suggest that the LODC endured greater upward shear force than the volunteers for both the 90° and 135° series. These differences suggest that the torso design of the LODC might not capture the unique torso response during shoulder loading of the pediatric population.

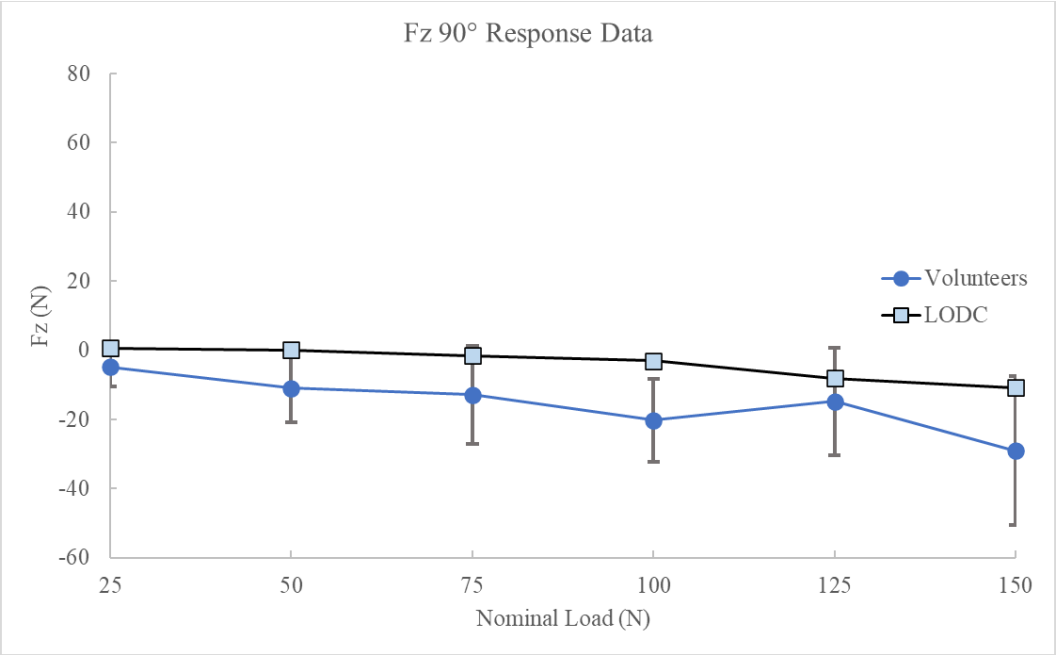

Figure 26: *Fz* for 90° series for volunteers (average ± 1 SD) and LODC

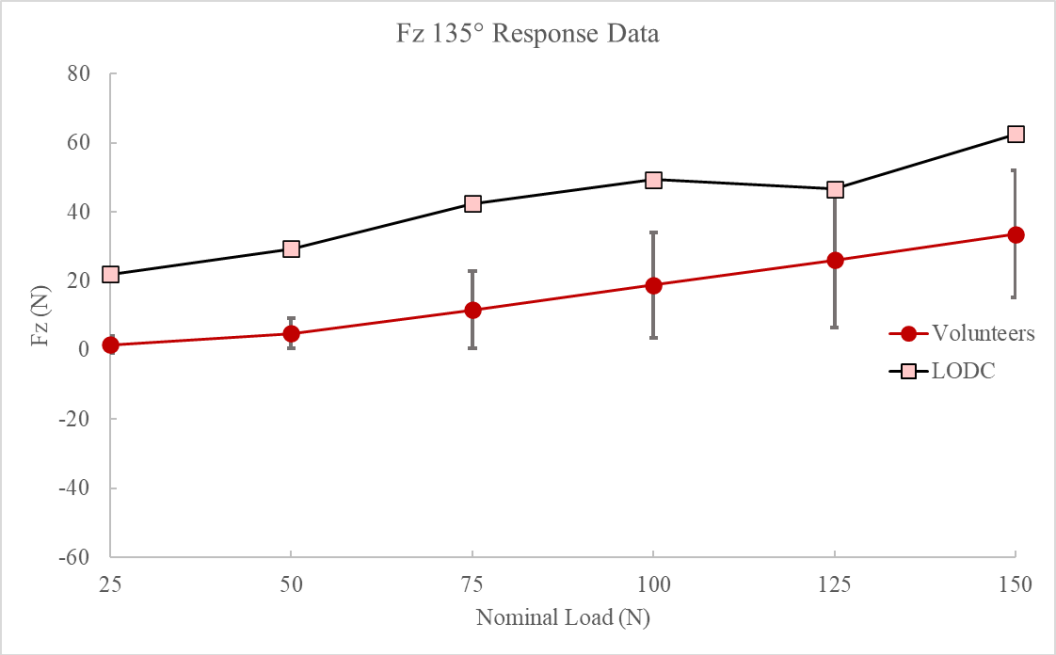

Figure 27: *Fz* for 135° series for volunteers (average ± 1 SD) and LODC

Lastly with the force data, *Fx* and *Fz* were directly compared for the 135° series for the volunteers and LODC. This analysis was completed since the effective load was equal for these two directions, so the response would provide insight into differences in torso response by direction. These values are displayed in Figure 28, but the standard deviations for the volunteers have been removed to clear up the comparison between the x direction and z direction. For the volunteers, the force in the x direction was much greater than in the z direction, indicating a greater force normal to the load cell than upward shear. However, the LODC was found to have the opposite be true, with more upward shear than force normal to the load cell. Additionally, the LODC was observed to have less difference between the x and z components than the volunteers. This comparison suggests that when an anterior, superior load is applied, the LODC has an

opposite relationship as the volunteers for the forward and upward response of the torso. For this force data, it is important to consider the differences in seated height and input loads that could lead to unequal loading conditions between the volunteers and LODC. Future testing that ensures precisely equal loading conditions could validate these findings.

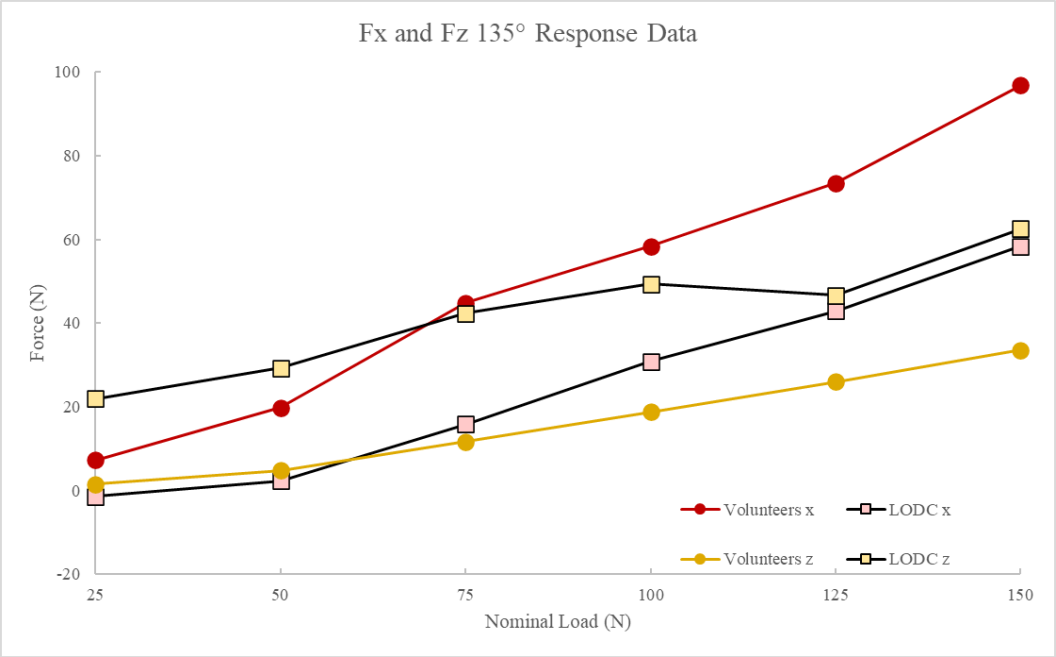

Figure 28: *Fx* and *Fz* for 135° series for volunteer average and LODC

Overall, the force data were found to have mostly identical trends between volunteers and LODC, however, the LODC would occasionally be shifted either upward or downward from the volunteer average, having a nearly constant difference across the nominal loads. The next step was to analyze the results of the moment data. The moment around x was the angular shear the volunteers and LODC applied to the force plate. For the 90° series

(Figure 29) and 135° series (Figure 30), the volunteer average was never greater than 0.2 Nm, suggesting no rotational shear. However, the LODC was found to have a negative shear (CCW) for the 90° series and a positive shear (CW) for the 135° series. These measured moments reached -0.26 Nm for the 90° series and 0.75 Nm for the 135° series. The magnitudes of these moments were determined to be insignificant, suggesting a negligible amount of angular shear on the chest plate.

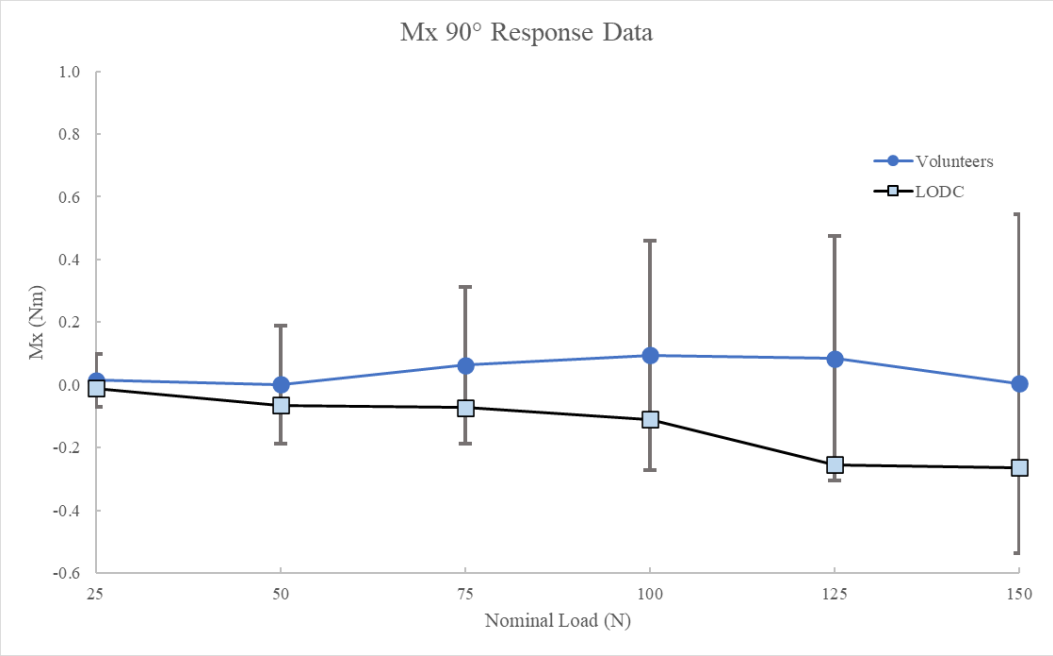

Figure 29: *Mx* for 90° series for volunteers (average ± 1 SD) and LODC

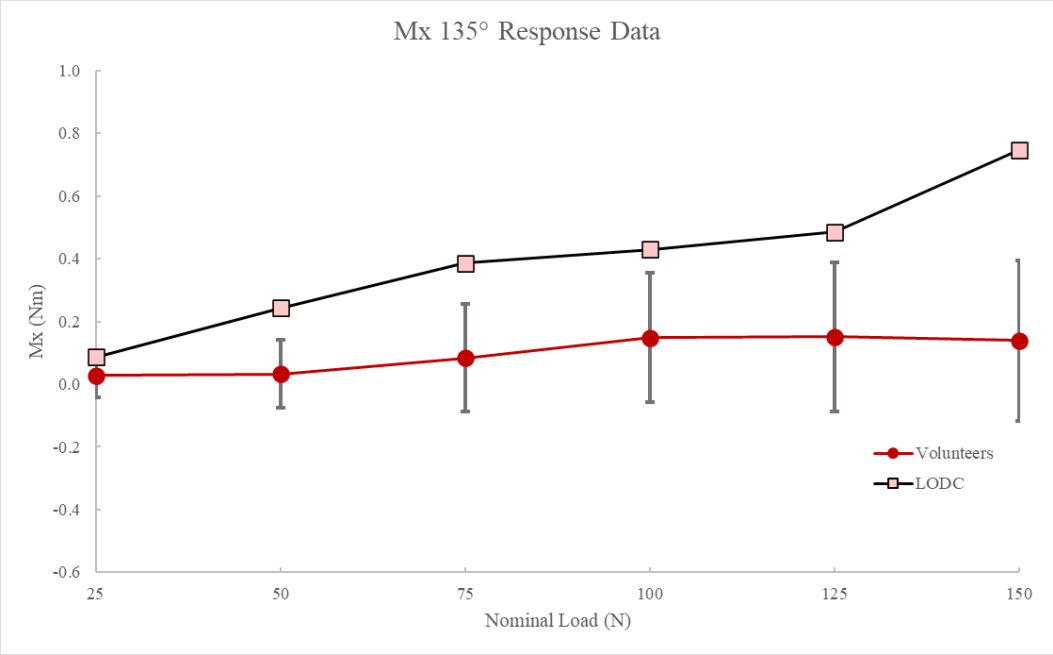

Figure 30: *Mx* for 135° series for volunteers (average ± 1 SD) and LODC

The moment around the z axis was used to quantify the difference in loading from the left side to the right side of the force plate. For the 90° series (Figure 31), the values demonstrated no clear trend, never exceeding a magnitude of 0.25 Nm for the volunteer average and 0.42 Nm for the LODC. For the 135° series (Figure 32), there was an observable increase in *Mz* as nominal load increased for both volunteers and LODC. The volunteers reached a maximum *Mz* of 0.62 Nm compared to 0.80 Nm for the LODC. The LODC slightly underestimated the volunteers at lower nominal loads, and slightly overestimated the volunteers at higher nominal loads, never exceeding one standard deviation away.

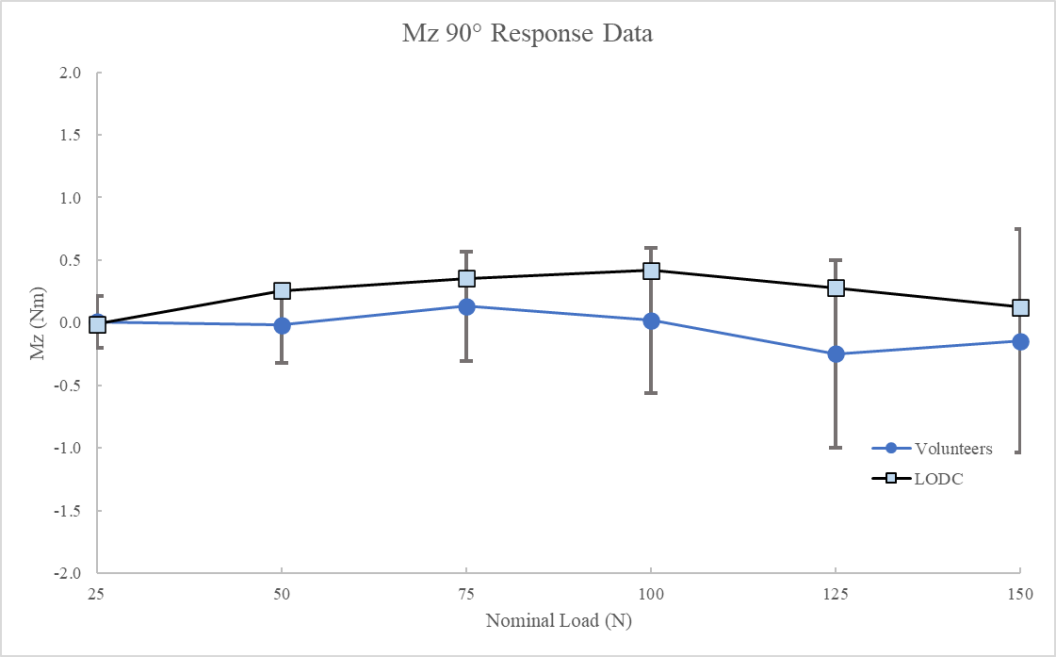

Figure 31: *Mz* for 90° series for volunteers (average ± 1 SD) and LODC

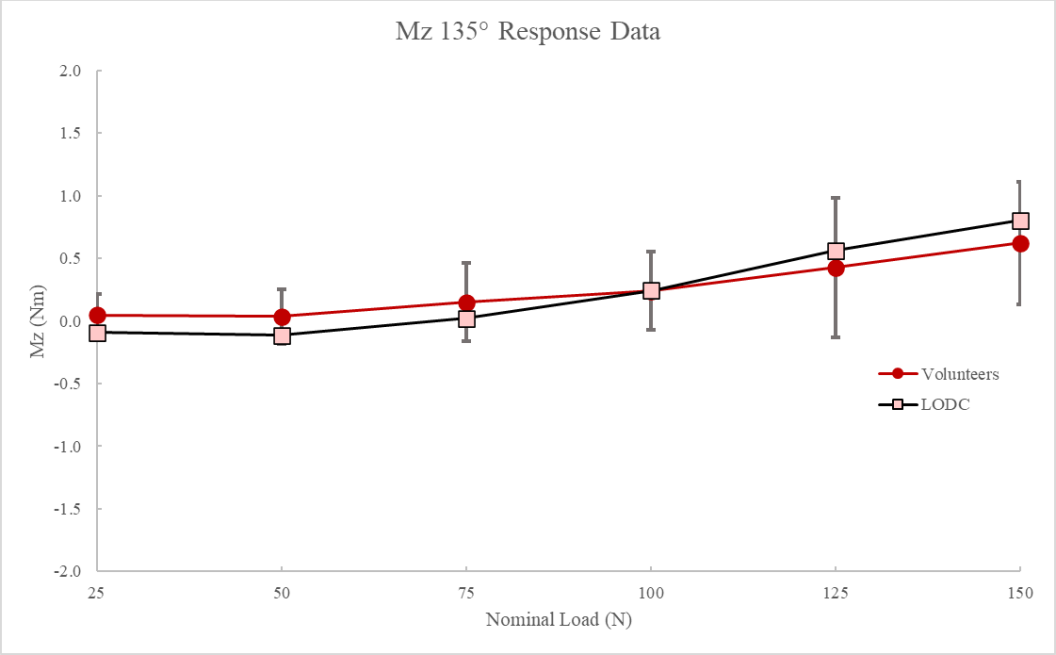

Figure 32: *Mz* for 135° series for volunteers (average ± 1 SD) and LODC

The moment about the y axis quantified the difference in force being applied from the top to the bottom of the chest plate. For the 90° series (Figure 33), the volunteers were observed to have no clear trends, only reaching a magnitude of 0.57 Nm at the highest nominal load. However, the LODC was observed to have a positive linear trend between *My* and nominal load, reaching 6.59 Nm at the highest nominal load. As a result, the LODC was further from the volunteer average as load increased. For the 135° series (Figure 34), there was a positive linear trend observed for both the LODC and volunteer average. At the highest nominal load, the LODC and volunteers reached 3.11 Nm and 2.85 Nm, respectively. At lower nominal loads, the LODC overestimated the volunteer average by over one standard deviation; however, at higher nominal loads, the LODC was nearly identical to the volunteer average.

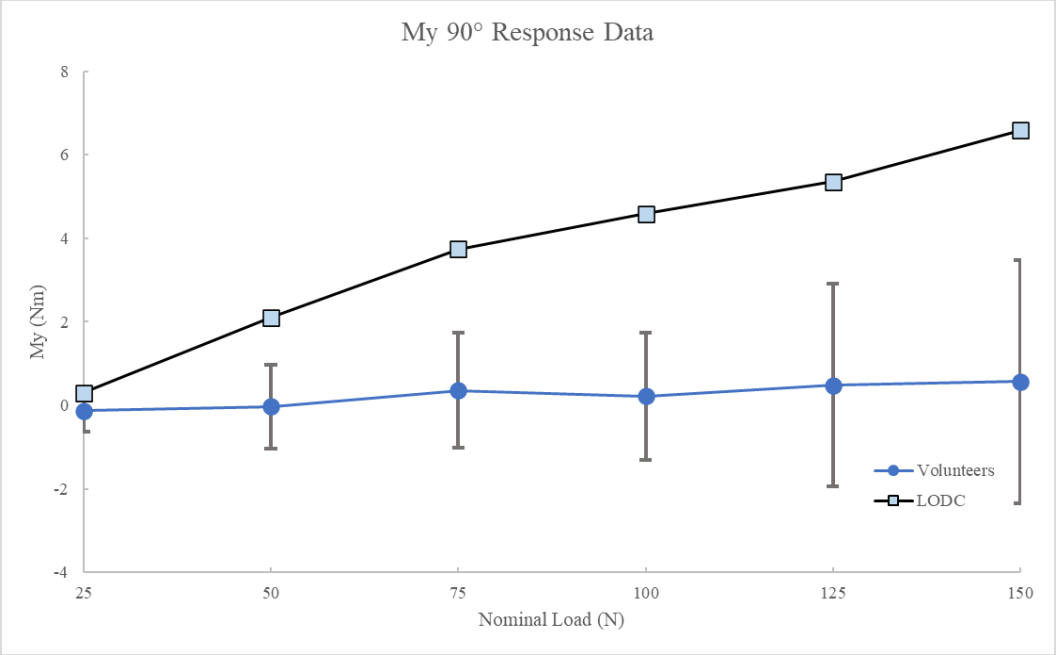

Figure 33: *My* for 90° series for volunteers (average ± 1 SD) and LODC

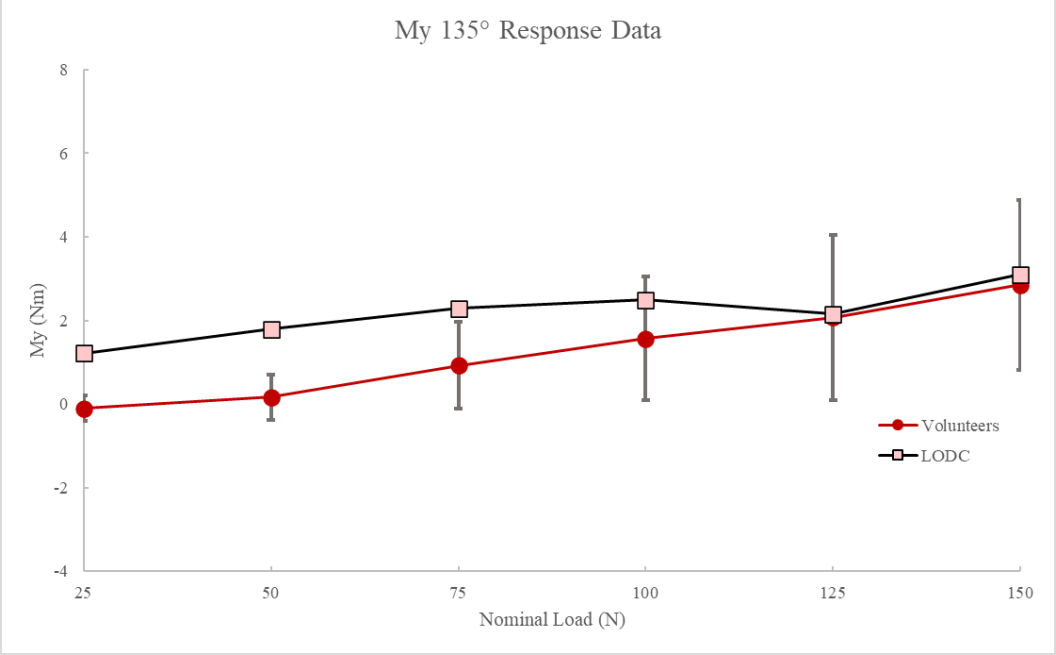

Figure 34: *My* for 135° series for volunteers (average ± 1 SD) and LODC

Of these three measured moments of the chest plate, only *My* was observed to have any values above 1 Nm, and this was only observed in the 135° series for volunteers and both 90° series and 135° series for the LODC. The *My* measurement for the 90° series was found to have a positive linear relationship with nominal load and volunteers were found to have none. Therefore, the torso of the LODC was loading the top of the plate more than the bottom, unlike the volunteers who loaded the plate evenly in the vertical direction. This difference suggests that volunteers respond to anterior loading of the shoulders by translating forward whereas the LODC rotates anteriorly about its pelvis. With regards to the LODC design, this difference suggests that the spine and torso articulation with the pelvis might not accurately represent the pediatric response to loading of the upper extremity. However, in scenarios with a lap belt, this difference would likely be insignificant since volunteers would then be likely to rotate about the pelvis instead of translating anteriorly. Overall, the moments revealed many similarities in torso response to shoulder loading between the LODC and volunteers, and all differences were determined to be insignificant. All data for forces and moments, including the 170° series, are tabulated in Appendix D (Tables D7-D25).

Quasi-Static Shoulder Displacement Comparison

Characterization of the LODC shoulder girdle response occurred through nearly the same data collection and analyses processes as with the volunteers. However, as stated in Chapter 2: Materials and Methods, only one pre-photo was used for the 135° series since the shoulder could not successfully undergo flexion in loaded states. In this single pre-

photo, the shoulders were positioned at 90° of shoulder flexion, matching the initial condition of the volunteers for both directions and the LODC for the 90° series. Post-loading photos for the LODC are shown for both 90° and 135° loading series in Figure 35. Similar to the volunteers for the 135° series, the arms of the LODC did not appear to reach 135° of shoulder flexion until the 100N of nominal load. This similar response suggests that the LODC accurately represents the shift in musculature away from shoulder flexors at higher loads once the angle of loading is reached.

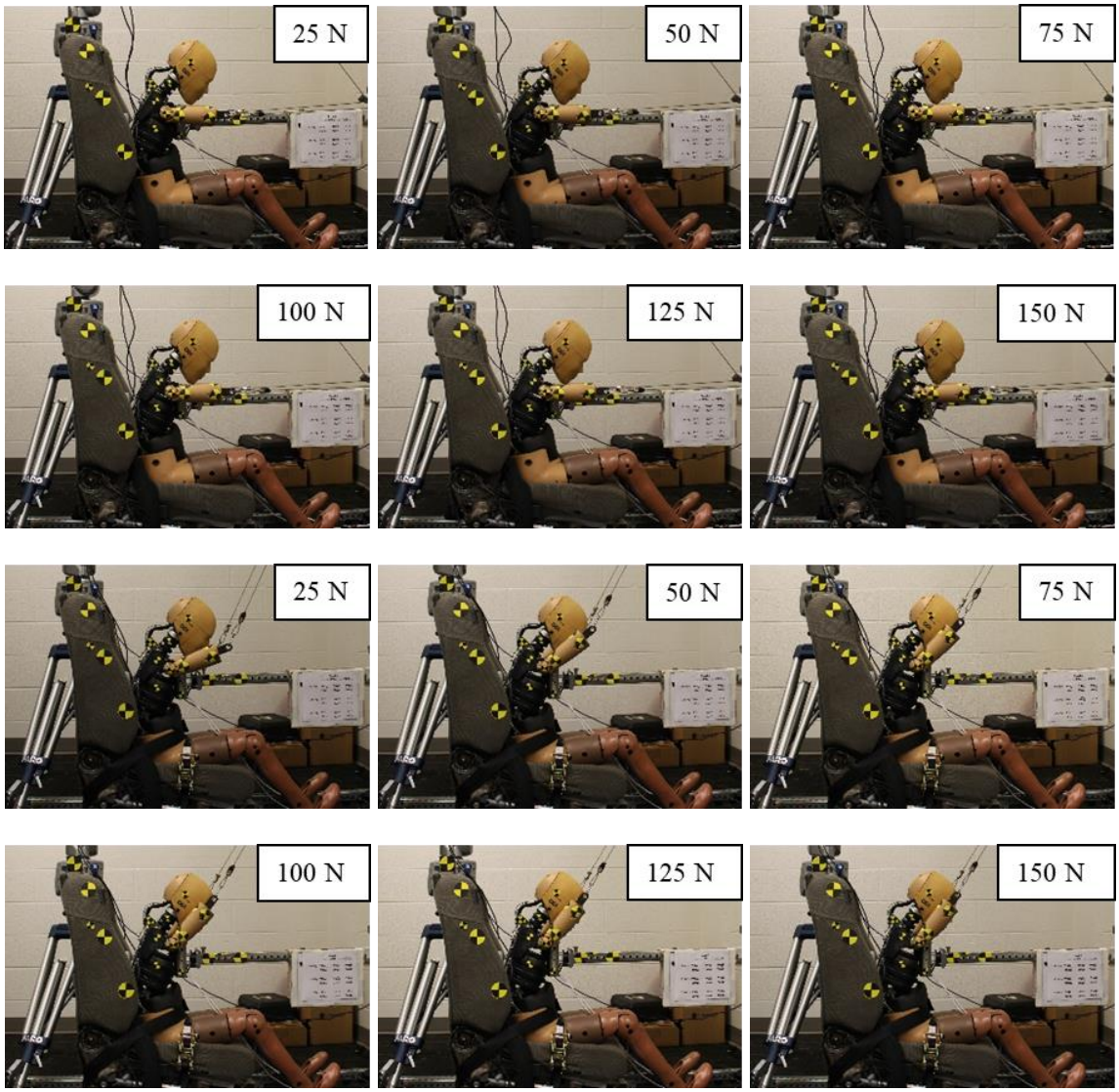

Figure 35: LODC ATD post-loading photos for 90° (top two rows) and 135° (bottom two rows) loading series

As with the volunteers, acromion displacement was found relative to T1, helping isolate the displacement of the shoulder girdle complex. These relative acromion to T1 displacements were plotted with the normalized volunteer averages and one standard deviation for the 90° and 135° loading series in Figure 36. It was observed visually that

the LODC was more similar to the volunteer average in the 90° series than the 135° series. Within the 135° series, the x displacement was closer to the volunteer response than the z displacement.

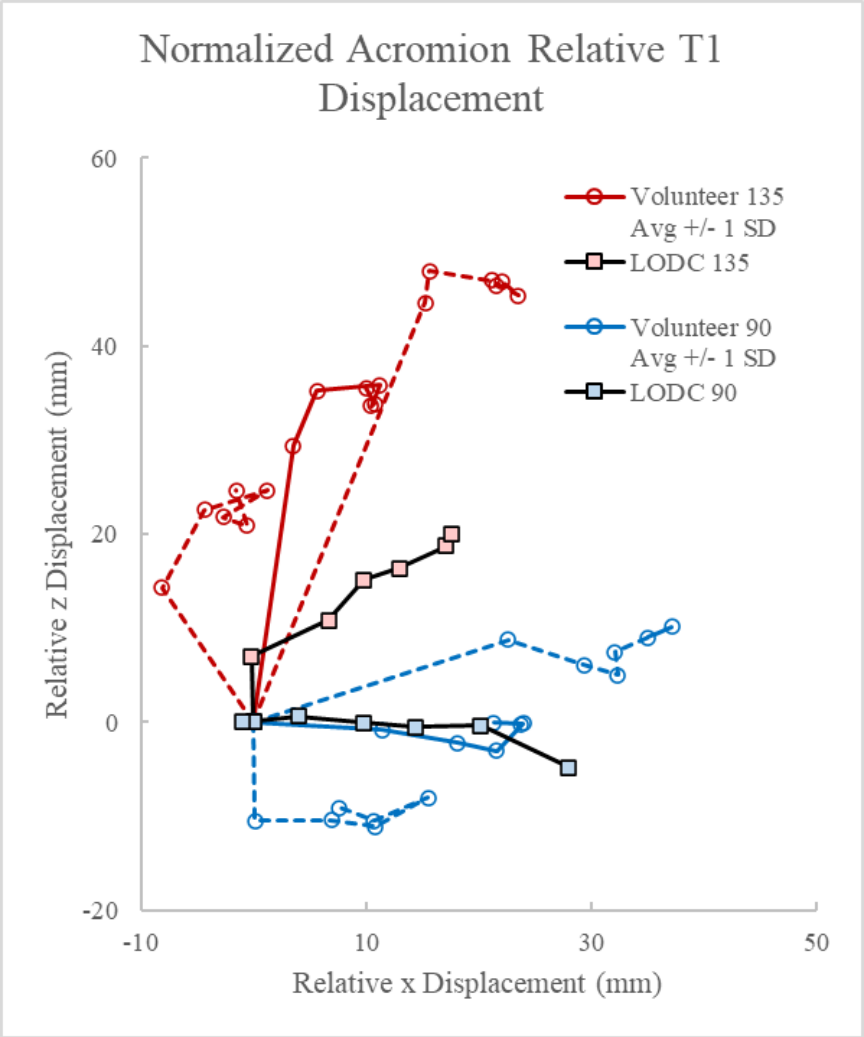

Figure 36: LODC acromion relative to T1 x-z displacement compared to normalized volunteer average and standard deviation

Each marker indicates increases of nominal load by increments of 25 N

As with the volunteers, the displacements of the LODC were broken into the x component for the 90° series, and into x and z components and resultant vector for the 135° series. These components were displayed in Figure 37 with respect to effective load in that direction. Effective loads were utilized to accurately depict how the shoulder girdle complex was responding under a known load. It was visually observed that the LODC underestimated the volunteer response at lower effective loads, but approached the volunteer average as effective load increased, sometimes surpassing the volunteer response. For the 135° series, the LODC was closest to the volunteer response in the x direction, always within one standard deviation of the average. Contrastingly, the LODC was never within one standard deviation of the volunteer response in the z direction.

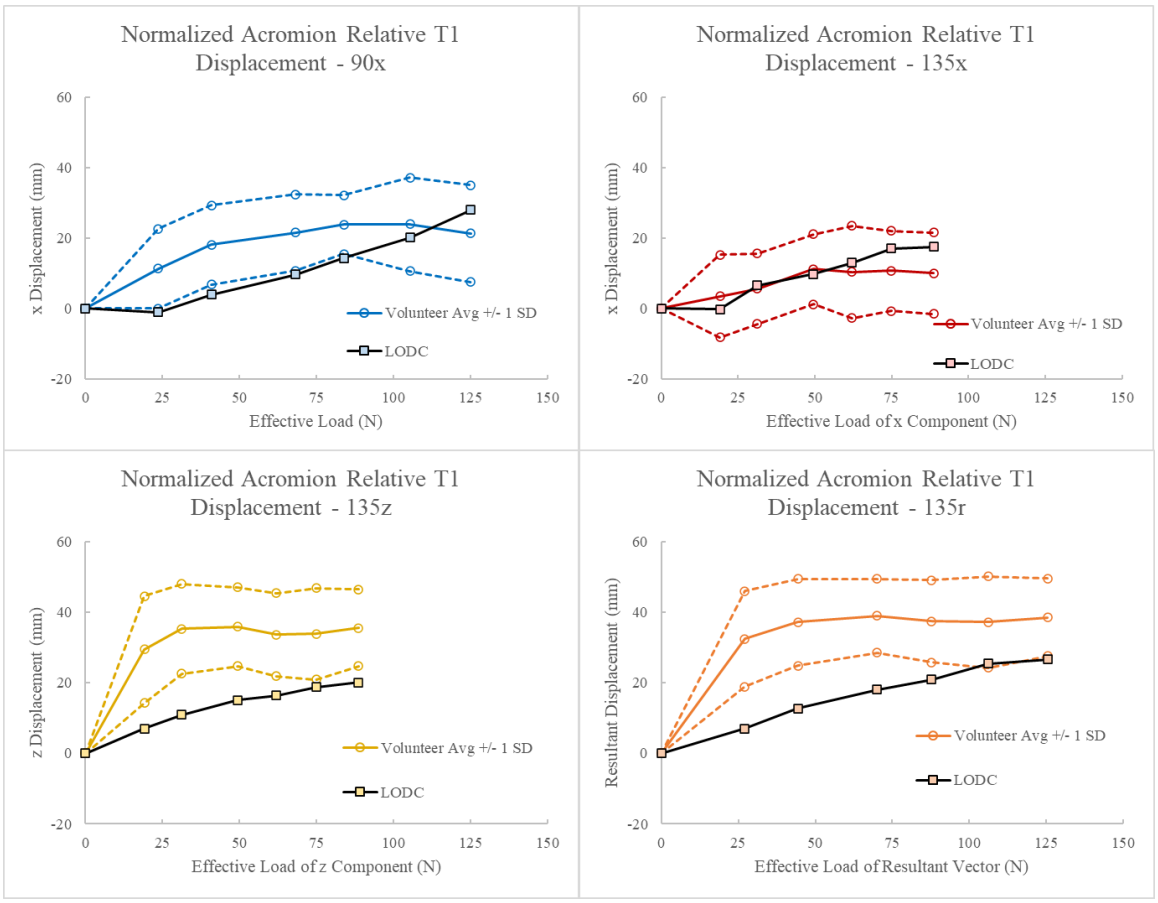

Figure 37: LODC acromion relative to T1 x and z displacement across loads at 90° and 135° compared to volunteers

Each marker corresponds to the effective load at each condition, in increments of 25 N of nominal load

Biofidelity Ranking System

While visually observing the displacement data is useful for recognizing trends, assessing biofidelity requires quantitative computation. Therefore, a Biofidelity Ranking System (BRS) score was calculated to quantify biofidelity using Equation 1. The BRS score was

found for each component, and then averaged to assess the overall biofidelity of the LODC. A weighted average was utilized such that the LODC would receive a BRS score for the x direction and another for the z direction. These two values were then averaged to find an overall BRS score for the LODC. A flowchart of this averaging process is shown in Figure 38. The results by direction are shown in Table 9. All values were less than 2, suggesting “good biofidelity” by component and overall for the LODC ATD. Despite concluding “good biofidelity”, it should be noted that the LODC is more biofidelic in the x direction than the z direction, seen by a worse BRS score for the z direction. In anatomical terms, the LODC is therefore more accurate at representing shoulder protraction than shoulder elevation.

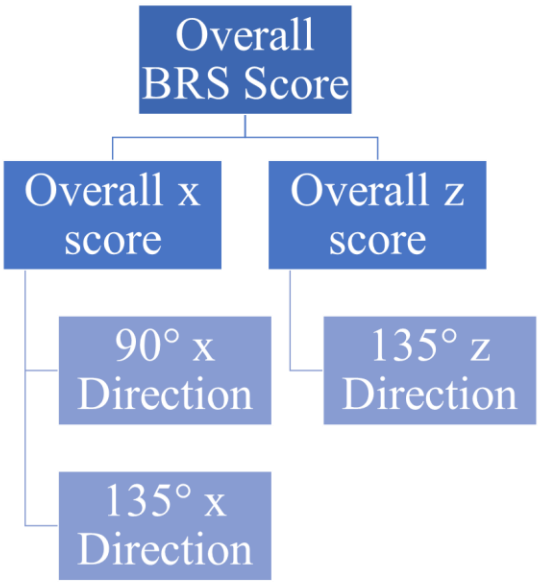

Figure 38: Flowchart of BRS Score calculation for overall biofidelity

Table 9: BRS scores by component and weighted average

Direction	BRS Score
90°: x component	0.85
135°: x component	0.33
135°: z component	1.55
Overall x	0.59
Overall z	1.55
Overall	1.07

These results of BRS suggest that on average, the LODC is outside one volunteer standard deviation from the volunteer average. For the x and z directions, the LODC is

1.5 and 0.6 volunteer standard deviations away from the volunteer average, respectively. In all of these instances, the BRS suggests good biofidelity even though the LODC is typically outside one standard deviation in the force-displacement relationship. This discrepancy suggests that the BRS score might not be an appropriate metric to apply to these data. One reason for this inconsistency is that BRS was developed for comparing a dynamic response of ATDs to post-mortem human subjects (PMHSs). These dynamic impacts have more complex interactions than the quasi-static response completed in this study. Therefore, a score of 2 was designated as "good biofidelity". In the relatively simpler context of quasi-static response, a score of 2 might not be an appropriate threshold for assessment of good biofidelity. Future quasi-static studies can be used to compare how robust current BRS methods are with assessment of ATDs in quasi-static scenarios. Despite these limitations of BRS with assessing "good biofidelity", the scoring system is still useful with concluding better shoulder biofidelity of the LODC in the x direction than the z direction.

Stiffness Comparison

As with the volunteers, the stiffness of the LODC was also calculated utilizing the same procedure of identifying the increasing linear relationship between force and displacement. Figure 39 displays the LODC displacement data with an indicator of where the end of the linear stiffness region was identified.

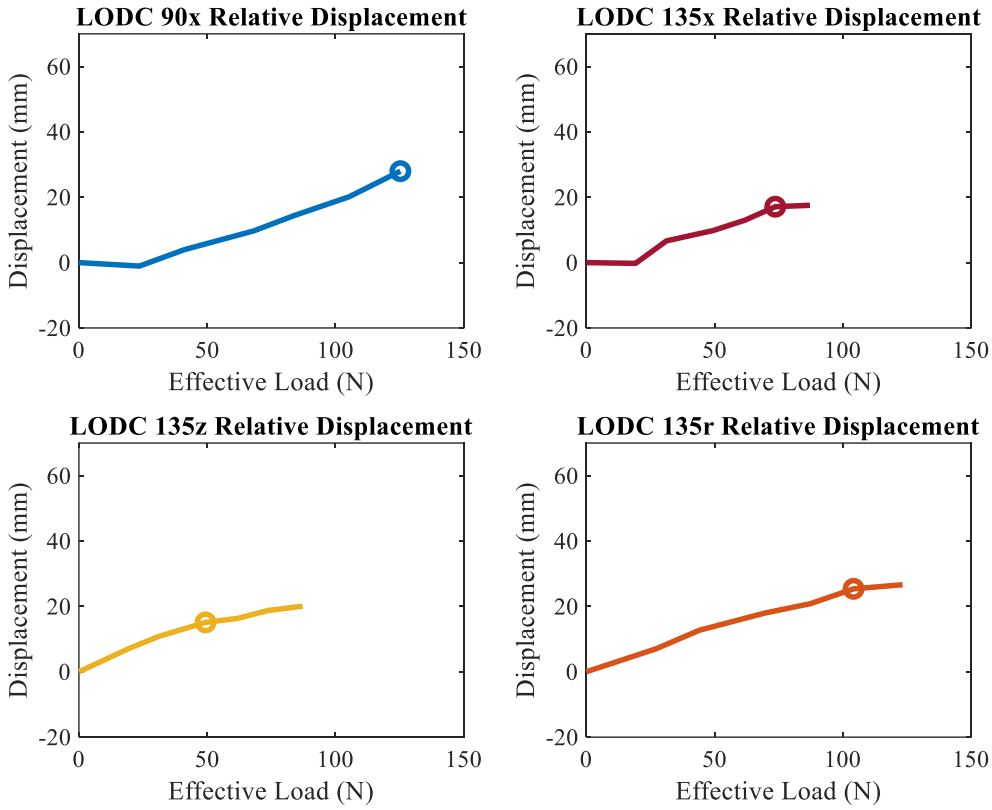

Figure 39: LODC displacement data with marker at end of linear stiffness region

The points leading up to and including the marker were utilized in the calculation of the linear regression, where the slope (in units of N/mm) was determined to be the stiffness. The values are shown in Figure 40 along with those of the volunteers. The LODC was observed to be inside one standard deviation of the volunteer average for the x components of the 90° series and 135° series but outside one standard deviation for the z component and resultant vector of the 135° series. In both directions where the LODC was outside one standard deviation, the LODC was overestimating the stiffness, which was observed in the LODC displacements being less than those of the volunteers at each

given load. Overall, the stiffness values suggest that the LODC is more biofidelic in the x direction than the z direction and therefore more biofidelic in anterior and superior loading at 90° of shoulder flexion than at 135° of shoulder flexion. These results match those of the BRS score calculations where the LODC was concluded to be more biofidelic in the x direction than the z direction.

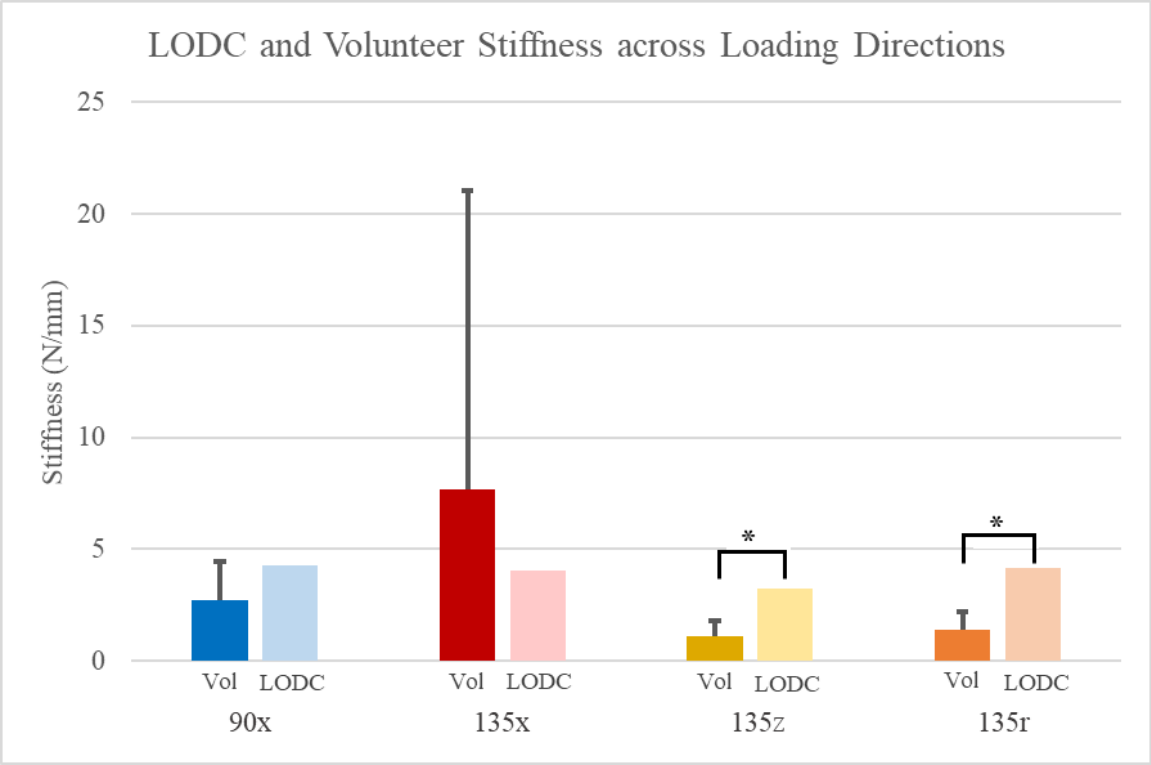

Figure 40: LODC and volunteer stiffness in different loading directions

(* Denotes LODC outside 1 SD of volunteer average)

These BRS and stiffness metrics can be used for different applications for predicting pediatric dynamic response. The stiffness values are useful for comparison to the results

of adult studies (Törnvall et al., 2010) to create scaling factors specific to the shoulder region. This quasi-static ratio can then be applied to adult PMHS dynamic response to estimate the pediatric dynamic response. The BRS scores are useful with drawing conclusions of biofidelity in this quasi-static environment and expanding these results for dynamic response scenarios of the LODC.

These results can also be applied to dynamic impact scenarios that utilized the LODC. With regards to accurate shoulder kinematics, instances of shoulder displacement in the anterior-posterior direction would be more robust than shoulder displacement in the superior-inferior direction. For injury values with the head, neck, and thorax, it is important to evaluate the cause and mechanisms of these metrics and how much other regions, specifically the shoulder, influence these values. The shoulder of the LODC was found to be stiffer than the volunteers in the inferior-superior direction, which would cause it to take a disproportionate percentage of the shoulder belt load, therefore underpredicting chest deflection metrics. Additionally, a stiffer shoulder could decrease head excursion, therefore underpredicting injuries metrics and head contact. Dynamic testing with the LODC should take these results into consideration when evaluating pediatric response.

Lastly, there were some qualitative differences in the LODC response that should be noted with assessing its biofidelity. One difference was with the elevation out of the seat for the 135° and 170° series. Even though several of the volunteers elevated during the

highest nominal loads of the 170° series, there were clear differences in the height off the seat and the load at which elevation occurred. These differences suggest that the spine and torso of the LODC do not respond in the same manner as the pediatric population. This difference could have injury prediction ramifications with ramping in rear impacts with not accurately representing the elevation off the seat due to an upward force. The other qualitative difference in loading patterns was for the shoulder of the LODC in the 135° and 170° series. When the LODC shoulder started at 90° of shoulder flexion for the pre-loading position, a bolt in the shoulder was dislocated when loads were applied in the anterior and superior directions. However, the shoulders could be flexed at slow velocities when the arms were not loaded, allowing for the placement of the unused pre-loading positions in the 130° and 170° series, seen in Figure 9. This shoulder dislocation suggests the design does not accurately represent the pediatric population during shoulder flexion while the shoulder is loaded along the long axis of the humerus. During a frontal dynamic impact, the kinematics of the shoulder of the LODC would be affected as the shoulder is being flexed with a high velocity, therefore loading the shoulder along the long axis of the humerus.

The comparison of the volunteers to the LODC evaluated the differences in anthropometric measurements. Differences in size demonstrated the need for normalization when comparing volunteer displacement data to that of the LODC. Right load cell data suggested that the LODC experienced a higher input load than the volunteers; however, the comparison of quasi-static displacement was still completed

between the volunteers and LODC. The results of the 6-axis load cell demonstrated that the volunteers and LODC followed similar trends with their torso response to the different series of loading. Additionally, all observed differences were determined to be negligible due to small magnitude and unrealistic boundary conditions. With the quasi-static displacement data, the LODC tended to underestimate the volunteer response, but this difference decreased as effective load increased. The BRS score calculation supported the visual comprehension of the displacement data, suggesting that the LODC was more biofidelic in the x direction than the z direction. Both BRS scores for the x and z directions concluded “good biofidelity” for the LODC; however, the application of BRS to this quasi-static loading condition is not well established. Lastly, the calculated stiffness of the LODC continued this trend of being outside one standard deviation of the volunteers in the z direction but within one standard deviation for the x direction of both series. These results are useful for making conclusions for the pediatric population by using the LODC in dynamic impact scenarios.

Chapter 5: Limitations and Conclusions

Limitations

Limitations were noted and should be considered when applying these conclusions to future work. This study utilized nominal loads that ranged from 25-150 N per shoulder, which is significantly less than those experienced in motor vehicle crashes, based on measured forces of the shoulder belt in dynamic testing (Bohman et al., 2018). Additionally, the volunteers and LODC utilized a pre-loading position of 90° of shoulder flexion. During a collision, the arms are at rest, closer to 0° of shoulder flexion, so this testing procedure eliminated the first 90° of shoulder flexion during a frontal collision. The reason for this decision was to allow an accurate comparison to adults who underwent the same procedure (Törnvall et al., 2010). The weight source of the loading input changed after the 13th volunteer from sandbags in a bucket to hook with free weights. This change was made so that larger volunteers at larger nominal loads did not "bottom out" with the bucket still resting on the lowest position of the drop table. Additionally, the cable uniaxial load cell data suggested that the LODC experienced a greater loading input than the volunteers. Comparisons were still drawn between the LODC and volunteers with this different input, but future work could target loading input conditions that exactly match the average of the volunteers. Similarly, the exact loading

angles of the 135° and 170° could have varied based on seated height of the volunteers and LODC. This difference was determined to be negligible, allowing for a reasonable comparison between the volunteers and LODC, but future work could quantify the exact angle at which loads were applied. Lastly, despite volunteers being instructed to relax, muscle contraction may have also influenced the results. Any muscle activation could have influenced displacement and stiffness results.

Other limitations occurred in the motion tracking procedures. Fiducials placed on the skin do not always directly match the motion of skeletal components beneath the skin, resulting in error in motion tracking. Additionally, only one individual completed one round of motion tracking, resulting in no measurement of interobserver or intra-observer error. However, there was the benefit of having the same individual complete motion tracking for all the volunteers and ATD, creating consistency between the tests. Future work could evaluate the tracking with quantifying interobserver error. Additionally, movement occurring normal to the plane of analysis, either from linear or rotational motion, was not assessed from two-dimensional sagittal images. However, adult volunteer results have shown little relative acromion displacement in the lateral-medial direction (Törnvall et al., 2010). Future work could quantify this y displacement using the frontal camera photos.

Conclusions

The objective of this study was to quantify the healthy 8–12-year-old shoulder girdle complex and use those results to assess the biofidelity of the LODC shoulder girdle complex. From this study, the healthy shoulder girdle complex was characterized from 25 pediatric volunteers using anthropometric and active assisted range of motion measurements. Under quasi-static loading, displacements were found across effective loads to quantify the x and z position of the acromion relative to T1 for 90° series and 135° series. Volunteers experienced greater displacement in the x direction for the 90° series and greater displacement in the z direction for the 135° series. For both loading series, the volunteers were observed to have reached the end of their range of motion, observable by little displacement as the nominal load was increased. Displacements were normalized by shoulder breadth to account for size differences across the sample. The normalized displacements were used to find the stiffness by each component of the loading series. Stiffness was observed by the positive, linear portions of the force-displacement relationship, which was found by cutting the data at the first load where the volunteers reached the end of their range of motion. The stiffnesses and displacements were useful for detecting differences across and within the loading series and for comparison to the LODC.

The comparison of the volunteers to the LODC evaluated the differences in anthropometric measurements. Differences in size demonstrated the need for normalization when comparing volunteer displacement data to that of the LODC. Right

load cell data suggested that the LODC experienced a higher input load than the volunteers; however, comparisons between the LODC and volunteers were still completed. The results of the 6-axis load cell demonstrated that the volunteers and LODC followed similar trends with their torso response to the different series of loading. Additionally, any observed differences were determined to be negligible due to small magnitudes or unrealistic boundary conditions. With the quasi-static displacement data, the LODC tended to underestimate the volunteer response, but this difference decreased as effective load increased. The BRS score calculation supported the visual comprehension of the displacement data, suggesting that the LODC was more biofidelic in the x direction than the z direction. Lastly, the calculated stiffness of the LODC continued this trend of decreased biofidelity in the z direction by being outside one standard deviation of the volunteers in the z direction but within one standard deviation for the x direction of both series. This comparison suggested that if changes were to be made to the LODC, shoulder elevation should be evaluated first for potential improvements.

Future directions with these data outside of changes to the LODC include comparing the displacement responses to those of adults in similar testing conditions (Törnvall et al., 2010). Specifically, stiffness values for the x and z direction could be used for comparison to adults and to create scaling ratios between adult and pediatric populations. With adult dynamic testing, most likely with PMHSs, this process could lead to the prediction of the pediatric dynamic shoulder response. This corridor could then be used to

evaluate the LODC in dynamic loading scenarios, providing better insight to the biofidelity in dynamic scenarios, similar to those experienced in a motor vehicle collision.

Bibliography

Agnew, A.M., Schafman, M., Moorhouse, K., White, S.E., Kang, Y.S., 2015. The effect of age on the structural properties of human ribs. J. Mech. Behav. Biomed. Mater. 41, 302–314. https://doi.org/10.1016/J.JMBBM.2014.09.002

Arbogast, K.B., Locey, C.M., Zonfrillo, M.R., Maltese, M.R., 2010. Protection of children restrained in child safety seats in side impact crashes. J. Trauma 69, 913–923. https://doi.org/10.1097/TA.0B013E3181E883F9

Baker, G., Stockman, I., Bohman, K., Jakobsson, L., Osvalder, A.L., Svensson, M., Wimmerstedt, M., 2018. Kinematics and shoulder belt engagement of children on belt-positioning boosters during evasive steering maneuvers. Traffic Inj. Prev. 19, S131–S138. https://doi.org/10.1080/15389588.2017.1398401

Bohman, K., Arbogast, K.B., Loeb, H., Charlton, J.L., Koppel, S., Cross, S.L., 2018. Frontal and oblique crash tests of HIII 6-year-old child ATD using real-world, observed child passenger postures. https://doi.org/10.1080/15389588.2017.1385781 19, S125–S130. https://doi.org/10.1080/15389588.2017.1385781

Bohman, K., Stockman, I., Jakobsson, L., Osvalder, A.L., Bostrom, O., Arbogast, K.B., 2011. Kinematics and Shoulder Belt Position of Child Rear Seat Passengers during Vehicle Maneuvers. Ann. Adv. Automot. Med. / Annu. Sci. Conf. 55, 15.

Chandran, A., Hyder, A.A., Peek-Asa, C., 2010. The global burden of unintentional

injuries and an agenda for progress. Epidemiol. Rev. 32, 110–120. https://doi.org/10.1093/epirev/mxq009

Davidsson, J., 2013. Volunteer shoulder range of motion and stiffness: data for evaluation of crash test dummies and human body models. publications.lib.chalmers.se.

Dayanidhi, S., Orlin, M., Kozin, S., Duff, S., Karduna, A., 2005. Scapular kinematics during humeral elevation in adults and children. Clin. Biomech. 20, 600–606. https://doi.org/10.1016/J.CLINBIOMECH.2005.03.002

Forman, J.L., Lopez-Valdes, F.J., Duprey, S., Bose, D., Del Pozo De Dios, E., Subit, D., Gillispie, T., Crandall, J.R., Segui-Gomez, M., 2015. The tolerance of the human body to automobile collision impact - A systematic review of injury biomechanics research, 1990-2009. Accid. Anal. Prev. 80, 7–17. https://doi.org/10.1016/j.aap.2015.03.004

Hagedorn, A., Stammen, J., Ramachandra, R., Rhule, H., Thomas, C., Suntay, B., Kang, Y.S., Kwon, H.J., Moorhouse, K., Bolte Iv, J.H., 2022. Biofidelity Evaluation of THOR-50M in Rear-Facing Seating Configurations Using an Updated Biofidelity Ranking System. SAE Int. J. Transp. Saf. 10, 9–10. https://doi.org/10.4271/09-10-02-0013

Hontschik, H., Ruter, G., 1980. I NVESTIGATIONS INTO THE EFFICACY OF THREE-POINT SEAT-BELTS IN OBL IQUE IMPACT EXPERIMENTS H . Hontsc h ik , 128–138.

Horsch, J.D., Hering, W.E., 1989. A kinematic analysis of lap-belt submarining for test dummies. SAE Tech. Pap. 98, 1847–1854. https://doi.org/10.4271/892441

Hynd, D., Carroll, J., Cuerden, R., Kruse, D., Böstrom, O., 2012. Restraint system safety diversity in frontal impact accidents. 2012 IRCOBI Conf. Proc. - Int. Res. Counc. Biomech. Inj. 44, 114–129.

Isaacs, J.L., George, J., Campolettano, E., Cutcliffe, H., Miller, B., 2022. The Role of Three-Point Restraints for Occupants in Moderate Severity Frontal Collisions. SAE Tech. Pap. 4–6. https://doi.org/10.4271/2022-01-0845

Ita, M., Kang, Y.S., Seacrist, T., Dahle, E., Bolte, J., 2014. Comparison of Q3s ATD Biomechanical Responses to Pediatric Volunteers. Traffic Inj. Prev. 15, S215–S222. https://doi.org/10.1080/15389588.2014.934368

Javed, O., Maldonado, K.A., Ashmyan, R., 2022. Anatomy, Shoulder and Upper Limb, Muscles. StatPearls.

Jindal, A., Mukherji, S., 2005. World report on road traffic injury prevention. Med. J. Armed Forces India 61, 91. https://doi.org/10.1016/s0377-1237(05)80135-2

Kent, R., Shaw, G., Lessley, D., Crandall, J., Kallieris, D., Svensson, M., 2003. Comparison of Belted Hybrid III, THOR, and cadaver thoracic responses in oblique frontal and full frontal sled tests. SAE Tech. Pap. 112. https://doi.org/10.4271/2003-01-0160

Miniato, M.A., Anand, P., Varacallo, M., 2022. Anatomy, Shoulder and Upper Limb, Shoulder. StatPearls.

National Center for Injury Prevention and Control Centers for Disease Control and Prevention, 2021. 10 Leading causes of death, united states. Cdc 4.

National Center for Statistics and Analysis, 2022. Traffic safety facts 2020: A

compilation of motor vehicle crash data (Report No. DOT HS 813 375). Natl. Highw. Traffic Saf. Adm. 24.

NHTSA, n.d. Car Seat & Booster Seat Safety, Ratings, Guidelines | NHTSA [WWW Document]. URL https://www.nhtsa.gov/equipment/car-seats-and-booster-seats (accessed 4.5.23).

Rhule, H., Stricklin, J., Moorhouse, K., Donnelly, B., 2018. IRC-18-11 IRCOBI conference 2018 114–124.

Stammen, J., Moorhouse, K., Suntay, B., Carlson, M., Kang, Y.-S., 2016. (PDF) The Large Omnidirectional Child (LODC) ATD: Biofidelity Comparison with the Hybrid III 10 Year Old [WWW Document]. Stapp Car Crash J. URL https://www.researchgate.net/publication/310604437_The_Large_Omnidirectional_Child_LODC_ATD_Biofidelity_Comparison_with_the_Hybrid_III_10_Year_Old (accessed 2.11.22).

Struyf, F., Nijs, J., Baeyens, J.P., Mottram, S., Meeusen, R., 2011. Scapular positioning and movement in unimpaired shoulders, shoulder impingement syndrome, and glenohumeral instability. Scand. J. Med. Sci. Sports 21, 352–358. https://doi.org/10.1111/J.1600-0838.2010.01274.X

Törnvall, F. V., Holmqvist, K., Martinsson, J., Davidsson, J., 2010. Comparison of shoulder range-of-motion and stiffness between volunteers, Hybrid III and THOR Alpha in static frontal impact loading. http://dx.doi.org/10.1533/ijcr.2005.0334 10, 151–160. https://doi.org/10.1533/IJCR.2005.0334

Appendix A: Anthropometry and Range of Motion Data

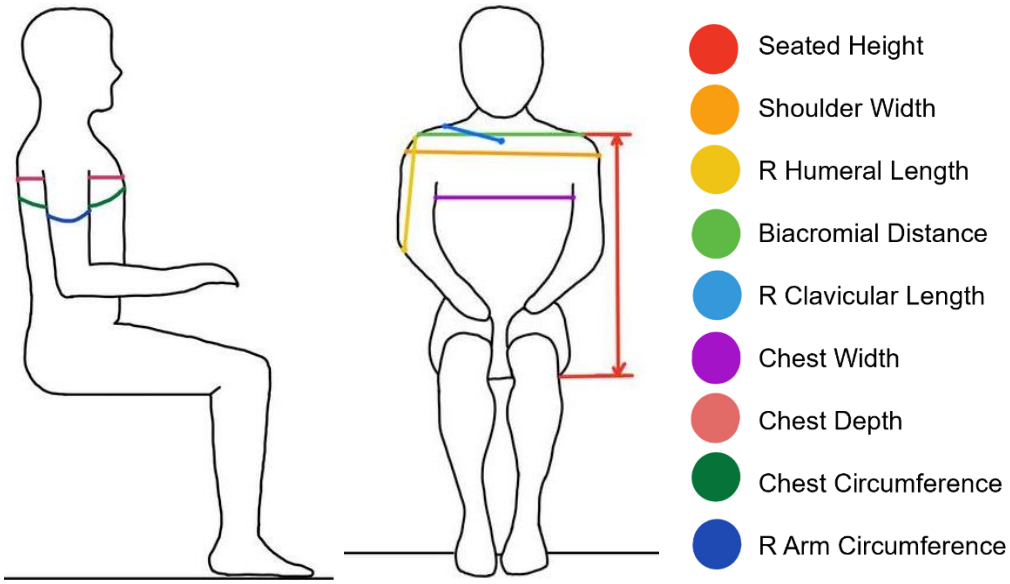

Figure A1: Anthropometric measurements collected

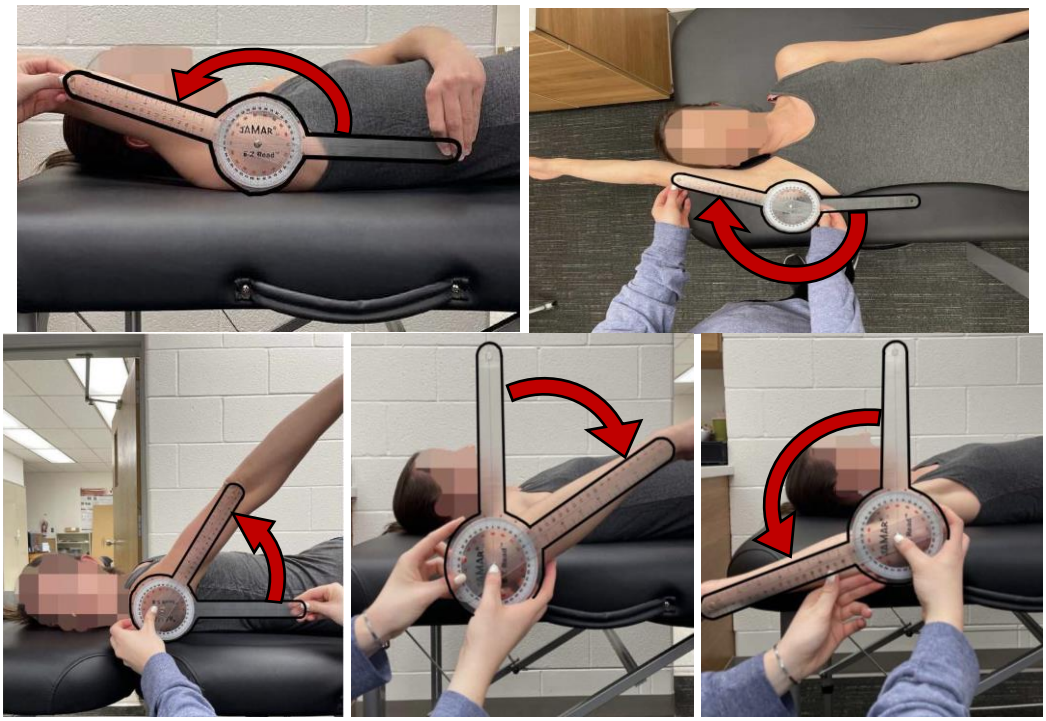

Figure A2: Collection of range of motion measurements of flexion (top left), abduction (top right), extension (lower left), internal rotation (lower middle), and external rotation (lower right)

Table A1: Complete anthropometric data

Subject	*Age (yrs)*	*Sex*	*Arm Dominance*	*Weight (kg)*	*Height (cm)*	*Seated Height (cm)*	*Shoulder Width (cm)*	*Bi-acromial Distance (cm)*	*Clavicular Length (R) (cm)*	*Humeral Length (R) (cm)*	*Chest Width (cm)*	*Chest Depth (cm)*	*Chest Circumference (cm)*	*Arm Circumference (cm)*
PS01	12.3	M	R	50.4	172.7	86.5	41.2	34.3	15.7	30.0	24.5	18.1	73.1	22.6
PS02	12.3	M	R	54.6	173.0	83.8	41.6	36.6	15.9	30.4	26.0	14.8	77.9	24.1
PS03	12.6	M	R	59.2	152.5	76.6	41.2	31.2	15.9	26.5	30.1	21.4	92.0	27.1
PS04	11.1	M	L	49.7	145.0	71.8	38.7	31.1	15.4	27.2	24.6	16.5	82.2	26.7
PS05	11.1	M	R	38.7	144.3	71.2	34.7	30.8	16.2	25.1	22.9	16.4	72.5	21.5
PS06	11.1	M	R	44.7	146.9	72.5	37.4	31.0	16.2	28.1	24.1	17.8	78.1	22.6
PS07	12.2	M	R	79.4	160.1	80.9	42.1	35.2	18.7	30.5	26.4	19.8	99.4	31.8
PS08	12.7	F	L	39.4	156.9	79.0	36.7	32.5	15.6	28.9	24.9	15.7	74.3	19.2
PS09	9.9	M	R	27.9	139.5	72.2	31.7	27.0	14.6	26.5	22.9	24.3	64.5	17.5
PS10	10.2	F	R	28.4	132.5	68.7	30.9	24.5	13.1	24.6	19.3	16.8	62.7	19.9
PS11	12.5	M	R	42.2	156.6	78.0	38.1	30.2	15.2	29.1	24.6	19.3	78.5	20.9
PS12	9.7	M	R	26.8	136.2	70.5	32.3	27.8	14.7	25.1	20.6	14.2	59.7	17.5
PS13	12.8	F	R	57.5	166.0	84.6	43.0	34.9	17.3	30.6	29.5	17.1	86.9	25.5
PS14	11.0	F	R	32.5	140.0	70.0	33.0	29.0	14.0	28.0	23.5	15.5	67.0	20.0
PS15	10.3	M	R	49.2	142.5	74.0	38.0	33.5	16.0	29.0	28.0	19.0	80.0	26.5
PS16	11.3	M	R	43.1	147.0	73.0	39.5	31.0	14.5	28.5	25.0	18.5	76.0	23.5
PS17	12.0	M	R	39.4	146.0	71.0	35.5	27.6	14.8	27.6	28.0	15.7	71.0	19.2
PS18	11.8	F	R	44.0	157.5	77.4	38.2	32.1	16.9	29.3	25.5	17.0	79.5	20.9
PS19	9.7	F	R	29.7	139.5	72.8	33.1	27.3	13.8	24.6	21.9	13.6	65.0	19.0
PS20	8.5	F	R	28.3	136.5	69.4	32.2	27.1	13.3	25.9	23.2	14.5	66.9	18.4
PS21	8.7	M	R	26.1	131.2	67.5	31.6	27.0	13.6	23.6	22.0	16.0	63.2	19.0
PS22	11.3	F	L	55.9	151.0	77.5	40.2	29.3	15.7	29.2	28.8	17.7	85.5	27.9
PS23	9.2	F	R	37.2	139.0	71.0	36.5	30.0	15.0	25.0	23.5	17.0	16.0	24.0
PS24	11.6	M	R	46.2	150.0	76.0	36.0	32.0	15.5	28.5	26.0	18.5	77.5	24.0
PS25	9.4	M	R	35.8	147.0	74.0	34.5	31.5	14.5	26.5	25.5	16.5	71.0	19.5
Avg	**11.0**			**42.7**	**148.4**	**74.8**	**36.7**	**30.6**	**15.3**	**27.5**	**24.9**	**17.3**	**72.8**	**22.4**
SD	**1.3**			**12.7**	**11.4**	**5.1**	**3.7**	**3.0**	**1.3**	**2.1**	**2.7**	**2.4**	**15.2**	**3.7**
LODC	**10.0**			**34.6**	**130.0**	**67.9**	**34.0**					**18.8**	**75.5**	

Table A2: Complete active assisted range of motion data

Subject	*Flexion (°)*	*Extension (°)*	*Abduction (°)*	*Internal Rotation (°)*	*External Rotation (°)*
PS01	155	74	160	100	76
PS02	142	76	136	97	87
PS03	175	50	180	92	95
PS04	168	61	166	100	105
PS05	189	62	188	94	115
PS06	182	64	178	83	110
PS07	165	58	152	90	102
PS08	170	54	168	98	118
PS09	150	64	160	70	96
PS10	159	76	164	69	117
PS11	173	58	183	58	84
PS12	169	80	175	66	105
PS13	191	81	185	70	113
PS14	168	74	188	85	80
PS15	184	93	190	133	103
PS16	201	66	195	97	105
PS17	176	55	189	61	98
PS18	167	85	192	71	100
PS19	176	74	192	66	109
PS20	183	90	194	56	101
PS21	189	89	195	94	109
PS22	193	86	193	73	108
PS23	177	73	181	83	97
PS24	190	44	186	73	100
PS25	169	56	176	77	95
Avg	**174**	**70**	**179**	**82**	**101**
SD	**14**	**14**	**15**	**18**	**11**

Appendix B: Non-normalized Acromion Relative to T1 Displacement Data

Table B1: Acromion relative to T1 non-normalized displacement (mm) in x direction from 90° load

Nominal Load (N)	0.0	25	50	75	100	125	150
Effective Load on R shoulder (N)	0.0	23.6	40.9	68.2	83.9	105.3	125.0
PS01	0.00	22.13	31.12	29.84	29.20	22.92	29.93
PS02	0.00	12.06	22.61	24.92	32.40	36.35	38.15
PS03	0.00	37.59	45.71	47.45	47.70	58.33	55.18
PS04	0.00	4.03	10.15	11.18	16.04	16.98	12.00
PS05	0.00	5.09	16.08	22.74	22.71	8.82	8.88
PS06	0.00	20.46	23.94	34.19	24.13	24.44	11.11
PS07	0.00	-1.32	17.14	18.83	26.50	28.25	28.18
PS08	0.00	8.63	17.55	23.68	24.66		
PS09	0.00	-2.67	15.73	17.29	19.32		
PS10	0.00	19.07	4.80	4.13	0.00		
PS11	0.00	-0.52	8.25	12.08	12.99		
PS12	0.00	30.19	26.61				
PS13	0.00	-7.37	8.62	27.56	32.64	27.90	17.48
PS14	0.00	-7.81	-5.07	9.36	7.10	2.77	3.86
PS15	0.00	21.58	40.64	38.34	33.06	24.36	23.68
PS16	0.00	15.68	26.76	50.30	44.90	53.51	48.63
PS17	0.00	22.14	23.56				
PS18	0.00	0.83	23.64	38.95	32.00	32.70	
PS19	0.00	28.17	30.12				
PS20	0.00	8.83	3.03	7.39			
PS21	0.00	6.26	13.19				
PS22	0.00	24.52	43.31	37.44			
PS23	0.00	10.18	8.79	14.81			
PS24	0.00	7.66	10.90	20.71	30.86		
PS25	0.00	18.42	29.36	18.58	21.03		
Avg	0.00	12.15	19.86	24.28	25.40	28.11	25.19
SD	0.00	12.09	12.74	13.02	11.92	16.07	16.74
Upper Corridor	0.00	24.24	32.60	37.30	37.32	44.18	41.93
Lower Corridor	0.00	0.07	7.12	11.25	13.49	12.04	8.45

Table B2: Acromion relative to T1 non-normalized displacement (mm) in z direction from 90° load

Nominal Load (N)	0.0	25	50	75	100	125	150
Effective Load on R shoulder (N)	0.0	23.6	40.9	68.2	83.9	105.3	125.0
PS01	0.00	7.05	1.45	1.43	2.06	-3.75	-4.93
PS02	0.00	-1.13	4.83	11.49	10.77	14.47	11.09
PS03	0.00	0.43	7.98	3.82	7.20	25.07	16.82
PS04	0.00	-5.54	-4.72	-0.22	0.51	6.34	0.24
PS05	0.00	1.61	3.70	4.79	5.95	3.18	10.46
PS06	0.00	13.87	7.79	3.59	2.26	-6.53	-7.65
PS07	0.00	-11.01	-6.34	-11.78	-6.89	-9.09	-12.69
PS08	0.00	3.37	-7.71	-6.05	-0.62		
PS09	0.00	-1.41	-1.74	-8.78	-4.50		
PS10	0.00	-4.63	-0.92	-9.74	0.00		
PS11	0.00	4.65	4.38	3.12	-4.05		
PS12	0.00	-25.64	-17.76	0.00	0.00		
PS13	0.00	7.76	-10.17	-16.12	-17.72	-13.35	-18.41
PS14	0.00	10.40	4.21	-2.86	-3.93	-6.08	-0.43
PS15	0.00	1.74	5.41	1.38	3.09	7.36	-4.89
PS16	0.00	6.00	5.09	0.74	-0.95	-0.03	7.22
PS17	0.00	-0.38	-1.25				
PS18	0.00	8.08	-11.20	-24.04	-11.11	-18.53	
PS19	0.00	-21.69	-18.07				
PS20	0.00	9.06	6.00	5.07			
PS21	0.00	2.87	1.67				
PS22	0.00	-8.13	-10.79	-11.30			
PS23	0.00	0.99	1.92	1.46			
PS24	0.00	0.63	2.10	2.12	19.86		
PS25	0.00	-16.58	-21.55	-16.54	-8.03		
Avg	0.00	-0.70	-2.23	-3.11	-0.32	-0.08	-0.29
SD	0.00	9.74	8.56	8.76	8.22	12.21	10.83
Upper Corridor	0.00	9.03	6.33	5.65	7.90	12.13	10.54
Lower Corridor	0.00	-10.44	-10.78	-11.87	-8.55	-12.29	-11.12

Table B3: Acromion relative to T1 non-normalized displacement (mm) in x direction from 135° load

Nominal Load (N)	0.0	17.7		35.4	53.0	70.7	88.4	106.1
Effective Load on R shoulder (N)	0.0	19.2		31.3	49.5	62.0	75.0	88.6
PS01	0.00	-12.99		-4.79				
PS02	0.00	9.58		7.12	15.73	12.71		
PS03	0.00	1.59		8.74	9.03	2.86		
PS04	0.00	26.23		23.50	26.24	17.73	19.96	16.24
PS05	0.00	4.59		13.19	14.45	13.57	17.69	15.41
PS06	0.00	-5.69		7.81	12.49	-6.99	-8.01	-4.07
PS07	0.00	-10.02		-4.80	1.65	12.96		
PS08	0.00	1.35		7.83	14.21			
PS09	0.00	-3.30		-6.06	2.30	-2.29		
PS10	0.00	7.62		4.86	10.57	6.66		
PS11	0.00	-11.15		-7.67	-3.38	-6.68	-0.88	-3.76
PS12	0.00	6.80		9.76	8.16			
PS13	0.00	-10.77		-6.82	29.11	25.36	30.63	
PS14	0.00	-6.57		0.67	1.20	-0.16	-2.56	-3.05
PS15	0.00	44.46		29.80	43.38	49.52	36.19	39.32
PS16	0.00	11.98		29.19	25.16	21.65	29.02	23.67
PS17	0.00	8.36		2.25	5.68			
PS18	0.00	2.70		-10.50	20.84	29.43	16.87	
PS19	0.00	19.58		21.50	23.73	29.07		
PS20	0.00	-9.94		-4.58	3.73			
PS21	0.00	9.72		7.22				
PS22	0.00	0.04		9.66	15.80	22.85	20.69	27.05
PS23	0.00	3.66		1.76	6.05	2.23		
PS24	0.00	-0.75		5.82	-0.79	7.68	10.49	8.14
PS25	0.00	4.42		4.94	10.15	8.59		
Avg	0.00	3.66		6.02	12.31	11.58	12.39	11.58
SD	0.00	12.87		11.04	11.31	14.64	13.07	13.24
Upper Corridor	0.00	16.53		17.05	23.62	26.22	25.45	24.82
Lower Corridor	0.00	-9.21		-5.02	1.01	-3.07	-0.68	-1.65

Table B4: Acromion relative to T1 non-normalized displacement (mm) in x direction from 135° load

Nominal Load (N)	0.0	17.7	35.4	53.0	70.7	88.4	106.1
Effective Load on R shoulder (N)	0.0	19.2	31.3	49.5	62.0	75.0	88.6
PS01	0.00	28.96	34.48				
PS02	0.00	19.38	17.94	33.18	30.44		
PS03	0.00	42.03	42.85	48.53	51.37		
PS04	0.00	34.27	42.57	51.80	46.39	57.68	53.25
PS05	0.00	22.44	40.18	43.89	42.49	43.08	42.55
PS06	0.00	11.75	24.31	35.60	12.05	11.71	22.11
PS07	0.00	18.77	18.58	31.78	35.09		
PS08	0.00	50.61	50.12	44.88			
PS09	0.00	16.82	15.02	15.89	18.24		
PS10	0.00	23.53	26.42	21.23	22.35		
PS11	0.00	29.97	33.85	37.14	39.99	41.83	43.03
PS12	0.00	55.44	53.01	50.48			
PS13	0.00	21.74	53.42	25.67	29.75	32.73	
PS14	0.00	33.50	42.49	41.93	52.22	42.57	44.74
PS15	0.00	31.68	25.42	36.54	40.00	35.97	40.51
PS16	0.00	35.27	47.64	40.96	37.84	50.76	50.36
PS17	0.00	28.65	41.04	45.82			
PS18	0.00	-12.28	21.62	15.25	16.50	22.25	
PS19	0.00	32.35	26.02	34.28	35.47		
PS20	0.00	52.25	56.60	49.22			
PS21	0.00	39.68	44.98				
PS22	0.00	40.89	44.01	36.25	35.84	31.78	25.64
PS23	0.00	54.28	58.09	57.13	54.75		
PS24	0.00	23.12	38.21	48.09	53.29	64.60	62.24
PS25	0.00	43.20	41.12	44.76	44.76		
Avg	0.00	31.13	37.60	38.55	36.74	38.11	40.01
SD	0.00	15.10	12.67	11.02	12.24	13.34	10.63
Upper Corridor	0.00	46.23	50.27	49.57	48.98	51.46	50.64
Lower Corridor	0.00	16.03	24.93	27.53	24.51	24.77	29.38

Appendix C: Volunteer Displacement and Stiffness Data

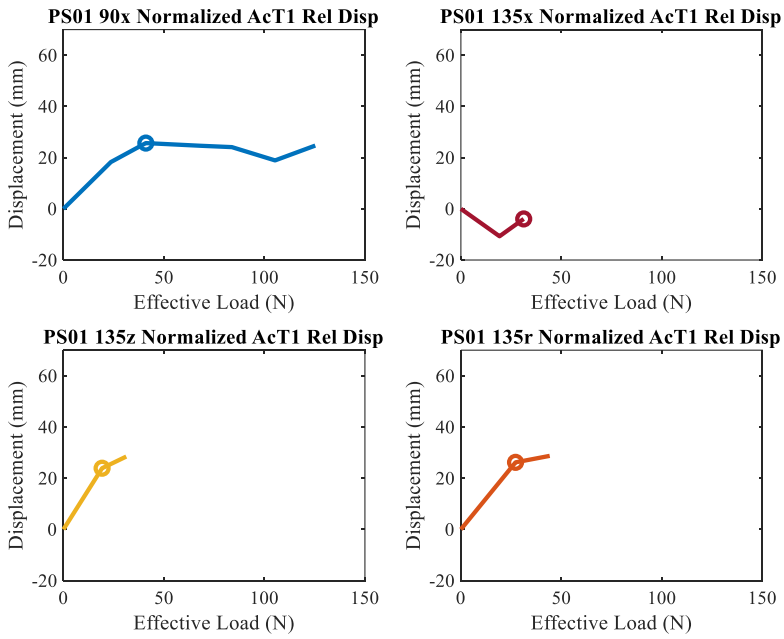

Figure C1: PS01 normalized displacement by component with marker at cut for stiffness

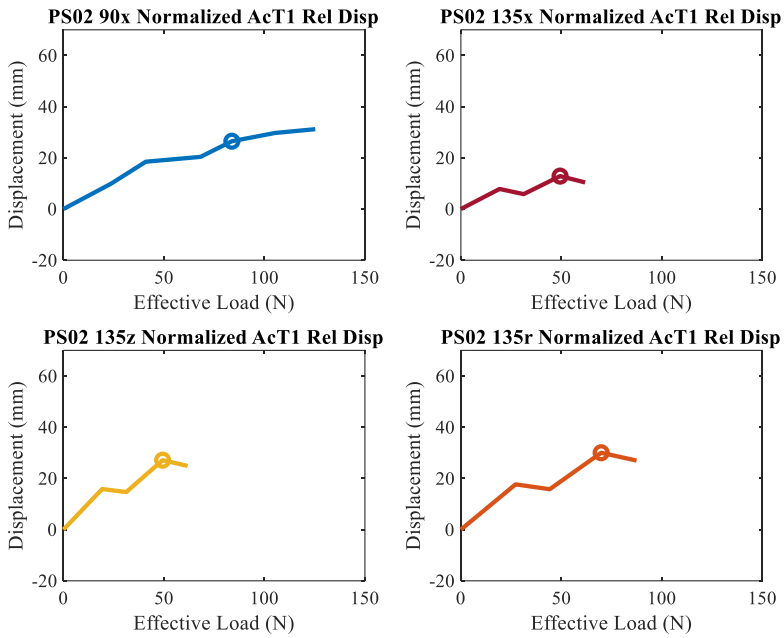

Figure C2: PS02 normalized displacement by component with marker at cut for stiffness

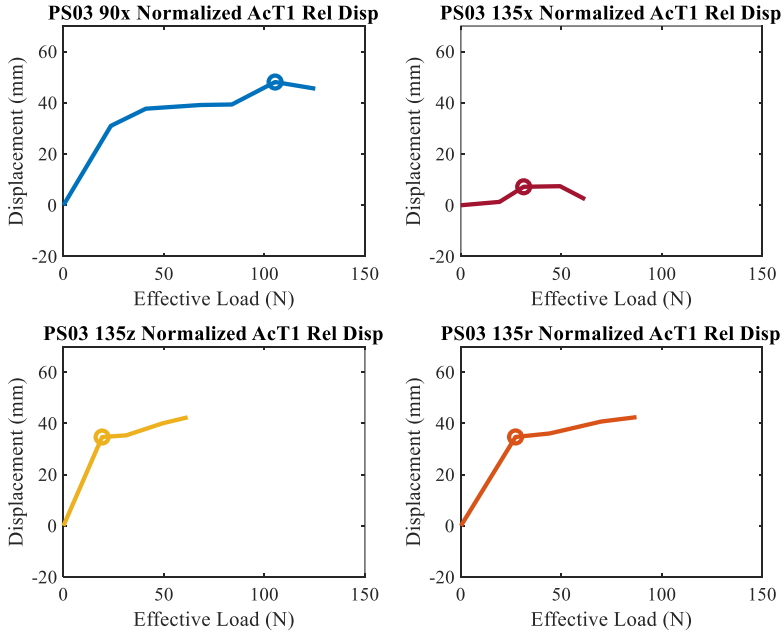

Figure C3: PS03 normalized displacement by component with marker at cut for stiffness

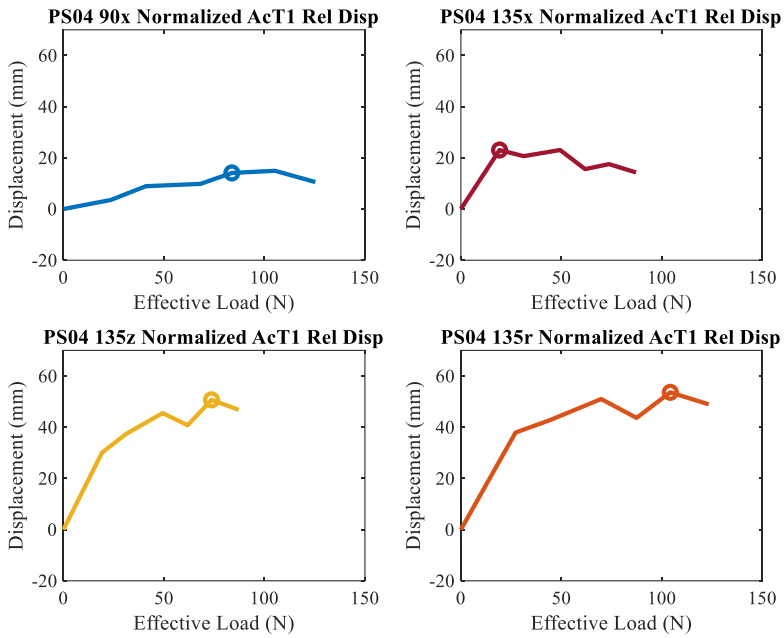

Figure C4: PS04 normalized displacement by component with marker at cut for stiffness

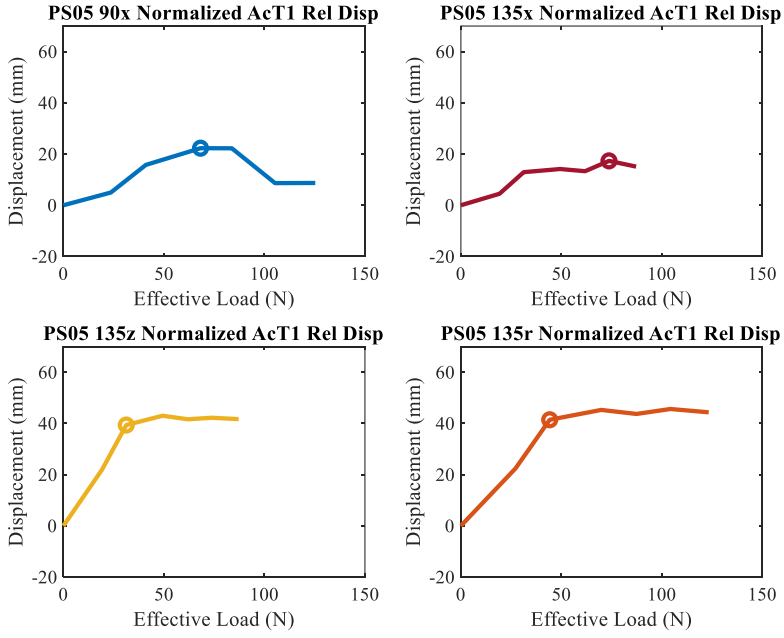

Figure C5: PS05 normalized displacement by component with marker at cut for stiffness

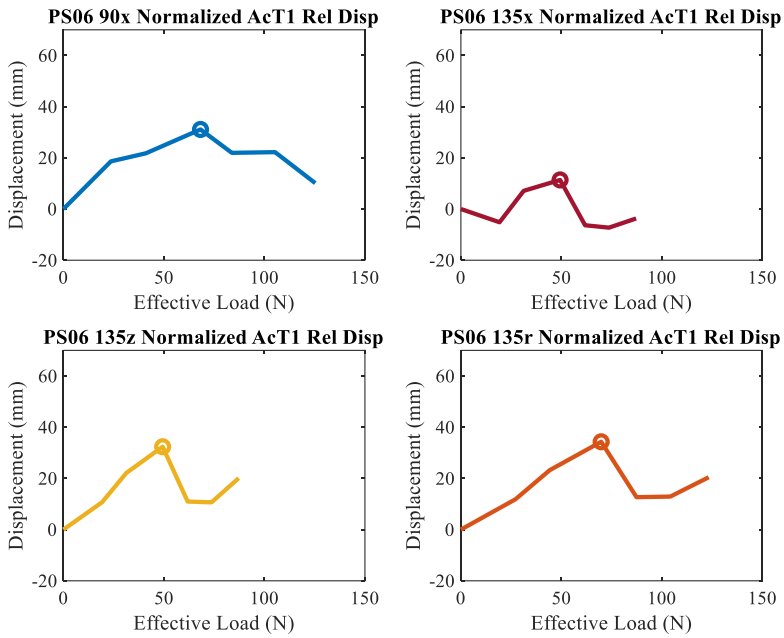

Figure C6: PS06 normalized displacement by component with marker at cut for stiffness

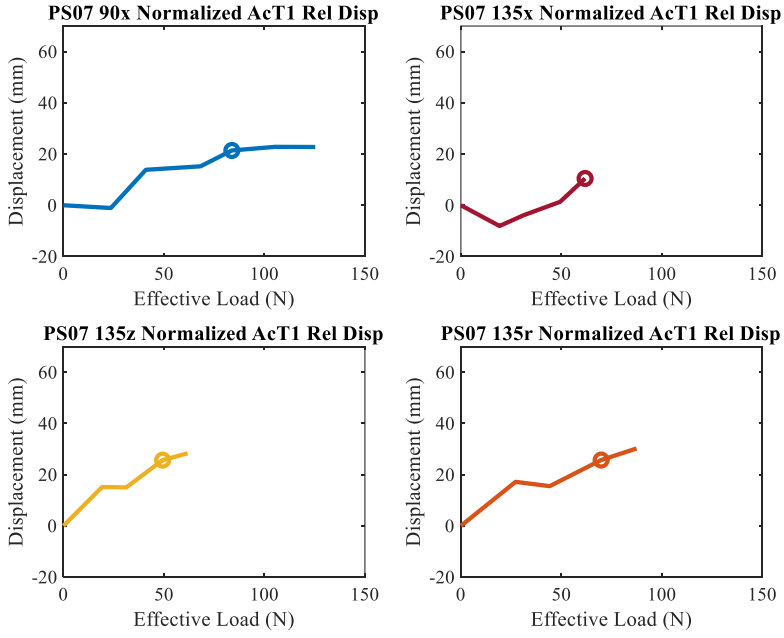

Figure C7: PS07 normalized displacement by component with marker at cut for stiffness

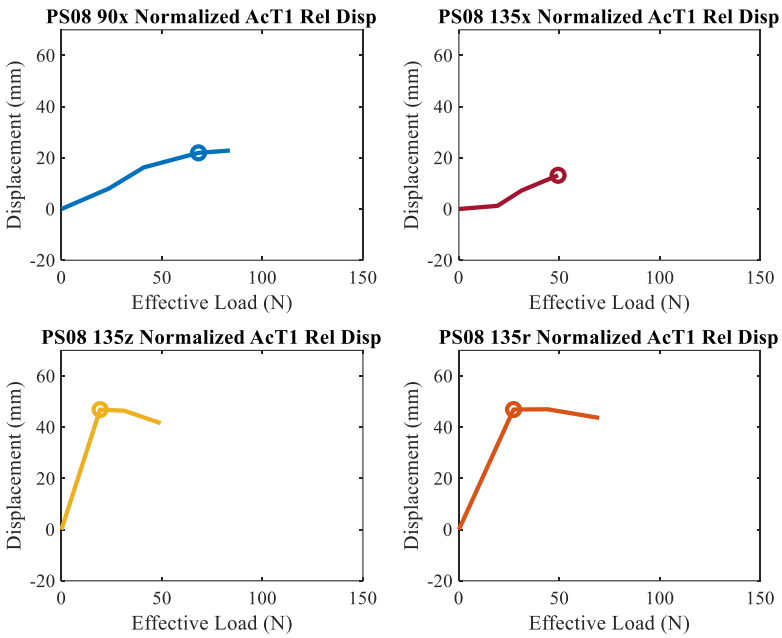

Figure C8: PS08 normalized displacement by component with marker at cut for stiffness

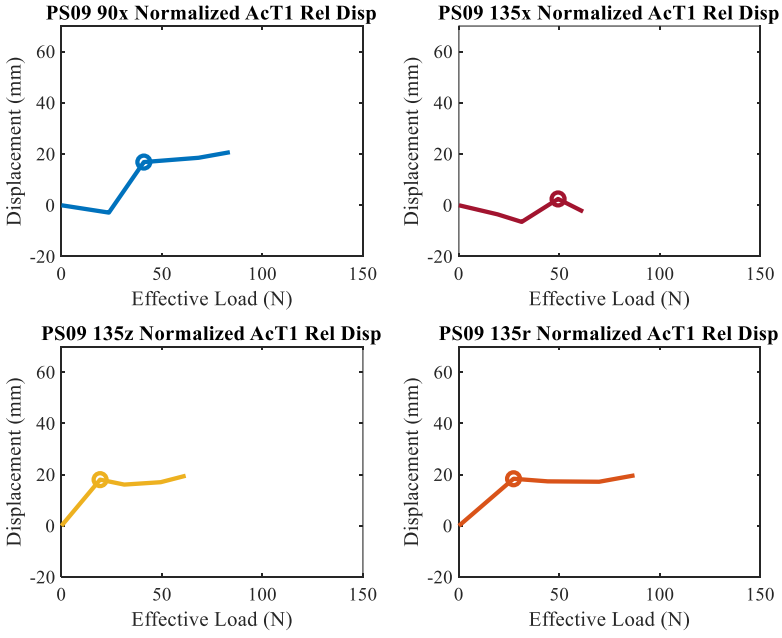

Figure C9: PS09 normalized displacement by component with marker at cut for stiffness

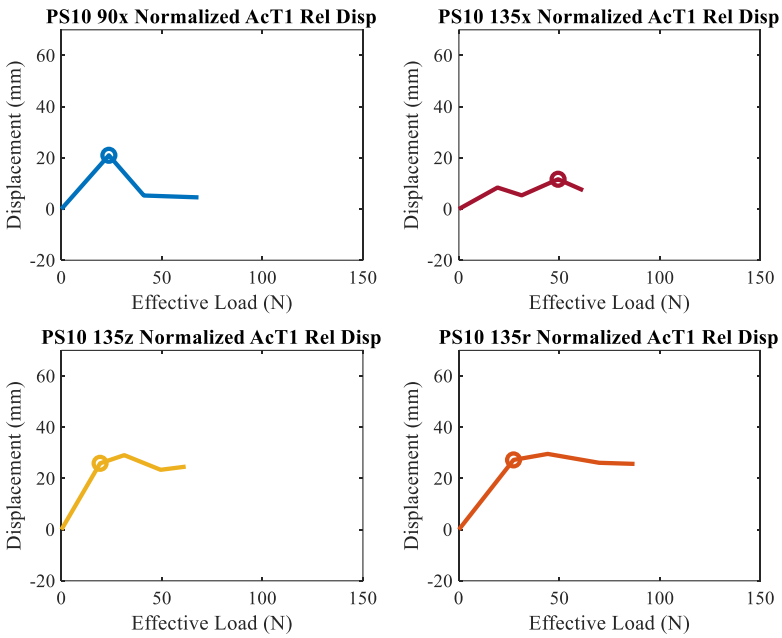

Figure C10: PS10 normalized displacement by component with marker at cut for stiffness

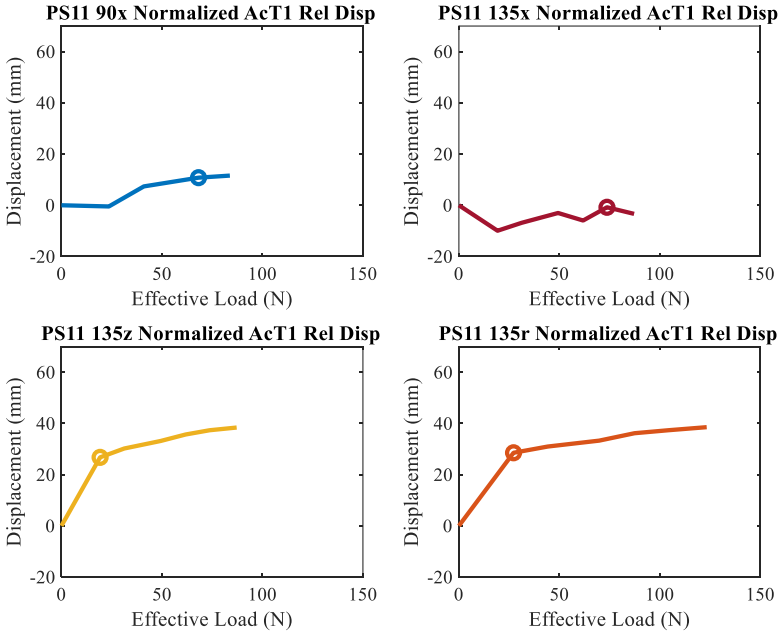

Figure C11: PS11 normalized displacement by component with marker at cut for stiffness

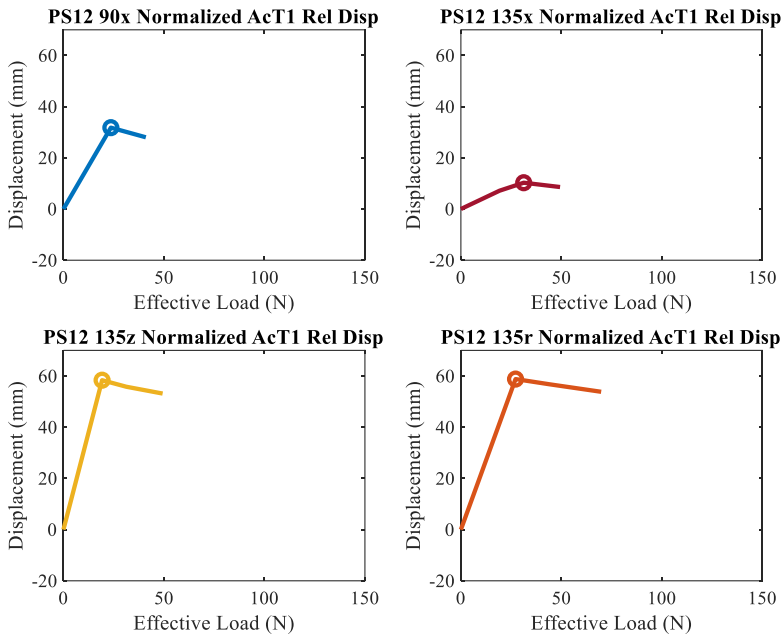

Figure C12: PS12 normalized displacement by component with marker at cut for stiffness

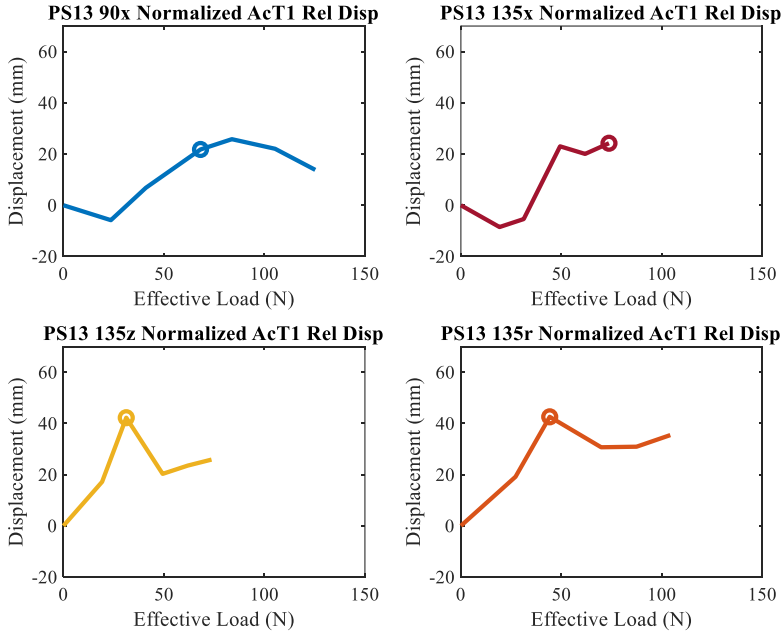

Figure C13: PS13 normalized displacement by component with marker at cut for stiffness

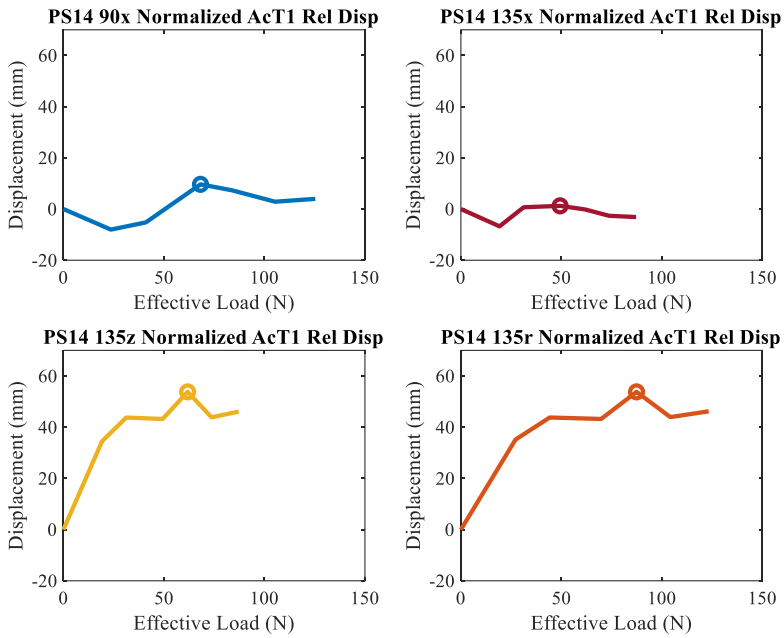

Figure C14: PS14 normalized displacement by component with marker at cut for stiffness

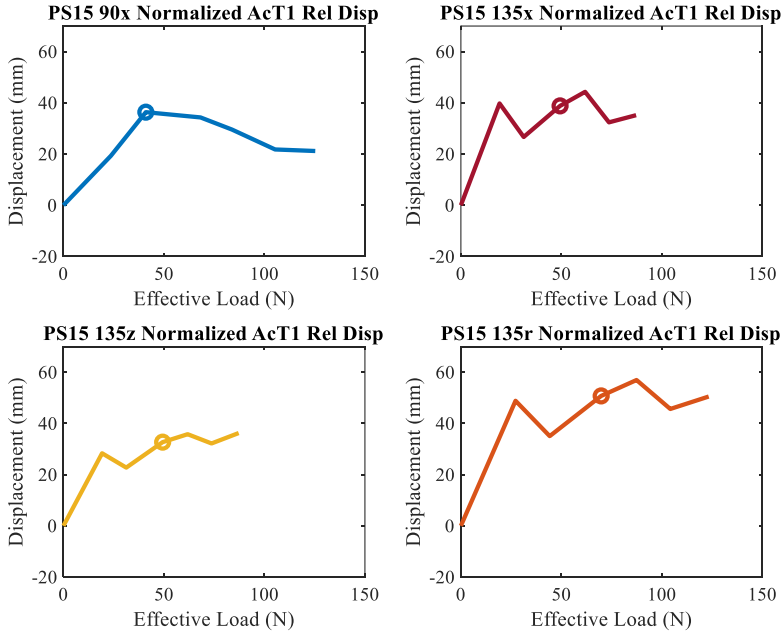

Figure C15: PS15 normalized displacement by component with marker at cut for stiffness

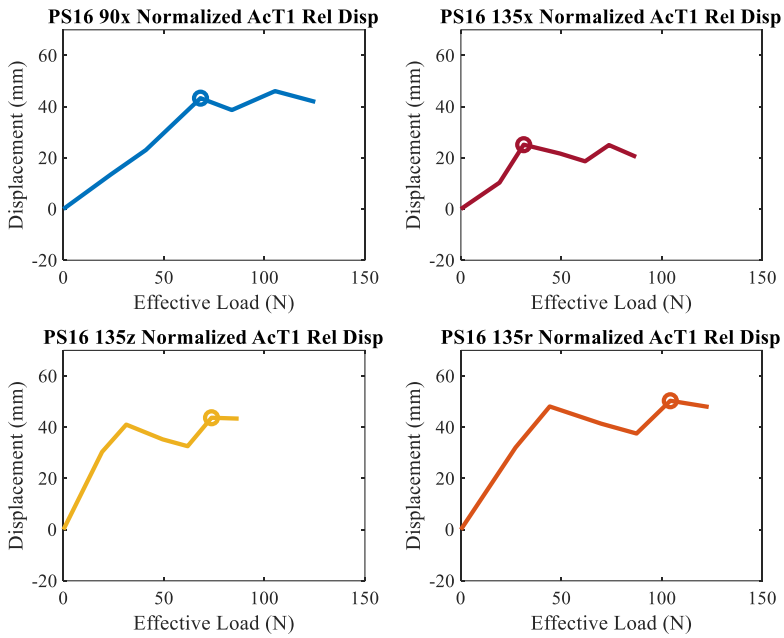

Figure C16: PS16 normalized displacement by component with marker at cut for stiffness

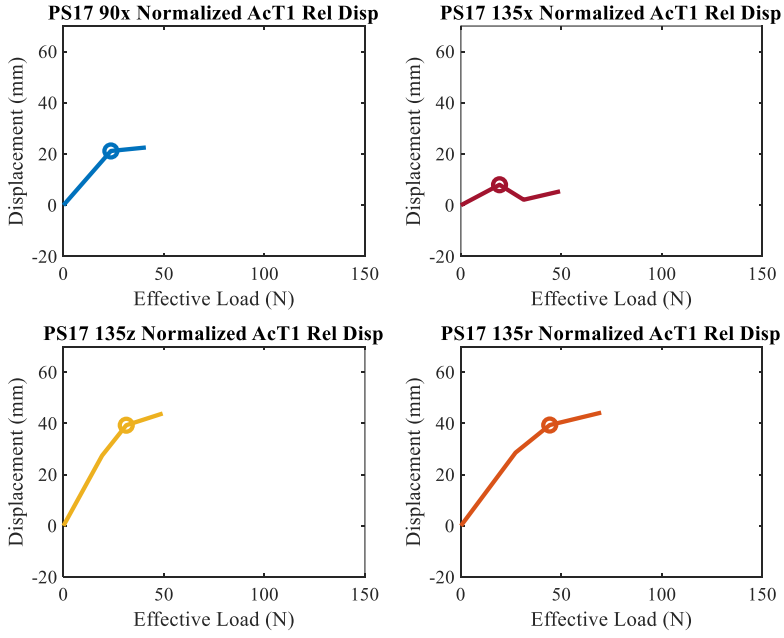

Figure C17: PS17 normalized displacement by component with marker at cut for stiffness

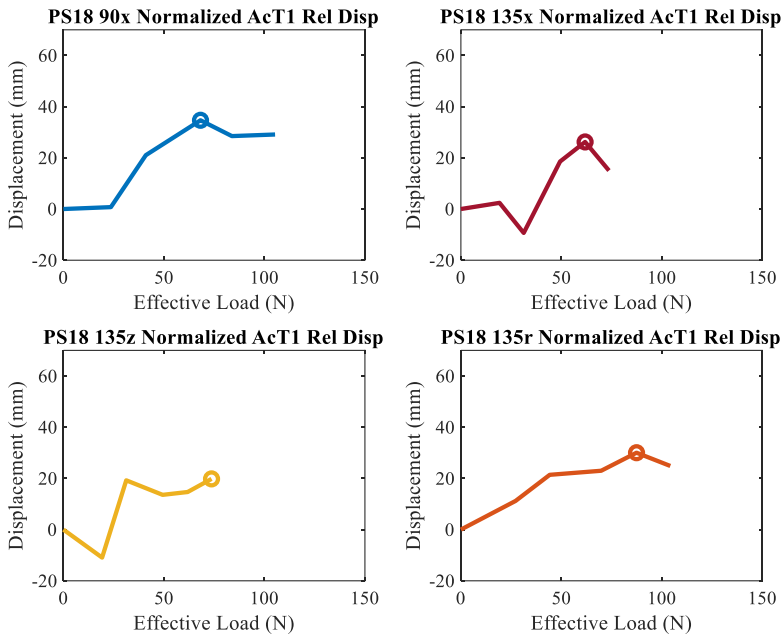

Figure C18: PS18 normalized displacement by component with marker at cut for stiffness

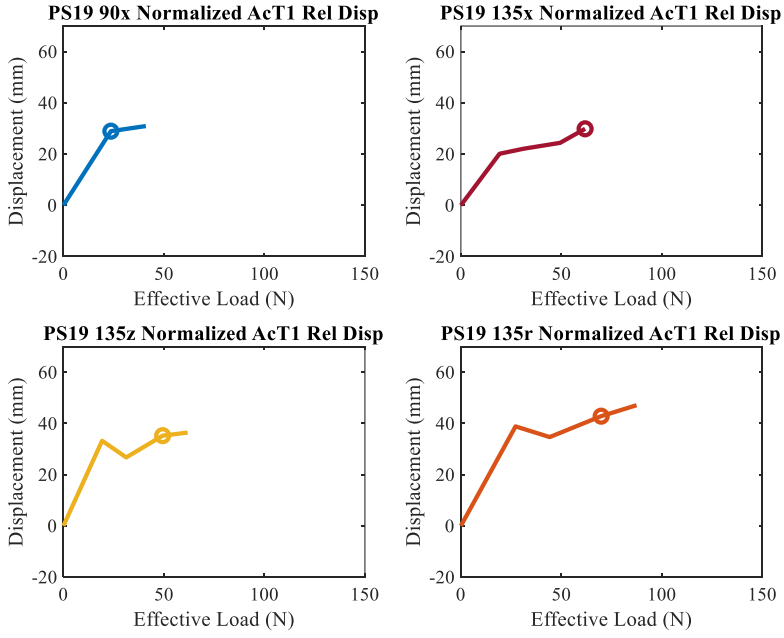

Figure C19: PS19 normalized displacement by component with marker at cut for stiffness

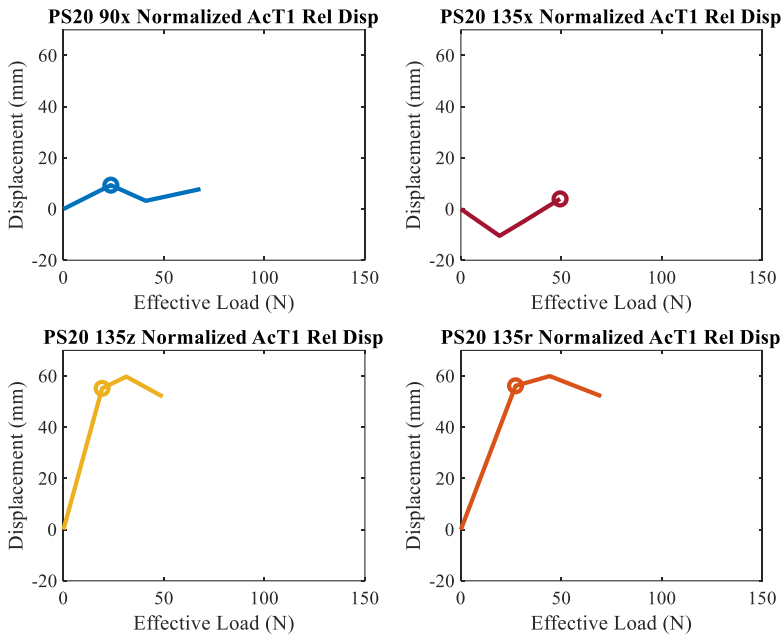

Figure C20: PS20 normalized displacement by component with marker at cut for stiffness

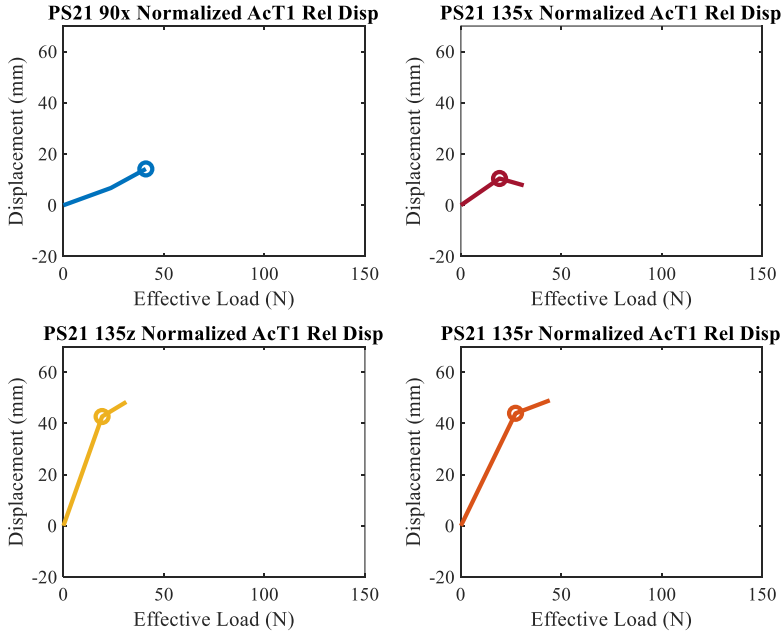

Figure C21: PS21 normalized displacement by component with marker at cut for stiffness

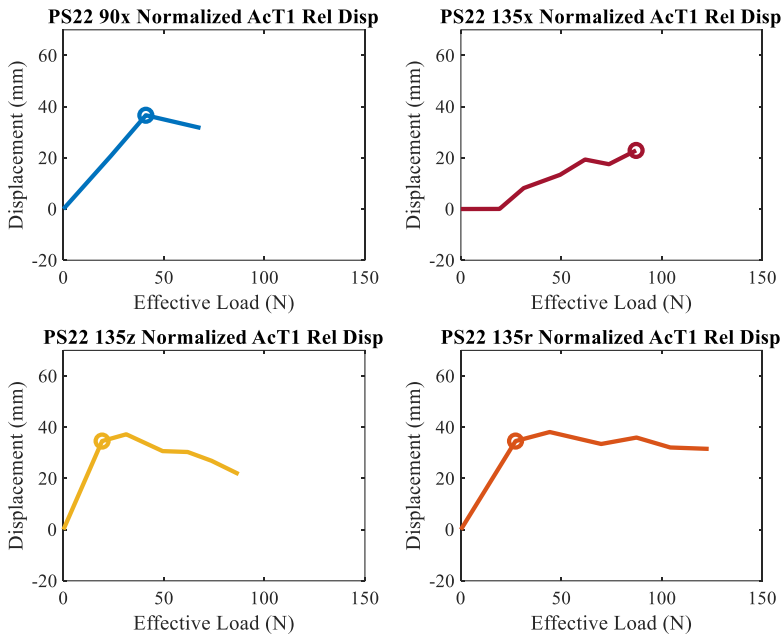

Figure C22: PS22 normalized displacement by component with marker at cut for stiffness

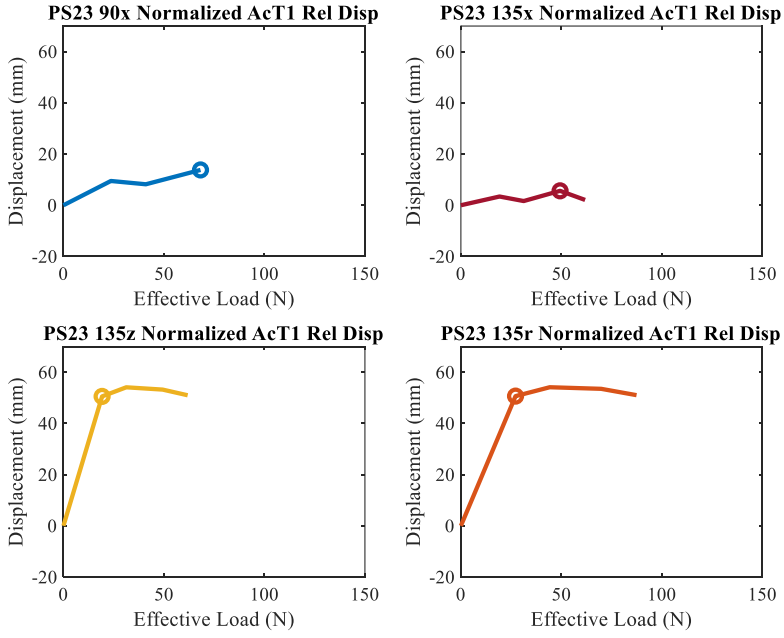

Figure C23: PS23 normalized displacement by component with marker at cut for stiffness

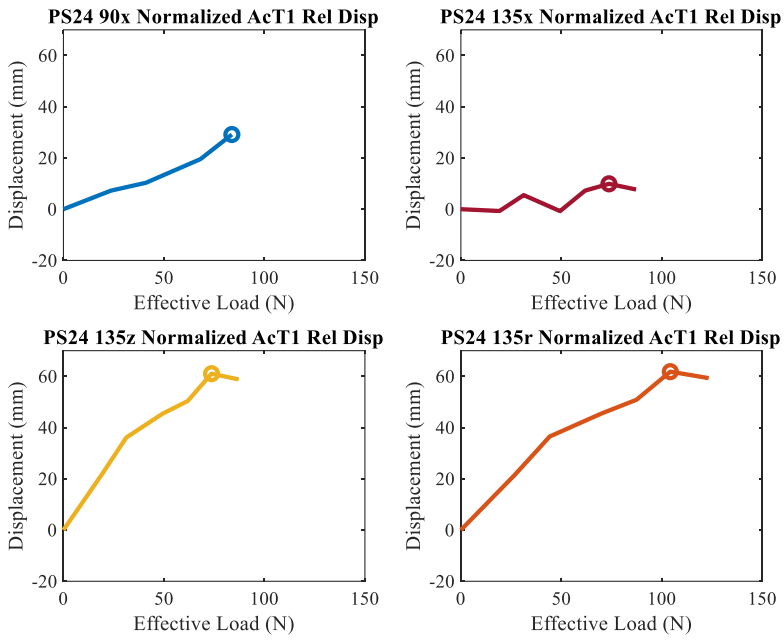

Figure C24: PS24 normalized displacement by component with marker at cut for stiffness

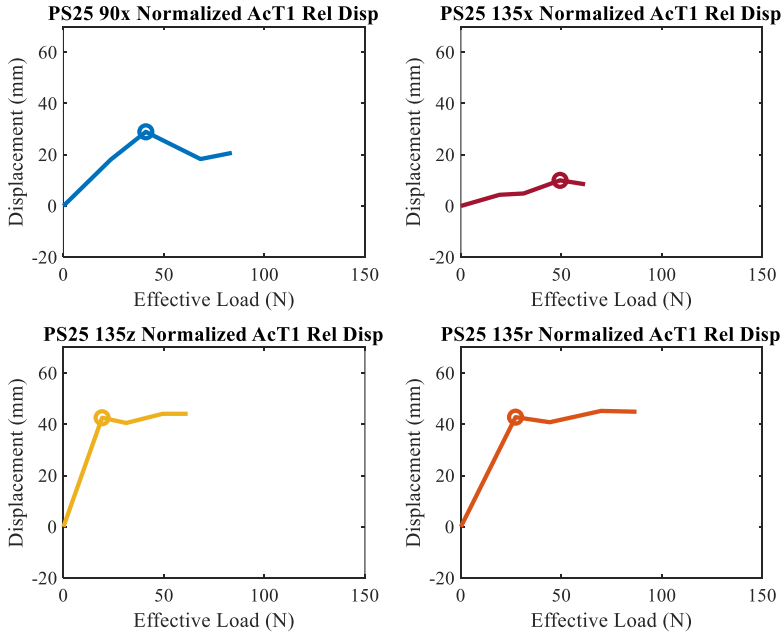

Figure C25: PS25 normalized displacement by component with marker at cut for stiffness

Table C1: Stiffnesses by direction for all volunteers

Subject	Direction of Stiffness (N/mm)			
	90x	**135x**	**135z**	**135r**
PS01	1.58	-6.00	0.80	1.04
PS02	3.38	4.23	1.95	2.50
PS03	2.73	4.64	0.55	0.78
PS04	6.25	0.83	1.71	2.39
PS05	2.90	4.48	0.80	1.08
PS06	2.30	3.67	1.49	2.00
PS07	3.67	5.38	2.04	2.92
PS08	3.03	3.59	0.41	0.58
PS09	2.63	32.65	1.07	1.48
PS10	1.12	4.79	0.74	1.00
PS11	5.65	62.08	0.72	0.95
PS12	0.74	3.00	0.33	0.46
PS13	2.84	2.19	0.76	1.06
PS14	6.63	17.64	1.30	1.85
PS15	1.13	1.46	1.66	1.55
PS16	1.58	1.28	2.28	2.72
PS17	1.11	2.40	0.79	1.10
PS18	1.81	2.23	3.12	3.04
PS19	0.82	2.36	1.54	1.75
PS20	2.53	10.27	0.35	0.48
PS21	2.92	1.84	0.45	0.62
PS22	1.12	3.50	0.56	0.79
PS23	5.44	10.06	0.38	0.54
PS24	3.02	8.13	1.28	1.79
PS25	1.41	5.17	0.45	0.64
Avg	**2.73**	**7.67**	**1.10**	**1.40**
SD	**1.69**	**13.36**	**0.72**	**0.81**
LODC	**4.28**	**4.07**	**3.25**	**4.18**

Appendix D: Load Cell Data

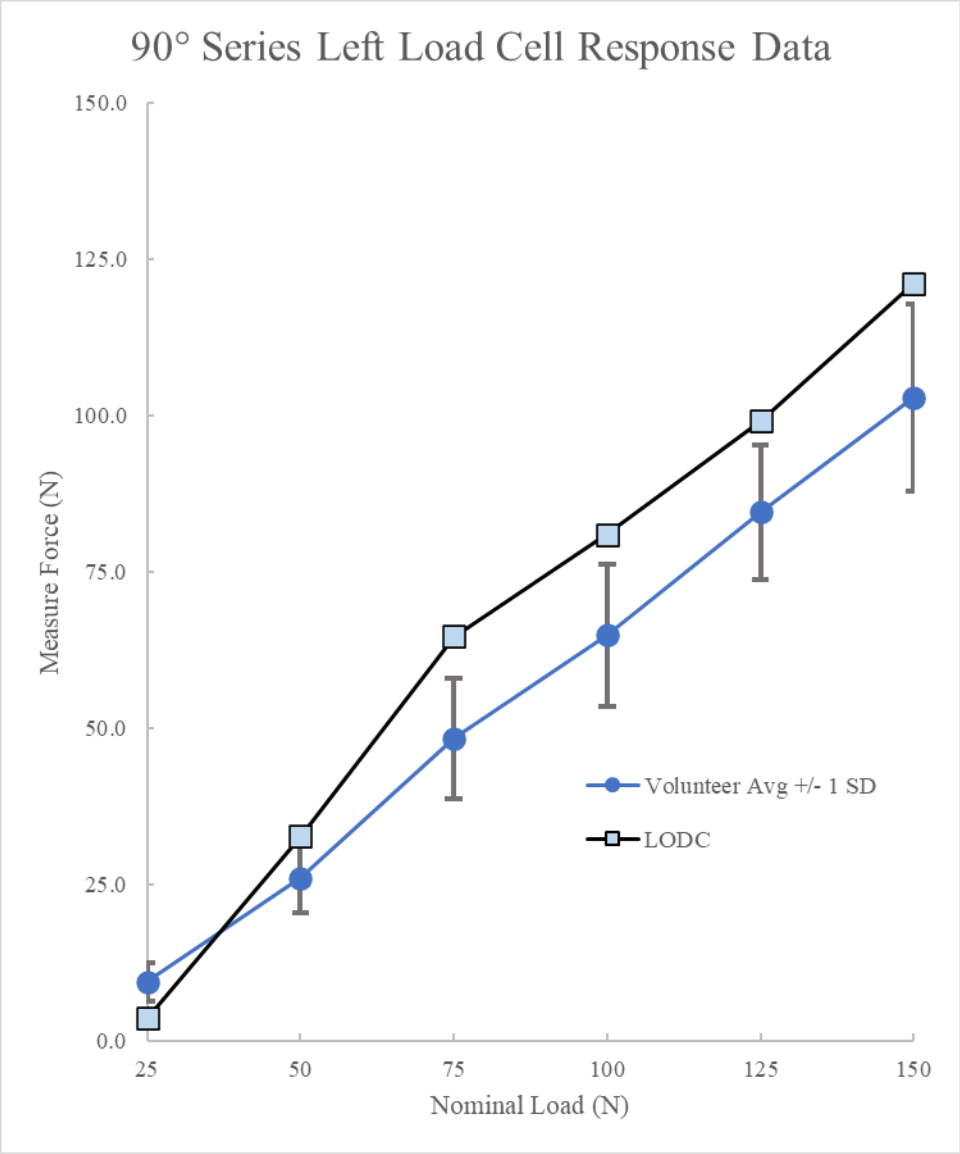

Figure D1: Left load cell measured force for 90° series across nominal loads

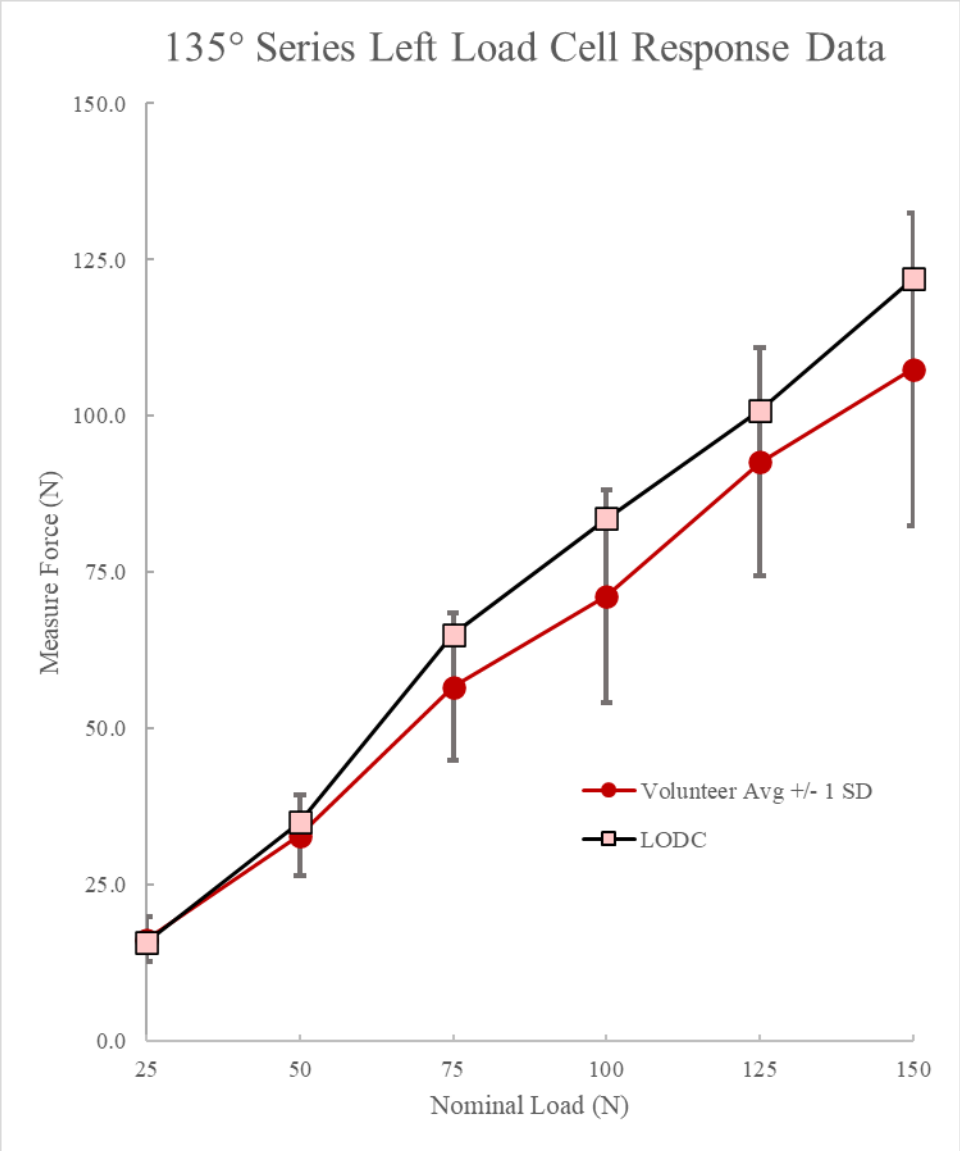

Figure D2: Left load cell measured force for 135° series across nominal loads

Table D1: Right load cell measured force for 90° series across nominal loads

Subject	Nominal Load (N)					
	25	**50**	**75**	**100**	**125**	**150**
PS01	17.87	34.17	67.71	88.13	108.69	131.66
PS02	11.84	30.77	32.05	69.91	83.45	116.31
PS03	22.37	48.95	65.45	78.76	104.09	127.48
PS04	14.47	18.14	54.79	67.32	92.21	116.17
PS05	16.45	26.87	51.25	50.48	99.47	124.11
PS06	14.68	33.11	56.15	60.55	92.24	123.08
PS07	9.57	32.90	51.68	70.33	92.45	125.49
PS08	9.35	32.09	41.08	66.58		
PS09	6.28	25.06	53.72	63.99		
PS10	12.23	34.04	46.86			
PS11	10.23	26.77	50.13	63.66		
PS12	12.71	34.47				
PS13	8.65	29.28	55.26	61.84	86.29	109.51
PS14	2.98	21.13	34.67	68.56	81.67	74.37
PS15	5.39	29.35	58.70	83.59	123.64	121.24
PS16	9.36	22.69	51.47	84.79	101.45	124.99
PS17	7.80	22.33				
PS18	9.50	29.85	59.48	70.54	93.94	
PS19	11.34	32.40				
PS20	11.41	29.28	57.43			
PS21	8.86	32.90				
PS22	11.34	22.26	59.27			
PS23	9.50	29.85	63.24			
PS24	10.71	26.94	62.18	78.84		
PS25	9.07	27.51	48.28	84.01		
Avg	**10.96**	**29.32**	**53.37**	**71.29**	**96.63**	**117.67**
SD	**4.04**	**6.10**	**9.23**	**10.28**	**11.79**	**15.61**
LODC	**3.88**	**35.63**	**65.23**	**83.11**	**101.22**	**122.40**

Table D2: Right load cell measured force for 135° series across nominal loads

Subject	Nominal Load (N)					
	25	**50**	**75**	**100**	**125**	**150**
PS01	26.02	31.98				
PS02	25.45	33.04	65.86	65.58		
PS03	28.24	38.85	38.49	25.14		
PS04	25.11	45.35	71.58	77.75	84.18	87.91
PS05	26.52	42.54	71.25	71.46	78.84	81.39
PS06	12.41	42.68	57.21	89.61	110.17	129.10
PS07	19.64	43.04	64.37	62.81		
PS08	25.85	41.87	50.17			
PS09	21.46	43.25	67.51	75.14		
PS10	23.47	44.24	71.04	84.97		
PS11	18.63	45.53	70.60	85.76	112.03	139.43
PS12	15.62	38.89	72.71			
PS13	22.60	38.14	61.23	85.66		
PS14	18.65	39.35	68.42	90.68	109.11	128.46
PS15	24.39	38.85	70.61	90.75	111.59	129.81
PS16	11.27	32.26	61.18	79.62	104.36	122.93
PS17	13.97	42.25	61.61			
PS18	17.58	35.31	63.10	86.64	106.63	
PS19	15.95	36.44	66.86	84.72		
PS20	18.50	36.37	66.08			
PS21	19.28	37.01				
PS22	17.37	39.91	63.10	88.12	104.50	122.51
PS23	14.89	36.09	69.55	85.29		
PS24		12.83	33.53	61.40	86.71	102.09
PS25	15.60	33.89	65.37	83.73		
Avg	**19.94**	**38.00**	**63.11**	**77.62**	**100.81**	**115.96**
SD	**4.88**	**6.61**	**10.05**	**15.70**	**12.55**	**20.43**
LODC	**14.98**	**37.48**	**70.12**	**89.68**	**105.00**	**126.98**

Table D3: Right load cell measured force for 170° series across nominal loads

Subject	Nominal Load (N)					
	50	**100**	**150**	**200**	**250**	**300**
PS01	14.53	17.58	17.44			
PS02	14.25	16.31				
PS03	18.47	16.26				
PS04	16.67	21.50	21.61	22.11	22.00	24.53
PS05						
PS06	14.75					
PS07	13.12					
PS08						
PS09	21.55	30.42	67.02	77.60		
PS10	11.73	29.72	53.26	65.72		
PS11	11.73	33.26	57.41	72.72	98.89	104.97
PS12	17.39	34.23	64.43	79.46		
PS13	-0.48	14.35	28.09	54.86	64.43	89.71
PS14	4.89	22.55	55.58	79.55	94.65	117.90
PS15	2.62	27.44	58.56	77.70	99.89	115.35
PS16	7.94	30.49	60.47	84.44	96.99	119.53
PS17			58.56			
PS18	9.57	34.03	63.03	77.49	87.13	
PS19	11.49	33.39	62.96	81.46	99.40	
PS20	9.85	27.58				
PS21	8.08	32.33	58.42	70.19		
PS22	7.30	31.69	62.46	79.55	103.08	120.60
PS23	10.07	30.98	63.88	78.20	100.25	119.96
PS24	13.26	34.53	62.74		101.45	116.98
PS25	11.20	29.28	63.03	77.84	99.33	124.92
Avg	**11.36**	**27.40**	**54.39**	**71.93**	**88.96**	**105.45**
SD	**5.16**	**6.75**	**15.22**	**15.60**	**23.55**	**30.18**
LODC	**16.91**	**36.43**	**64.04**	**85.93**	**99.50**	**124.16**

Table D4: Left load cell measured force for 90° series across nominal loads

Subject	Nominal Load (N)					
	25	**50**	**75**	**100**	**125**	**150**
PS01	10.92	26.75	45.48	60.73	80.35	101.66
PS02	9.54	25.59	23.23	55.29	66.52	89.93
PS03	15.59	31.11	46.62	58.28	81.99	106.46
PS04	13.20	12.83	44.86	62.07	80.25	101.34
PS05	11.95	19.26	45.70	40.13	86.54	102.50
PS06	14.71	24.70	45.52	50.25	78.38	104.07
PS07	8.07	21.80	42.13	57.25	76.33	108.93
PS08	9.16	27.21	40.54	62.55		
PS09	6.98	29.25	56.68	68.59		
PS10	12.34	35.98	46.42			
PS11	10.50	26.86	53.84	71.13		
PS12	14.16	36.74				
PS13	11.74	31.47	57.09	68.90	98.91	119.90
PS14	2.67	19.47	29.77	59.31	77.41	65.82
PS15	5.61	32.04	55.04	84.05	104.72	117.96
PS16	5.26	16.89	45.77	77.67	94.87	113.99
PS17	6.28	20.45				
PS18	9.49	31.24	57.95	71.92	88.46	
PS19	8.91	27.50				
PS20	8.69	26.51	54.68			
PS21	7.84	29.16				
PS22	8.51	23.26	57.89			
PS23	7.98	27.63	63.23			
PS24	8.69	22.95	55.61	75.40		
PS25	7.49	25.45	48.53	79.63		
Avg	**9.45**	**26.08**	**48.41**	**64.89**	**84.56**	**102.96**
SD	**3.11**	**5.68**	**9.60**	**11.35**	**10.72**	**14.95**
LODC	**3.61**	**32.69**	**64.68**	**81.02**	**99.13**	**121.20**

Table D5: Left load cell measured force for 135° series across nominal loads

Subject	Nominal Load (N)					
	25	**50**	**75**	**100**	**125**	**150**
PS01	17.88	21.13				
PS02	18.55	28.85	53.64	53.37		
PS03	19.01	25.27	26.00	21.20		
PS04	16.55	29.84	54.72	52.94	62.25	69.15
PS05	20.73	29.56	56.00	62.96	59.70	65.32
PS06	7.36	30.94	40.66	67.15	90.87	105.23
PS07	13.47	34.73	54.89	54.17		
PS08	16.94	28.50	36.41			
PS09	17.91	41.12	64.90	72.59		
PS10	22.32	43.75	68.02	80.35		
PS11	20.83	39.77	65.80	80.86	103.92	131.51
PS12	12.73	34.47	66.11			
PS13	21.25	38.36	57.48	80.99		
PS14	15.46	36.18	65.60	86.05	106.15	126.34
PS15	17.02	34.36	68.23	87.97	109.45	127.32
PS16	10.83	29.01	53.43	74.82	97.37	115.15
PS17	12.43	38.99	60.25			
PS18	19.65	35.47	63.81	85.61	105.84	
PS19	13.10	32.31	60.92	81.06		
PS20	12.97	34.98	63.95			
PS21	16.67	35.20				
PS22	17.11	37.08	61.76	86.76	104.81	125.18
PS23	16.18	36.72	66.22	81.86		
PS24		14.26	32.58	60.38	86.54	101.96
PS25	14.08	31.91	62.30	81.55		
Avg	**16.29**	**32.91**	**56.68**	**71.19**	**92.69**	**107.46**
SD	**3.64**	**6.41**	**11.84**	**17.00**	**18.21**	**24.95**
LODC	**15.91**	**35.07**	**65.03**	**83.58**	**100.98**	**121.95**

Table D6: Left load cell measured force for 170° series across nominal loads

Subject	Nominal Load (N)					
	50	**100**	**150**	**200**	**250**	**300**
PS01	10.66	12.13	9.99			
PS02	12.40	12.40				
PS03	11.43	12.08				
PS04	13.17	15.22	16.05	15.82	15.69	19.17
PS05						
PS06	13.02					
PS07	9.01					
PS08						
PS09	16.85	25.83	59.52	72.72		
PS10	16.69	32.18	61.66	73.95		
PS11	15.58	31.09	52.85	68.28	93.09	123.20
PS12	15.32	29.99	62.19	75.89		
PS13	-0.27	16.18	31.47	61.43	74.01	99.13
PS14	5.97	21.61	55.53	78.56	97.33	117.56
PS15	7.04	26.92	58.56	75.58	96.70	118.63
PS16	5.08	24.73	53.52	78.61	93.05	120.23
PS17			57.93			
PS18	10.03	29.90	58.38	76.02	82.04	
PS19	6.24	27.58	57.40	77.98	96.26	
PS20	10.16	28.12				
PS21	9.36	31.86	58.82	72.10		
PS22	8.20	28.97	53.07	75.71	95.99	113.55
PS23	13.15	29.63	63.59	81.46	103.79	122.95
PS24	10.03	29.77	57.98		97.15	113.23
PS25	13.24	29.50	62.88	77.49	95.72	117.60
Avg	**10.56**	**24.78**	**51.74**	**70.77**	**86.73**	**106.52**
SD	**4.17**	**7.11**	**15.78**	**15.95**	**23.70**	**31.46**
LODC	**12.91**	**33.57**	**62.12**	**84.81**	**101.07**	**123.58**

Table D7: Chest plate *Fx* for 90° series across nominal loads

Subject	Nominal Load (N)					
	25	**50**	**75**	**100**	**125**	**150**
PS01	22.02	52.30	62.38	99.93	107.99	172.89
PS02	4.39	51.00	54.94	127.85	153.95	193.38
PS03	9.70	50.08	70.72	99.04	143.55	211.11
PS04	18.21	42.29	126.77	148.44	171.56	236.00
PS05	17.06	41.27	80.01	76.44	137.37	133.44
PS06	4.50	41.92	98.62	111.36	148.20	194.19
PS07	-6.01	12.25	8.90	30.85	-1.65	140.68
PS08	10.22	43.20	37.37	81.52		
PS09	6.53	38.08	103.54	106.82		
PS10	17.29	83.23	118.35			
PS11	11.48	31.66	74.62	96.03		
PS12	31.90	57.23				
PS13	2.56	46.90	98.48	118.15	158.17	203.35
PS14	-0.07	15.17	51.29	78.32	93.75	95.30
PS15	8.61	43.49	28.46	109.88	173.85	194.34
PS16	19.08	54.86	82.12	101.33	156.96	173.89
PS17	14.28	59.83				
PS18	1.12	0.95	10.93	13.80	44.21	
PS19	36.31	72.76				
PS20	8.39	43.15	82.18			
PS21	18.42	54.67				
PS22	40.08	84.40	115.88			
PS23	12.57	26.33	53.31			
PS24	6.22	20.11	64.03	88.90		
PS25	13.76	57.55	73.55	125.01		
Avg	**13.14**	**44.99**	**71.26**	**94.92**	**123.99**	**177.14**
SD	**11.04**	**20.16**	**33.00**	**33.20**	**54.25**	**40.15**
LODC	**6.33**	**54.29**	**105.36**	**135.52**	**169.82**	**204.53**

Table D8: Chest plate *Fx* for 135° series across nominal loads

Subject	Nominal Load (N)					
	25	**50**	**75**	**100**	**125**	**150**
PS01	8.98	14.91				
PS02	1.84	20.86	48.83	47.07		
PS03	-0.66	4.46	7.45	11.03		
PS04	13.11	29.78	54.72	67.47	65.44	72.86
PS05	10.88	34.42	56.96	54.82	60.64	71.12
PS06	-6.04	12.37	23.30	50.20	74.54	97.42
PS07	-4.58	-1.97	36.24	39.80		
PS08	7.88	24.79	37.85			
PS09	14.27	34.42	62.74	75.65		
PS10	10.90	18.35	51.12	56.80		
PS11	7.64	15.59	34.74	45.76	71.68	96.80
PS12	6.48	20.14	79.43			
PS13	-0.38	10.45	65.30	74.39		
PS14	-0.01	14.99	43.65	76.73	97.23	116.20
PS15	17.37	21.13	64.46	87.69	121.14	125.75
PS16	0.85	13.43	26.89	44.03	63.91	89.56
PS17	3.04	22.83	38.30			
PS18	2.00	2.85	7.37	8.51	5.20	
PS19	17.06	36.82	61.77	87.08		
PS20	21.72	26.38	47.74			
PS21	8.66	27.87				
PS22	7.94	40.48	63.10	91.68	100.80	117.34
PS23	4.63	16.54	47.89	80.56		
PS24		0.26	10.98	40.08	73.82	84.40
PS25	19.84	33.34	60.46	68.66		
Avg	**7.22**	**19.82**	**44.84**	**58.32**	**73.44**	**96.83**
SD	**7.51**	**11.57**	**19.66**	**23.98**	**30.86**	**19.61**
LODC	**-1.41**	**2.33**	**15.80**	**30.83**	**42.91**	**58.39**

Table D9: Chest plate *Fx* for 170° series across nominal loads

Subject	Nominal Load (N)					
	25	**50**	**75**	**100**	**125**	**150**
PS01	0.70	1.75	-4.42			
PS02	-0.01	0.08				
PS03	-0.70	-4.57				
PS04	1.19	-1.65	0.97	-1.83	-2.67	-2.88
PS05						
PS06	0.08					
PS07	-7.94					
PS08						
PS09	12.68	7.98	16.01	18.64		
PS10	-0.03	0.23	-0.54	1.41		
PS11	-0.28	-0.64	-0.21	-0.55	-0.14	-0.19
PS12	-10.85	6.61	6.36	4.97		
PS13	1.44	0.08	-0.74	-0.47	-0.76	-0.05
PS14	-5.11	-5.27	-2.32	4.91	2.78	7.22
PS15	-2.59	-4.21	-1.69	3.33	1.60	3.41
PS16	0.56	0.39	0.11	0.98	-0.04	4.64
PS17			2.75			
PS18	0.96	-0.16	-0.01	-0.11	0.19	
PS19	0.33	5.07	4.80	3.63	-0.01	
PS20	-0.94	6.57				
PS21	0.45	0.16	-0.26	9.43		
PS22	0.13	-2.12	0.93	1.98	-1.98	1.59
PS23	-1.19	-2.78	-1.19	0.13	-2.51	0.93
PS24	1.85	-0.13	-1.32	-3.97	1.85	1.19
PS25	-4.23	-7.28	3.17	-0.93	-0.66	6.75
Avg	**-0.61**	**0.01**	**1.24**	**2.60**	**-0.20**	**2.26**
SD	**4.34**	**4.07**	**4.49**	**5.35**	**1.70**	**3.21**
LODC	**-9.27**	**-26.45**	**-25.09**	**-30.19**	**-23.89**	**-33.21**

Table D10: Chest plate *Fy* for 90° series across nominal loads

Subject	Nominal Load (N)					
	25	**50**	**75**	**100**	**125**	**150**
PS01	-3.07	5.12	2.77	4.99	8.58	7.53
PS02	0.63	-0.97	-0.08	-1.37	-2.65	-2.34
PS03	1.47	4.36	2.53	3.45	6.90	7.58
PS04	0.26	1.24	3.87	4.23	2.92	3.85
PS05	1.98	3.12	3.60	1.64	-0.85	2.01
PS06	1.41	2.53	1.23	-1.93	-4.36	9.03
PS07	-0.47	2.88	0.36	4.31	-1.58	6.78
PS08	-0.21	0.61	-0.87	-1.20		
PS09	-0.74	-1.32	-2.59	0.75		
PS10	0.19	-0.37	1.81			
PS11	-0.45	1.59	-0.10	1.24		
PS12	-2.29	-0.74				
PS13	0.10	-1.90	2.99	8.97	4.32	9.62
PS14	0.27	-0.98	2.06	3.62	-2.44	-2.75
PS15	0.92	-0.78	-3.72	0.95	6.82	-3.23
PS16	3.68	6.14	8.68	3.94	0.51	14.21
PS17	0.04	-1.09				
PS18	0.19	1.07	1.16	3.73	2.86	
PS19	0.50	-1.04				
PS20	-0.64	0.06	0.90			
PS21	0.62	2.48				
PS22	0.29	-0.49	4.36			
PS23	0.25	1.03	4.94			
PS24	-0.74	-0.74	4.74	-1.69		
PS25	-0.29	-2.26	-2.31	3.46		
Avg	**0.16**	**0.78**	**1.73**	**2.30**	**1.75**	**4.75**
SD	**1.29**	**2.25**	**2.89**	**2.89**	**4.28**	**5.74**
LODC	**0.33**	**-0.44**	**-0.38**	**0.08**	**-0.95**	**-1.10**

Table D11: Chest plate *Fy* for 135° series across nominal loads

Subject	Nominal Load (N)					
	25	**50**	**75**	**100**	**125**	**150**
PS01	4.20	3.64				
PS02	-0.16	0.95	0.76	0.79		
PS03	1.41	1.99	0.56	0.91		
PS04	2.12	0.67	3.05	2.09	2.64	0.39
PS05	0.24	1.32	2.63	1.67	3.58	1.02
PS06	1.66	0.82	0.01	0.42	1.43	3.26
PS07	-1.57	-0.13	3.39	-0.31		
PS08	-0.36	0.87	0.28			
PS09	-0.43	1.21	0.76	0.78		
PS10	-0.51	-0.88	0.46	0.35		
PS11	-0.35	0.82	0.06	1.35	0.88	1.91
PS12	0.00	2.31	0.97			
PS13	0.00	-0.32	-0.01	0.10		
PS14	0.18	-0.94	-0.65	0.79	-0.01	1.05
PS15	-0.94	-3.46	-0.47	1.42	0.38	0.22
PS16	0.13	0.09	-1.27	-1.15	-0.69	-1.92
PS17	-0.18	-1.23	-2.09			
PS18	-0.38	-0.27	0.13	0.47	-1.48	
PS19	-0.79	0.43	-0.43	1.59		
PS20	-1.08	0.43	0.35			
PS21	0.99	1.24				
PS22	-0.41	-0.99	-0.99	-1.28	2.39	3.21
PS23	0.16	-1.03	-0.74	0.25		
PS24	-2.64	-0.62	0.16	-0.08	1.52	-2.80
PS25	-1.36	1.61	-1.28	0.58		
Avg	**0.00**	**0.34**	**0.24**	**0.56**	**1.06**	**0.70**
SD	**1.34**	**1.42**	**1.33**	**0.89**	**1.57**	**2.06**
LODC	**1.17**	**1.77**	**1.04**	**1.92**	**0.81**	**0.10**

Table D12: Chest plate *Fy* for 170° series across nominal loads

Subject	Nominal Load (N)					
	25	**50**	**75**	**100**	**125**	**150**
PS01	-0.49	-0.45	-1.52			
PS02	0.27	-0.31				
PS03	0.83	-0.73				
PS04	2.02	0.27	0.63	0.30	-0.04	0.06
PS05						
PS06	0.76					
PS07	1.05					
PS08						
PS09	0.66	0.51	1.23	1.01		
PS10	0.08	-0.30	0.18	0.19		
PS11	0.19	-0.04	-0.31	-0.13	0.20	-0.14
PS12	0.24	1.17	2.22	1.50		
PS13	-0.15	-0.03	0.06	0.04	0.27	0.31
PS14	-0.04	0.58	2.09	1.72	1.13	0.96
PS15	-0.64	-0.51	-0.31	1.43	0.97	0.81
PS16	-0.08	-0.13	0.08	-0.42	0.26	0.40
PS17			-0.29			
PS18	-0.12	0.15	0.11	0.30	0.06	
PS19	0.07	-0.11	-0.66	0.04	0.10	
PS20	-0.13	-0.19				
PS21	-0.49	-0.49	-0.54	0.16		
PS22	-0.21	0.16	-0.41	-0.12	0.33	-0.08
PS23	0.70	0.86	1.98	0.04	0.29	-0.08
PS24	-0.33	1.03	-0.58	0.66	0.82	-0.54
PS25	1.24	1.36	-0.21	0.33	-0.08	-1.36
Avg	**0.25**	**0.14**	**0.21**	**0.44**	**0.36**	**0.03**
SD	**0.65**	**0.60**	**1.04**	**0.64**	**0.40**	**0.67**
LODC	**0.99**	**1.10**	**1.00**	**-0.02**	**0.37**	**3.20**

Table D13: Chest plate *Fz* for 90° series across nominal loads

Subject	Nominal Load (N)					
	25	**50**	**75**	**100**	**125**	**150**
PS01	-10.35	-14.75	-8.33	-31.08	-14.73	-34.20
PS02	-1.18	-7.39	-12.35	-32.71	-34.16	-44.26
PS03	-13.54	-20.81	-24.45	-33.82	-32.76	-54.62
PS04	-7.87	-10.69	-18.55	-16.31	-38.54	-26.13
PS05	-2.06	-1.05	3.70	2.97	6.18	12.49
PS06	-4.17	-11.98	-18.37	-29.80	-18.31	-19.06
PS07	-1.29	-2.50	0.56	-3.21	-6.91	-22.33
PS08	-2.14	-10.41	-12.51	-20.72		
PS09	-1.24	-11.56	-18.30	-15.03		
PS10	-5.84	-36.69	-57.14			
PS11	-5.69	-9.54	-23.46	-25.97		
PS12	-1.11	-2.65				
PS13	-1.77	-10.24	-13.04	-31.18	-27.33	-61.12
PS14	-0.10	-1.68	0.49	-29.16	-1.04	-1.81
PS15	1.65	-3.44	-12.16	-25.53	-10.26	-36.11
PS16	-14.80	-7.42	6.87	-10.43	6.56	-32.29
PS17	-2.85	-10.42				
PS18	0.38	-0.95	-1.37	-1.91	-5.99	
PS19	-18.34	-21.74				
PS20	-2.09	-2.18	1.00			
PS21	-3.21	-16.34				
PS22	-16.42	-37.78	-25.41			
PS23	-5.24	-3.88	-20.37			
PS24	-0.21	-0.66	-0.70	-9.77		
PS25	-1.53	-16.21	-14.97	-28.95		
Avg	**-4.84**	**-10.92**	**-12.80**	**-20.15**	**-14.78**	**-29.04**
SD	**5.59**	**10.02**	**14.20**	**11.98**	**15.60**	**21.50**
LODC	**0.64**	**0.16**	**-1.47**	**-3.03**	**-8.02**	**-10.79**

Table D14: Chest plate *Fz* for 135° series across nominal loads

Subject	Nominal Load (N)					
	25	**50**	**75**	**100**	**125**	**150**
PS01	6.01	4.42				
PS02	0.86	3.40	4.87	6.78		
PS03	1.75	1.50	2.22	-5.15		
PS04	-5.56	0.20	5.59	17.30	24.90	23.62
PS05	1.29	-0.11	18.23	20.34	14.63	16.62
PS06	0.12	2.61	3.93	15.97	26.39	27.87
PS07	3.32	5.02	2.43	3.54		
PS08	7.28	8.52	9.47			
PS09	3.33	7.94	9.64	14.96		
PS10	2.24	8.86	16.32	22.21		
PS11	3.23	9.28	19.37	22.84	29.56	41.88
PS12	1.76	15.15	20.33			
PS13	0.22	3.13	13.83	12.91		
PS14	3.64	9.73	30.16	34.93	50.64	53.35
PS15	0.88	-0.01	-3.89	12.94	8.59	20.69
PS16	0.34	4.00	44.58	68.82	66.96	70.65
PS17	1.28	3.94	6.37			
PS18	-0.93	0.28	4.18	6.22	3.21	
PS19	-1.04	0.01	6.47	24.83		
PS20	1.08	11.44	19.17			
PS21	-0.16	4.89				
PS22	-0.08	0.08	-3.88	12.87	12.83	29.98
PS23	2.10	3.79	14.85	24.79		
PS24	2.02	0.25	4.21	12.33	22.68	17.53
PS25	2.43	11.63	19.38	27.59		
Avg	**1.50**	**4.80**	**11.64**	**18.79**	**26.04**	**33.58**
SD	**2.45**	**4.38**	**11.14**	**15.32**	**19.54**	**18.34**
LODC	**21.97**	**29.30**	**42.38**	**49.36**	**46.59**	**62.57**

Table D15: Chest plate *Fz* for 170° series across nominal loads

Subject	Nominal Load (N)					
	25	**50**	**75**	**100**	**125**	**150**
PS01	6.58	6.56	5.74			
PS02	-0.26	-0.10				
PS03	-1.08	-0.74				
PS04	3.58	3.46	1.60	1.32	2.59	-0.61
PS05						
PS06	1.61					
PS07	5.98					
PS08						
PS09	14.81	18.50	23.65	26.75		
PS10	-0.28	0.00	0.07	0.19		
PS11	-0.08	0.33	0.24	0.14	-0.43	-0.20
PS12	6.05	2.48	4.93	4.88		
PS13	-0.06	-0.15	-0.20	0.30	-0.06	0.31
PS14	0.94	5.04	10.48	12.84	16.47	16.43
PS15	-0.63	2.23	1.93	2.93	3.82	4.03
PS16	-0.30	-0.40	-0.23	7.73	1.12	20.28
PS17	-0.16	1.24	1.88			
PS18	-0.25	0.20	0.11	0.17	0.10	
PS19	1.00	7.90	5.58	2.99	0.07	
PS20	4.64	10.19				
PS21	0.33	-0.16	-0.37	8.82		
PS22	0.21	0.49	0.16	-0.66	0.16	-0.49
PS23	0.16	0.08	4.33	-0.12	-0.29	0.12
PS24	-0.78	0.70	1.53	2.56	3.67	4.91
PS25	0.66	0.62	-1.07	-0.45	0.29	6.43
Avg	**1.85**	**2.78**	**3.35**	**4.40**	**2.29**	**5.12**
SD	**3.68**	**4.69**	**5.88**	**7.11**	**4.71**	**7.47**
LODC	**14.17**	**13.18**	**15.06**	**18.89**	**16.09**	**9.66**

Table D16: Chest plate *Mx* for 90° series across nominal loads

Subject	Nominal Load (N)					
	25	**50**	**75**	**100**	**125**	**150**
PS01	-0.017	-0.099	-0.072	0.121	0.118	0.183
PS02	0.015	0.052	0.092	0.047	0.243	0.181
PS03	-0.071	-0.364	-0.285	0.274	-0.063	0.042
PS04	0.118	0.106	-0.165	-0.004	-0.226	-0.314
PS05	0.044	0.126	0.328	0.297	-0.049	0.527
PS06	-0.059	-0.188	-0.272	-0.751	-0.710	-0.309
PS07	0.006	0.034	0.034	0.166	0.433	0.277
PS08	0.003	-0.015	0.028	-0.073		
PS09	0.054	0.055	-0.152	-0.069		
PS10	-0.242	-0.059	0.214			
PS11	0.011	0.006	0.091	-0.108		
PS12	-0.028	-0.063				
PS13	0.008	0.054	0.427	0.813	0.208	-1.303
PS14	-0.035	-0.179	0.167	0.226	-0.263	0.120
PS15	-0.128	-0.442	-0.143	-0.142	0.219	-0.111
PS16	0.114	0.301	0.737	0.848	0.839	0.761
PS17	0.085	-0.212				
PS18	0.020	-0.013	0.086	-0.046	0.258	
PS19	0.156	0.248				
PS20	0.098	0.154	0.084			
PS21	-0.026	0.297				
PS22	0.066	-0.031	-0.122			
PS23	0.098	-0.059	-0.192			
PS24	0.072	0.039	0.160	0.162		
PS25	-0.002	0.273	0.284	-0.151		
Avg	**0.014**	**0.001**	**0.063**	**0.095**	**0.084**	**0.005**
SD	**0.085**	**0.187**	**0.250**	**0.366**	**0.390**	**0.541**
LODC	**-0.010**	**-0.065**	**-0.072**	**-0.110**	**-0.254**	**-0.264**

Table D17: Chest plate *Mx* for 135° series across nominal loads

Subject	Nominal Load (N)					
	25	**50**	**75**	**100**	**125**	**150**
PS01	0.102	0.073				
PS02	-0.009	-0.138	-0.164	-0.147		
PS03	-0.004	0.028	0.032	0.123		
PS04	0.050	0.050	0.282	0.327	0.171	0.231
PS05	0.034	-0.038	0.322	0.199	0.125	0.040
PS06	-0.046		0.004	0.129	0.134	0.407
PS07	0.040	-0.043	-0.015	0.026		
PS08	-0.193	-0.099	-0.005			
PS09	0.041	0.067	0.072	0.034		
PS10	0.022	0.091	0.221	0.177		
PS11	0.032	0.061	0.158	0.361	0.355	0.314
PS12	0.030	-0.055	-0.160			
PS13	0.001	0.022	0.097	0.071		
PS14	0.012	0.064	0.263	0.464	0.190	0.331
PS15	0.137	0.228	0.351	0.680	0.438	0.084
PS16	0.039	0.178	0.003	-0.018	0.339	0.223
PS17	0.011	0.214	0.216			
PS18	0.008	0.039	0.051	0.091	0.106	
PS19	0.202	0.126	0.311	0.255		
PS20	0.061	-0.027	-0.239			
PS21	-0.020	-0.109				
PS22	-0.017	-0.020	-0.046	-0.002	-0.431	0.074
PS23	0.024	0.168	0.238	0.101		
PS24	0.087	0.096	0.090	0.144	0.085	-0.457
PS25	0.048	-0.188	-0.146	-0.194		
Avg	**0.028**	**0.033**	**0.084**	**0.148**	**0.151**	**0.139**
SD	**0.070**	**0.109**	**0.171**	**0.207**	**0.237**	**0.257**
LODC	**0.086**	**0.243**	**0.387**	**0.430**	**0.485**	**0.747**

Table D18: Chest plate *Mx* for 170° series across nominal loads

Subject	Nominal Load (N)					
	25	**50**	**75**	**100**	**125**	**150**
PS01	-0.084	-0.012	-0.048			
PS02	-0.005	-0.011				
PS03	-0.055	0.001				
PS04	-0.006	0.018	-0.031	0.001	0.032	0.016
PS05						
PS06	-0.063					
PS07	0.054					
PS08						
PS09	0.048	0.073	0.080	0.177		
PS10	-0.001	0.003	-0.001	0.005		
PS11	0.001	0.001	-0.001	0.000	0.002	0.000
PS12	0.036	-0.023	0.048	0.034		
PS13	0.009	-0.011	0.004	-0.006	0.002	0.007
PS14	-0.003	-0.032	-0.052	0.018	0.040	0.064
PS15	0.010	0.023	0.003	-0.028	-0.004	-0.002
PS16	0.003	-0.008	0.003	-0.029	-0.006	-0.007
PS17			0.044			
PS18	-0.011	0.008	0.004	0.010	-0.003	
PS19	0.004	0.018	0.064	-0.009	0.007	
PS20	-0.001	0.019				
PS21	0.002	0.007	-0.011	-0.055		
PS22	0.020	0.015	0.015	-0.017	-0.004	-0.013
PS23	0.037	0.020	-0.068	-0.009	-0.035	-0.015
PS24	-0.015	-0.044	0.028	-0.066	0.020	0.055
PS25	0.015	0.033	0.101	-0.031	-0.002	0.101
Avg	**0.000**	**0.005**	**0.010**	**0.000**	**0.004**	**0.020**
SD	**0.033**	**0.025**	**0.045**	**0.054**	**0.019**	**0.039**
LODC	**0.082**	**0.167**	**0.138**	**0.209**	**0.130**	**0.099**

Table D19: Chest plate *My* for 90° series across nominal loads

Subject	Nominal Load (N)					
	25	**50**	**75**	**100**	**125**	**150**
PS01	0.426	1.565	2.905	4.149	4.085	4.814
PS02	0.034	0.671	0.058	2.495	3.400	5.677
PS03	-0.526	-0.417	-0.222	-0.990	0.583	-0.853
PS04	-0.659	-0.146	-1.361	-0.719	-3.457	-1.316
PS05	-0.009	0.136	0.127	0.622	0.469	0.777
PS06	0.096	-0.890	-1.371	-1.608	-1.271	-1.769
PS07	0.172	0.870	1.028	0.590	0.381	2.469
PS08	-0.137	1.110	3.189	2.288		
PS09	-0.210	-0.358	-0.105	-0.173		
PS10	0.483	-0.050	-0.755			
PS11	-0.045	0.180	0.008	0.132		
PS12	0.686	0.816				
PS13	-0.194	-2.288	-0.645	-1.008	2.856	-0.860
PS14	-0.013	0.678	1.150	0.656	2.461	2.431
PS15	0.399	0.316	0.798	0.320	-2.606	-3.280
PS16	-0.218	-0.394	1.046	-1.373	0.809	-1.880
PS17	-0.749	-1.059				
PS18	-0.061	-0.191	-0.537	-0.763	-1.903	
PS19	-1.180	-1.170				
PS20	0.269	1.296	3.390			
PS21	0.665	1.257				
PS22	-1.223	-2.262	-0.202			
PS23	-0.462	0.497	0.336			
PS24	-0.180	-0.313	-1.131	-0.730		
PS25	-0.523	-0.577	-0.157	-0.206		
Avg	**-0.126**	**-0.029**	**0.360**	**0.217**	**0.484**	**0.565**
SD	**0.501**	**1.005**	**1.379**	**1.528**	**2.431**	**2.918**
LODC	**0.304**	**2.101**	**3.743**	**4.587**	**5.352**	**6.588**

Table D20: Chest plate *My* for 135° series across nominal loads

Subject	Nominal Load (N)					
	25	**50**	**75**	**100**	**125**	**150**
PS01	0.608	0.384				
PS02	-0.041	0.062	0.382	1.004		
PS03	0.108	0.021	-0.050	-0.608		
PS04	-0.349	-0.089	0.143	1.817	1.772	1.643
PS05	-0.435	-1.075	1.795	1.742	1.553	0.811
PS06	0.221	-0.386	-0.463	-0.379	-0.427	-0.653
PS07	0.305	0.463	0.419	0.347		
PS08	0.242	0.911	1.591			
PS09	-0.078	-0.140	0.639	1.735		
PS10	0.002	0.563	1.861	2.652		
PS11	-0.141	0.681	1.321	1.901	2.876	3.984
PS12	0.013	1.353	2.635			
PS13	0.000	-0.050	0.872	0.577		
PS14	0.057	0.377	1.110	1.060	2.641	3.630
PS15	-0.432	-0.503	0.680	2.573	3.600	4.394
PS16	-0.021	-0.190	3.636	5.278	6.445	5.551
PS17	-0.117	-0.230	0.204			
PS18	-0.085	-0.133	0.000	0.160	0.090	
PS19	-0.515	0.603	0.541	3.291		
PS20	-0.364	0.711	2.318			
PS21	0.073	0.993				
PS22	-0.264	-0.489	-0.512	1.070	1.429	4.413
PS23	0.038	0.111	1.494	2.732		
PS24	-0.669	0.019	-0.065	-0.214	0.714	1.861
PS25	-0.688	0.229	0.779	3.037		
Avg	**-0.101**	**0.168**	**0.927**	**1.567**	**2.069**	**2.848**
SD	**0.307**	**0.544**	**1.035**	**1.484**	**1.978**	**2.027**
LODC	**1.217**	**1.791**	**2.295**	**2.489**	**2.155**	**3.106**

Table D21: Chest plate *My* for 170° series across nominal loads

Subject	Nominal Load (N)					
	25	**50**	**75**	**100**	**125**	**150**
PS01	0.234	0.470	0.413			
PS02	-0.004	-0.011				
PS03	-0.055	0.183				
PS04	0.241	0.330	0.082	0.165	0.242	0.064
PS05						
PS06	0.138					
PS07	0.609					
PS08						
PS09	0.348	0.816	0.747	0.878		
PS10	0.000	0.002	0.005	0.011		
PS11	-0.001	0.001	0.000	0.002	-0.004	0.000
PS12	0.002	-0.004	0.141	0.101		
PS13	0.006	-0.008	-0.009	0.005	0.000	0.008
PS14	0.189	0.493	0.587	0.457	0.781	0.677
PS15	0.083	0.303	0.181	0.041	0.154	0.133
PS16	0.000	0.020	0.011	0.753	0.066	1.767
PS17			-0.053			
PS18	0.003	0.018	-0.010	0.006	0.005	
PS19	0.051	0.218	0.138	0.077	0.011	
PS20	0.314	0.323				
PS21	0.023	0.031	-0.015	-0.149		
PS22	0.015	0.031	0.008	-0.038	0.067	0.046
PS23	0.061	0.050	0.351	0.023	0.073	-0.008
PS24	0.027	0.134	0.130	0.287	0.218	0.275
PS25	0.302	0.371	-0.050		0.011	0.118
Avg	**0.118**	**0.188**	**0.148**	**0.174**	**0.135**	**0.308**
SD	**0.164**	**0.226**	**0.231**	**0.298**	**0.220**	**0.552**
LODC	**0.763**	**1.285**	**1.576**	**1.882**	**1.499**	**1.127**

Table D22: Chest plate *Mz* for 90° series across nominal loads

Subject	Nominal Load (N)					
	25	**50**	**75**	**100**	**125**	**150**
PS01	0.223	0.089	-0.553	-0.755	-0.259	-0.504
PS02	-0.023	0.091	-0.056	-0.698	-0.944	-0.509
PS03	0.228	0.294	0.809	0.651	1.616	1.250
PS04	-0.154	-0.370	-0.878	-1.119	-0.339	-1.542
PS05	-0.382	-0.062	-0.427	-0.193	-1.547	-0.535
PS06	0.133	0.082	0.194	-0.012	-0.133	0.502
PS07	0.067	0.001	0.299	0.008	-0.029	1.491
PS08	0.033	0.121	0.073	0.489		
PS09	0.044	-0.232	0.109	0.306		
PS10	0.324	0.772	0.680			
PS11	0.089	0.145	0.715	1.321		
PS12	0.109	-0.299				
PS13	-0.019	-0.764	-0.264	-0.458	-0.116	-0.300
PS14	-0.044	-0.131	0.144	0.377	-0.429	-0.578
PS15	0.318	0.434	0.431	-0.012	-0.142	-0.723
PS16	-0.479	-0.065	0.847	0.321	-0.793	-0.178
PS17	0.005	0.030				
PS18	-0.003	-0.104	0.084	0.011	0.122	
PS19	-0.443	-0.319				
PS20	0.220	0.227	0.026			
PS21	-0.091	-0.313				
PS22	0.008	-0.291	0.193			
PS23	-0.030	0.034	-0.042			
PS24	0.049	0.091	0.155	0.234		
PS25	-0.011	0.034	0.223	-0.151		
Avg	**0.007**	**-0.020**	**0.132**	**0.019**	**-0.249**	**-0.148**
SD	**0.205**	**0.300**	**0.435**	**0.580**	**0.751**	**0.892**
LODC	**-0.010**	**0.258**	**0.354**	**0.417**	**0.279**	**0.123**

Table D23: Chest plate *Mz* for 135° series across nominal loads

Subject	Nominal Load (N)					
	25	**50**	**75**	**100**	**125**	**150**
PS01	-0.352	-0.264				
PS02	0.095	-0.501	-0.355	-0.246		
PS03	-0.078	-0.008	0.076	0.063		
PS04	0.075	0.127	0.172	0.575	0.496	0.530
PS05	0.110	0.431	0.319	0.050	0.001	0.457
PS06	-0.209	-0.038	0.176	0.477	0.428	1.220
PS07	0.072	0.196	0.652	0.799		
PS08	0.478	0.331	0.627			
PS09	0.295	0.223	0.380	0.208		
PS10	0.158	0.242	0.354	0.405		
PS11	0.206	0.189	0.612	0.216	0.198	0.348
PS12	0.007	-0.426	-0.693			
PS13	0.000	-0.080	-0.108	-0.234		
PS14	0.085	0.082	0.488	0.725	0.844	0.629
PS15	-0.211	-0.067	-0.074	-0.251	-0.102	0.119
PS16	0.015	0.126	-0.007	0.499	1.687	1.623
PS17	-0.004	0.103	0.235			
PS18	-0.039	0.066	0.120	0.250	0.196	
PS19	0.014	0.105	0.099	0.457		
PS20	0.101	0.107	-0.173			
PS21	0.019	-0.042				
PS22	-0.019	-0.257	0.060	-0.102	-0.181	0.211
PS23	-0.011	0.094	0.132	0.083		
PS24	0.257	0.004	0.113	0.294	0.725	0.461
PS25	0.170	0.170	0.253	0.287		
Avg	**0.049**	**0.037**	**0.150**	**0.240**	**0.429**	**0.622**
SD	**0.169**	**0.218**	**0.315**	**0.314**	**0.557**	**0.490**
LODC	**-0.090**	**-0.116**	**0.020**	**0.243**	**0.561**	**0.804**

Table D24: Chest plate *Mz* for 170° series across nominal loads

Subject	Nominal Load (N)					
	25	**50**	**75**	**100**	**125**	**150**
PS01	0.162	-0.023	0.222			
PS02	0.009	-0.013				
PS03	-0.036	-0.039				
PS04	-0.157	-0.042	-0.108	-0.045	-0.029	-0.011
PS05						
PS06	-0.044					
PS07	-0.035					
PS08						
PS09	0.037	0.067	0.066	0.225		
PS10	-0.002	0.001	-0.002	0.005		
PS11	0.001	-0.003	-0.003	-0.003	-0.003	-0.004
PS12	-0.193	-0.098	-0.016	-0.001		
PS13	0.006	-0.004	-0.009	0.010	0.002	-0.001
PS14	-0.017	0.170	0.191	0.214	0.415	0.378
PS15	0.026	0.107	0.115	0.035	0.047	0.037
PS16	0.003	-0.013	0.002	0.236	-0.001	0.134
PS17			0.115			
PS18	-0.022	0.015	0.008	-0.002	0.008	
PS19	-0.001	0.108	-0.006	0.011	0.023	
PS20	-0.046	0.062				
PS21	0.008	-0.042	-0.011	-0.075		
PS22	-0.023	0.057	0.023	-0.042	-0.026	-0.011
PS23	0.023	0.057	-0.189	-0.023	-0.008	0.023
PS24	-0.049	-0.004	0.106	0.121	0.204	0.344
PS25	-0.147	-0.106	0.015	-0.038	-0.008	-0.060
Avg	**-0.023**	**0.013**	**0.029**	**0.039**	**0.052**	**0.083**
SD	**0.073**	**0.069**	**0.097**	**0.101**	**0.130**	**0.155**
LODC	**-0.271**	**-0.548**	**-0.373**	**-0.450**	**-0.304**	**-0.544**